NASA TECHNICAL NOTE

NASA TN D-6335

NASA TN D-6335





# TRANSIENT THERMAL PERFORMANCE OF MULTILAYER INSULATION SYSTEMS DURING SIMULATED ASCENT PRESSURE DECAY

*by Irving E. Sumner and Joseph E. Maloy*

*Lewis Research Center*
*Cleveland, Ohio 44135*

NATIONAL AERONAUTICS AND SPACE ADMINISTRATION • WASHINGTON, D. C. • JULY 1971

| 1. Report No. NASA TN D-6335 | 2. Government Accession No. | 3. Recipient's Catalog No. |
|---|---|---|
| 4. Title and Subtitle TRANSIENT THERMAL PERFORMANCE OF MULTILAYER INSULATION SYSTEMS DURING SIMULATED ASCENT PRESSURE DECAY | | 5. Report Date July 1971<br>6. Performing Organization Code |
| 7. Author(s) Irving E. Sumner and Joseph E. Maloy | | 8. Performing Organization Report No. E-5764<br>10. Work Unit No. 180-31 |
| 9. Performing Organization Name and Address Lewis Research Center<br>National Aeronautics and Space Administration<br>Cleveland, Ohio 44135 | | 11. Contract or Grant No.<br>13. Type of Report and Period Covered Technical Note |
| 12. Sponsoring Agency Name and Address National Aeronautics and Space Administration<br>Washington, D.C. 20546 | | 14. Sponsoring Agency Code |
| 15. Supplementary Notes | | |

16. Abstract

Thermal tests were conducted to determine experimentally the transient heat flux and total integrated heat transferred to a liquid hydrogen tank during a simulated Saturn V ascent pressure decay. Three 30-layer helium-purged multilayer insulations systems, comprised of (1) glass-fiber paper or silk netting spacers between aluminized Mylar radiation shields and (2) fiber glass mat or sealed foam sublayers, were tested. All three insulation systems achieved space-hold heat-transfer conditions within 2 hours after initiation of pumpdown. The integrated heat transferred was approximately 25 percent greater than ideal, except for the system utilizing the foam sublayer which had not been optimized with regard to thickness.

| 17. Key Words (Suggested by Author(s)) | 18. Distribution Statement |
|---|---|
| Multilayer insulation<br>Purge gas venting<br>Liquid hydrogen propellant tanks<br>Space vehicles<br>Transient thermal performance | Unclassified - unlimited |

| 19. Security Classif. (of this report) | 20. Security Classif. (of this page) | 21. No. of Pages | 22. Price* |
|---|---|---|---|
| Unclassified | Unclassified | 78 | $3.00 |

*For sale by the National Technical Information Service, Springfield, Virginia 22151

# TRANSIENT THERMAL PERFORMANCE OF MULTILAYER INSULATION SYSTEMS DURING SIMULATED ASCENT PRESSURE DECAY

by Irving E. Sumner and Joseph E. Maloy

Lewis Research Center

## SUMMARY

Steady-state and transient experimental tests were conducted to determine the transient heat flux and total integrated heat transferred to a liquid hydrogen tank during a simulated Saturn V launch vehicle ascent pressure decay for each of three multilayer insulation systems. The multilayer insulation systems utilized (1) glass-fiber (Dexiglas) paper or silk netting as the spacers between the double-aluminized Mylar radiation shields and (2) helium-purged fiber glass mat or sealed polyurethane foam sublayers to reduce the ground-hold heat flux. The multilayer insulation panels were intended to be purged with gaseous nitrogen and the fiber glass mat sublayer purged with gaseous helium during the initial ground-hold conditions. However, transient rapid pumpdowns could be achieved only when using a gaseous helium purge throughout the entire insulation system during the initial ground-hold conditions.

The test results indicated that multilayer insulation (MLI) systems utilizing a helium-purged sublayer in conjunction with gaseous-nitrogen-purged multilayer insulation panels for ground-hold conditions are inadequate unless considerable care is taken to control the sublayer and MLI thickness during ground hold. These MLI systems, when entirely purged with helium during ground hold, did, however, provide reasonably good thermal performance. The integrated total heat input up to 150 minutes after initiation of a rapid pumpdown was only 22 to 28 percent greater than the ideal integrated heat input (i.e., MLI interstitial pressure equal to instantaneous ambient pressure) calculated from steady-state data. The MLI system utilizing a foam sublayer provided an integrated heat input 3.6 times greater than the ideal value; this was due, in part, to the heat storage capacity of the foam sublayer, which had not been optimized with regard to thickness for these tests.

# INTRODUCTION

The use of liquid hydrogen as a propellant for cryogenic spacecraft propulsion modules will require well-designed thermal protection systems to maintain the vented liquid hydrogen boiloff or the nonvented tank pressure rise at acceptably low values. The three major phases of a given mission during which the thermal protection system must provide predictable thermal performance are

(1) Ground hold prior to launch

(2) Transition from ground hold to space hold during and immediately after launch

(3) Space hold (earth orbit and planetary travel)

Numerous analytical and experimental investigations have been conducted to define the necessary performance factors of various thermal protection systems (most notably multilayer insulation (MLI) systems) during the ground-hold and space-hold phases. However, one area in which a lack of experimental data exists is the transient thermal response of the multilayer insulation to the ascent pressure decay that occurs in the transition from ground-hold to space-hold conditions during and immediately after launch. Failure of the multilayer insulation to rapidly vent the interstitial purge gases may result in large heat leaks into the propellant tanks and possible structural damage to the insulation systems. The investigation reported herein was conducted to measure experimentally the transient heat flux for a representative multilayer system during a simulated Saturn V launch vehicle ascent pressure decay.

The basic MLI system chosen for this investigation had already undergone a considerable amount of design and experimental testing, as reported by Sterbentz and Baxter (ref. 1). This insulation system was designed for the 4.20-meter (165.2-in.) diameter spherical liquid hydrogen tank of a hypothetical cryogenic spacecraft propulsion module; the thermal performance design goal was to limit the total liquid hydrogen boiloff to 5 percent or less for an assumed 8-day lunar mission. As originally designed, this MLI system consisted of (1) a 1.0-centimeter (0.4-in.) thick fiber glass mat sublayer (helium-purged during ground hold) and (2) 30 layers of multilayer insulation (nitrogen-purged during ground hold) fabricated in triangular $60^{\circ}$ gore-shaped panels. Each panel of insulation consisted of 10 double-aluminized Mylar radiation shields, each separated by a glass-fiber (Dexiglas) paper spacer. Nylon monofilament threads and Teflon buttons were utilized to assemble the 10 radiation shields and nine paper spacers in the modular panels. The multilayer insulation was separated from the fiber glass mat sublayer by a plastic (Aclar 22C) vapor barrier.

This MLI system was subsequently installed on a half-scale 2.10-meter (82.6-in.) diameter spherical tank and tested under ground-hold environmental conditions, a partially simulated transient ascent pressure decay representative of a Saturn V launch, and space-hold environmental conditions (the test results are noted in ref. 1). Further experimental tests to gain additional information on the thermal performance of this

insulation system installed on the half-scale tank have been recently completed at the Lewis Research Center (ref. 2). These more recent experimental tests also consisted of ground-hold and space-hold thermal tests. However, neither of these two test programs have provided adequate experimental data during a suitably simulated ascent pressure decay to determine (1) the transient heat flux and (2) the transient interstitial pressure decay of the ground-hold purge gases within the multilayer insulation during the transition from ground-hold to space-hold conditions.

Therefore, a program involving purged-multilayer-insulation venting tests was conducted in a 1.65-meter (65-in.) diameter by 2.3-meter (90-in.) high cylindrical vacuum chamber capable of providing a Saturn V launch vehicle ascent pressure decay (pressure against time) to pressures less than $10^{-4}$ torr. Three different multilayer insulation systems were ultimately investigated. The first insulation system consisted of a helium-purged fiber glass sublayer and 30 layers of nitrogen-purged multilayer insulation; this MLI system was almost identical to the insulation system previously tested on the 2.10-meter (82.6-in.) diameter spherical tank. The second insulation system utilized three layers of silk netting instead of the Dexiglas paper as the spacer material between radiation shields (the helium-purged fiber glass mat sublayer remained essentially the same). The third insulation system used the same multilayer insulation panels as the first system tested (aluminized Mylar separated by Dexiglas paper spacers) but utilized a sealed polyurethane foam as the sublayer rather than the helium-purged fiber glass mat sublayer.

Each of the three multilayer insulation systems was mounted on a 0.76-meter (30-in.) diameter, double-guarded cylindrical calorimeter. Liquid hydrogen was used as the cryogenic fluid for testing in all cases. The experimental data obtained included steady-state heat flux as a function of chamber pressure as well as transient heat flux and interstitial pressure decay for simulated Saturn V ascent ambient pressure decay. The multilayer insulation panels were intended to be purged with gaseous nitrogen and the fiber glass sublayer (when used) with gaseous helium during the initial ground-hold conditions. However, transient rapid pumpdowns could be achieved only when using a gaseous helium purge throughout the insulation systems (MLI as well as fiber glass sublayer) during the initial ground-hold conditions.

## EXPERIMENTAL APPARATUS

### Multilayer Insulation Systems

System 1 (aluminized Mylar/Dexiglas/fiber glass). - The MLI system originally considered and tested in this investigation was nearly identical to that designed and tested previously on a 2.10-meter (82.6-in.) diameter spherical tank (refs. 1 and 2).

This insulation system, a cross section of which is shown in figure 1, consisted of a fiber glass mat sublayer that was helium purged under ground-hold conditions, a relatively leak-free purge bag, and multilayer insulation that was intended to be gaseous nitrogen purged under ground-hold conditions.

The fiber glass mat sublayer consisted of a 1.3-centimeter (0.5-in.) thick fiber glass mat of about 9.6 kilograms per cubic meter (0.6 $lb/ft^3$) density sandwiched between two layers of Dacron cloth for strength. Velcro fasteners were sewed on each side of the fiber glass mat to provide support from the tank wall and also support for the purge bag. The idealized thickness of the sublayer (including the thickness of the Velcro fasteners) for this investigation was 1.9 centimeters (0.75 in.). This is the only departure from the insulation system specified in references 1 and 2, which utilized a fiber glass sublayer with an intended effective thickness of 1.0 centimeter (0.4 in.).

The fiber glass sublayer was enclosed by a 0.013-centimeter (5-mil) thick Aclar 22C plastic film treated for adhesive bonding. Velcro fasteners were adhesively bonded to each side of the purge bag to help support the purge bag from the fiber glass sublayer, and in turn, to help support the inner blanket of multilayer insulation. The purge bag was also bonded at the top and bottom of the cylindrical test tank to a 1.9-centimeter (0.75-in.) diameter stainless-steel helium purge manifold. The primary purpose of the purge bag was to prevent helium gas from leaving and nitrogen gas from entering the sublayer during purging of the insulation system during ground-hold conditions. The intended temperature on the outer surface of the purge bag was 78 K ($140^{\circ}$ R) or higher to prevent condensation or freezing of the nitrogen purge gas.

The multilayer insulation consisted of 30 layers of double-aluminized Mylar radiation shields with approximately 460 Å thickness of aluminizing on each side. A reflectivity-sensing emissometer was used to determine total hemispherical emittance of the aluminized surface, which varied between 0.023 and 0.033 at normal room temperature. The radiation shields were separated by Dexiglas paper spacers having a thickness of 0.0071 centimeter (2.8 mils). The multilayer insulation was fabricated in three blankets having 10 radiation shields and nine spacers per blanket. Nylon monofilament thread and Teflon buttons and tabs were used to assemble the alternating radiation shields and spacers together in modular panels. The resulting layer density of the multilayer insulation blanket was approximately 28 layers per centimeter (70 layers/in.).

Each of the three 10-layer blankets comprising the MLI system was made up of three panels, as noted in figures 1 and 2. The middle panel of each MLI blanket was identical in size except for the circumferential length. The middle panel of the inner MLI blanket was sized to have the same venting characteristics as a panel from the 2.10-meter (82.6-in.) tank program; that is, using the analysis described in appendix A, the center of the middle panel was calculated to experience nearly the same interstitial pressure decay rate as the corresponding point in a MLI panel of the 2.10-meter

(82.6-in.) diameter tank insulation system. This assumes that, for edgewise venting of the MLI panel, the largest portion of the pressure drop experienced by the interstitial purge gas occurs within the MLI panel, as compared to the pressure drop which might occur across the butt joints between adjacent panels of MLI.

A Dacron net was applied over the MLI after it was installed on the test tank. The Dacron net was utilized on the 2.10-meter (82.6-in.) spherical tank to restrain the MLI from ballooning during an ascent pressure decay and was included in this test for completeness of the MLI system.

System 2 (aluminized Mylar/silk net/fiber glass). - Experimental results for MLI system 1 (to be discussed later) indicated that the helium-purged sublayer was not maintaining its intended thickness and providing purge bag temperatures of 78 K ($140^{\circ}$ R) or higher during ground-hold conditions (required to preclude the possibility of freezing and/or condensing the MLI nitrogen purge gas). Consequently, the fiber glass sublayer was rebuilt for MLI system 2 in an attempt to get the sublayer to remain at its intended thickness of 1.9 centimeters (0.75 in.) during ground-hold conditions. Two layers of initially (uncompressed) 1.3-centimeter (0.50-in.) fiber glass mat were sandwiched together and sewed between two layers of Dacron cloth to provide an overall thickness of 1.9 centimeters (0.75 in.). Cutouts were then made in the fiber glass sublayer to allow for a total of 48 rigid polyurethane foam blocks to penetrate the sublayer, as shown in figure 3. The purpose of these foam blocks, which were adhesively bonded to the tank wall, was to provide a more positive standoff for the purge bag and, therefore, better thickness control of the sublayer. A 0.005-centimeter (2-mil) Mylar purge bag was utilized in place of the Aclar since tests indicated it contracted only 0.3 to 0.4 percent through a temperature change from room temperature to liquid nitrogen temperature, as compared to approximately 1 percent for the Aclar 22C material.

Multilayer insulation blankets having the same basic dimensions and method of construction as those for MLI system 1 were fabricated utilizing three layers of 14-by-14 mesh silk netting as the spacer between radiation shields. The resulting layer density of the MLI was approximately 20 layers per centimeter (50 layers/in.).

System 3 (aluminized Mylar/Dexiglas/foam). - A rigid polyurethane foam insulation, 1.9 centimeters (0.75 in.) thick with a density of 34 kilograms per cubic meter, (2.1 $lb/ft^3$) was utilized for the sublayer for insulation system 3, rather than the helium-purged fiber glass mat sublayer utilized on the two previous MLI systems. The formulation of the closed-cell polyurethane foam was identical to that successfully tested and described in reference 3. The cylindrical walls of the calorimeter were primed with G-207 adhesive, and the foam constituents were poured in place, directly on the tank, one-half at a time. The excess foam was then machined to provide a uniform thickness of 1.9 centimeters (0.75 in.). A vapor barrier (also identical to that described in ref. 3) consisting of a two-way stretch nylon cloth "bleeder ply" and a laminate of Mylar and aluminum foil was bonded over the sublayer and helium leak-checked to provide

a leak rate of less than $10^{-8}$ standard cubic centimeter of helium per second for any individual leak. The vacuum tap used to conduct the leak check was left on the vapor barrier so that the back side of the vapor barrier could be partially evacuated during and after each thermal test.

The thickness of the foam sublayer was not optimized to provide the surface temperature of 78 K ($140^{\circ}$ R) or slightly higher needed to prevent condensation and/or freezing of nitrogen purge gas within the MLI blankets (approx. 0.13 cm (0.050 in.) would have been theoretically required). Instead, a thickness of 1.9 centimeters (0.75 in.) was used to eliminate the necessity of fabricating new MLI blankets that would have been required otherwise. The multilayer insulation was comprised of the same aluminized Mylar/Dexiglas panels utilized for insulation system 1.

## Insulation System Installation

The fiber glass mat utilized in the sublayer of the first two insulation systems was wrapped around the calorimeter and supported from the tank by the Velcro fasteners. The mat was then sewn together along the longitudinal seam.

The purge bag was wrapped around the sublayer and adhesively bonded at the top and bottom to the helium purge manifolds. The longitudinal seam was either heat sealed (Aclar purge bag) or adhesively bonded (Mylar purge bag). A gross leak check was then performed to ensure that there were no large leaks in the vapor barrier.

The inner blanket of multilayer insulation was supported from the purge bag by the Velcro fasteners. The longitudinal butt joint between the ends of each panel and the circumferential butt joints between panels were laced with Dacron thread, as shown in figure 4(a), to complete the installation of the inner blanket. The final trimming of the edges of each panel and tension of the Dacron thread lacing was such that each panel was amply supported without being unduly compressed.

The MLI panels of intermediate and outer blankets were supported by Dacron thread lacing between the outside of each inner blanket already installed on the test tank and the inside of the next adjacent outer panel being installed (fig. 4(b)), starting from the lower panel. Once all three panels for any given blanket were positioned on the test tanks, Dacron thread lacing was again used across the longitudinal and circumferential butt joints to complete the blanket installation. The butt joints between insulation panels of any given blanket were offset from the butt joints in the next adjacent blanket so that no direct path through the insulation existed for thermal radiation.

A lightweight Dacron net was installed over the three blankets of MLI and held in place at the top and bottom of the test tank by drawstrings. The net did not bear against the insulation system in any manner and, therefore, did not produce compressive forces on the outer surface of the insulation blankets.

Generally, all the procedures for applying the helium-purged sublayer and MLI blankets to the test tank were identical or very similar to the procedures specified and utilized for the installation of the insulation system on the 2.10-meter (82.6-in.) diameter spherical tank (refs. 1 and 2).

The foam sublayer was applied to the wall of the test tank as noted previously. To provide support for the MLI blankets, Velcro fasteners were bonded to the outside of the vapor barrier (fig. 5) in the same positions as used for the Aclar and Mylar purge bags. Therefore, the procedure for installing the MLI blankets over the foam sublayer was identical to that used for the fiber glass sublayer.

## Liquid Hydrogen Test Tank

The basic liquid hydrogen test tank configuration was a double-guarded cylindrical calorimeter consisting of a 76.2-centimeter (30.0-in.) diameter by 76.2-centimeter (30.0-in.) high measure tank, and 76.2-centimeter (30.0-in.) diameter upper and lower cold guards, as shown in figure 6. The purpose of the cold guards was to suppress insulation system edge effects in order to ensure one-dimensional heat transfer over the area of the measure tank.

The test tank utilized for the first two insulation systems tested was fabricated from 1.27-centimeter (0.50-in.) thick, oxygen-free, high-conductivity copper. This construction reduced the temperature gradients laterally along the wall to reduce the effect of liquid hydrogen level on the measured boiloff rate. This is necessary for (1) high heat fluxes through the insulation and (2) low liquid levels in the tanks. A second test tank, fabricated from 1100 aluminum alloy, was utilized for the third insulation system; the lighter weight of the aluminum test tank made it more convenient to handle while applying the foam sublayer.

The measure tank and cold guards were supported in a stack by a heavy stainless-steel center support tube. The individual tanks were separated from each other and from the center support tube by Bakelite spacers to thermally isolate the measure tank. The 5-centimeter (2-in.) outside diameter by 0.165-centimeter (0.065-in.) thick wall stainless-steel vent lines were also centered by Bakelite spacers as they passed through the upper tanks in the stack. Copper wool was packed around the vent lines and center support tube as they passed through the upper cold guard to provide a good thermal short and, thereby, reduce or eliminate any extraneous heat leaks into the measure tank. The fill line for each individual tank was a smaller tube located concentrically within the vent line. In the case of the measure tank, the fill line was cut off 5 centimeters (2 in.) below the top of the tank so that the tube did not extend down into the liquid hydrogen during the thermal test. The top and bottom of the calorimeter were insulated with foam (fig. 1) and sealed to reduce the heat leak into the upper and lower

cold guards during ground-hold conditions and to prevent freezing and/or condensation of nitrogen gas (when used as the MLI blanket purge gas).

## Test Facility

The liquid hydrogen test tank was mounted inside a cylindrical vacuum chamber (fig. 7) approximately 1.65 meters (65 in.) in diameter and 2.29 meters (90 in.) high. Water was circulated through tubing attached to the wall of the lower half of the chamber and through an internal baffle in the upper half of the chamber to provide a relatively constant boundary temperature during the ground-hold and space-hold tests. The chamber wall temperature varied between 281 and 298 K ($523^{\circ}$ and $537^{\circ}$ R), depending on the heat lost to the liquid hydrogen test tank and the environmental temperature inside the test cell.

Three mechanical roughing pumps (shown in the test facility schematic, fig. 7) were utilized in varying combinations either to maintain a steady chamber pressure above the diffusion pump range during steady-state tests, or to provide sufficient pumping capability to evacuate the chamber from 1-atmosphere pressure at a rate simulating a Saturn V ascent pressure decay. A closed-loop control system in conjunction with control valves just upstream of the 24.1- and 8.5-cubic-meter-per-minute (cmm) (850- and 300-cu ft/min (cfm)) roughing pumps provided the desired pumpdown rate to chamber pressures less than 1 torr. During a rapid pumpdown, the control valves generally reached the full-open position at slightly less than 1 torr, and the pumpdown rate could no longer be controlled. At a chamber pressure of approximately $8\times10^{-2}$ torr, a 50.8-centimeter (20-in.) diameter oil diffusion pump was manually cut in to complete the chamber pumpdown. For the transient pumpdown tests where a noncondensable insulation purge gas was used, the vacuum chamber could be pumped to $10^{-4}$ torr in $6\frac{1}{4}$ minutes or less; ultimate chamber pressures in the $10^{-5}$- to $10^{-6}$-torr range could be achieved.

In experimental boiloff tests of a transient nature or when low rates of heat transfer into the liquid hydrogen tank are expected, it is desirable to maintain a steady pressure within the test tank so that sensible heating and cooling of the liquid hydrogen can be neglected. In this test program, three different systems to control the back pressure within the cold guards as well as in the measure tank were tried. Although difficulties were encountered with each of these systems, the system noted in figure 7 ultimately proved to have the greatest potential in maintaining a constant liquid hydrogen tank pressure.

The back-pressure control system utilized an electrically heated oven designed to maintain an interior temperature of $306\pm0.01$ K ($550\pm0.02^{\circ}$ R). The oven contained a reference volume of approximately 98 cubic centimeters (6 in.$^3$) and two differential

pressure gages having a full-scale range of 690 newtons per square meter ($N/m^2$) (0.1 psid). The reference volume was charged with dry air to a pressure of approximately $1.2 \times 10^5$ $N/m^2$ (17.4 psia). For oven temperature variations of ±0.01 K (±0.02° R), the reference volume should theoretically maintain a constant pressure of ±4 $N/m^2$ (±0.0006 psi). The difference between the reference volume pressure and the liquid hydrogen test-tank pressure was sensed by the two differential pressure gages (one for the measure tank and one for the cold guards). The electrical signal from the differential pressure gages was used to operate four control valves, two for the measure tank and two for the cold guards, which in turn controlled the back pressure in the measure tank and cold guards. Each set of control valves mounted in parallel consisted of a large flow control valve to handle the ground-hold boiloff rates and a small control valve to handle the space-hold boiloff rates. For a maximum inaccuracy and drift of the differential pressure gages of ±1 percent of full scale, the back-pressure control system should have theoretically been able to control the tank pressures to ±6.9 $N/m^2$ (±0.001 psi) for the expected space-hold boiloff flow rates. The electrical signal from the cold-guard differential pressure gage was biased slightly to maintain the cold-guard pressure from 34 to 690 $N/m^2$ (0.005 to 0.1 psi) above the measure-tank pressure. This prevented the measure-tank boiloff gas from condensing within the vent line passing through the upper cold guard. It also maintained the temperature difference between the measure tank and cold guards to a low value, which reduced any heat leak into the measure tank directly from the cold guards.

## Instrumentation

Each of the three multilayer insulation systems was instrumented with 30 copper-constantan thermocouples to experimentally determine the insulation temperature profile at six locations, as noted in figure 8. The thermocouples were fabricated from 0.025-centimeter (10-mil) diameter wire. Each thermocouple junction plus a 15-centimeter (6-in.) length of each lead wire were taped to the aluminized Mylar radiation shield with aluminized Mylar tape to provide an isothermal lead length. Each thermocouple was referenced to one of three dynamic reference junctions mounted on the outer insulation blanket similar to those utilized in the tests reported by references 1 and 2. The temperature of each dynamic reference junction was, in turn, measured by a copper-constantan thermocouple referenced to liquid nitrogen temperature.

The interstitial pressure was measured within the insulation system at two locations (as also noted in fig. 8), one at the no-flow boundary within the fiber glass sublayer and the other at the center (or at the no-flow boundary) of the middle multilayer insulation panel (between the first and second radiation shields numbered from inside out) of the inner blanket. The interstitial pressures at each location were sensed by

both (1) a 0- to 775-torr (0- to 15-psid) differential strain gage transducer and (2) a capacitance-type differential pressure transducer having a range of either 30 to $3\times10^{-4}$ torr or 10 to $1\times10^{-4}$ torr depending on the specific transducer utilized. The pressure transducers were located just outside the vacuum chamber; each set of transducers was connected to the point at which the pressure was to be measured by a stainless-steel tube. The tube or flowpath length for each interstitial pressure measurement system was approximately 2.8 meters (110 in.) long and consisted of (1) a 1.68-meter (66-in.) long tube having a 0.95-centimeter (0.375-in.) outside diameter by 0.041-centimeter (0.016-in.) wall running from within the insulation system to outside the chamber, and (2) a 1.12-meter (44-in.) length of tubing 0.64-centimeter (0.25-in.) outside diameter by 0.089-centimeter (0.035-in.) wall connecting the transducers, valves, etc., as shown in figure 9. The last 82.6 centimeters (32.5 in.) of tubing within the insulation was flattened to 0.64-centimeter (0.25-in.) thickness to reduce the physical interference with the insulation system. Each tube was instrumented with a copper-constantan thermocouple at the cold end within the insulation to allow for a temperature correction of the measured pressure in the molecular and transition flow range (ref. 4). The differential pressure transducers were referenced to a vacuum level of less than $10^{-4}$ torr; valves were located in the interstitial pressure measurement system (as noted in fig. 9) to allow the capacitance transducers to be zeroed immediately before and, if necessary, during each run.

The chamber pressure was measured throughout the entire range of pressures by the following gages:

(1) A 0- to 775-torr (0- to 15-psia) strain gage transducer

(2) A 0- to 10.3-torr (0- to 0.2-psia) strain gage transducer

(3) A $10^{-3}$- to 1-torr thermocouple gage

(4) A $<10^{-3}$-torr nude ionization gage

The sublayer helium-purge flow rate was determined by utilizing choked flow through a jeweled orifice in conjunction with an upstream strain gage pressure transducer and a thermocouple to measure the helium gas temperature.

The liquid hydrogen boiloff from the measure tank, which was used to evaluate the thermal performance of each insulation system, was measured at ambient conditions by one of three mass flowmeters:

(1) A 0 to 85 standard cubic meter per hour (scmh) (0 to 3000 std $ft^3$/hr (scfh))

(2) A 0 to 2.8 scmh (0 to 100 scfh)

(3) A 0 to 0.28 scmh (0 to 10 scfh)

The flowmeters were calibrated at Lewis Research Center with gaseous hydrogen at standard conditions, with an estimated uncertainty of $\pm1/2$ percent over the expected flow rate.

# PROCEDURE

## Steady State

For the steady-state data points (noted in table I) between ground hold and space hold, the desired chamber pressures were obtained by a combination of pumping on the chamber and purging the chamber with either nitrogen or helium at a purge rate that matched the pumping rate. The purge rates were arrived at by a trial-and-error technique until the chamber remained at the desired pressure level. When the chamber was purged with nitrogen, the fiber glass sublayer was actively purged with gaseous helium to prevent any nitrogen gas from entering the sublayer and freezing. When the chamber was purged with helium, no active sublayer helium purge was utilized since the initial data were obtained at the lowest chamber pressure, and the gaseous helium could backflow into the sublayer as the chamber pressure was slowly increased to the next higher value.

To ensure that the liquid hydrogen was at saturated conditions during tests, the filling or retopping of the measure tank with liquid hydrogen was done at $1.4 \times 10^5$ $N/m^2$ (20 psia) or above. Once the measure tank was filled, the tank pressure was allowed to decay to the normal operating pressure as determined by the reference pressure of the back-pressure control system for measure-tank boiloff flow rates below 42.5 scmh (1500 scfh). When the measure-tank boiloff flow rate was above 42.5 scmh (1500 scfh), the tank pressure settled at a pressure somewhat higher than the nominal operating pressure because of the higher pressure differential required to flow the boiloff gas through the vent line, flowmeter, and control valve (which was fully open).

The insulation temperature profiles and the boiloff rate were monitored until steady conditions were reached. The experimental data were then recorded over a period of at least 30 minutes (longer as the measured heat flux decreased) to ensure that equilibrium thermal conditions actually had been reached.

## Transient Pumpdown

To set up the proper conditions for the initiation of a transient pumpdown or evacuation of the vacuum chamber, the chamber was first slowly pumped down to the $10^{-5}$-torr vacuum level and then slowly brought back to 1-atmosphere pressure by establishing the proper chamber and insulation system purges. The test tank was then filled with liquid hydrogen in the same manner as that noted for the steady-state tests. When steady-state ground-hold conditions were established, the test tank was topped off with liquid hydrogen. The transient pumpdown was not initiated until 20 to 30 minutes after the test tank had been topped off to ensure thermal equilibrium within the insulation

system. Hopefully, fully saturated liquid hydrogen within the test tank had been attained.

When the transient pumpdown was initiated, the chamber and sublayer purges were shut off, and the sublayer was allowed to vent through both the upper and lower helium purge manifolds (figs. 6 and 7) to a point just upstream of the control valves to the roughing pumps. The 8.5- and 24.1-cmm (300- and 850-cfm) roughing pumps were utilized to evacuate the chamber to a pressure of approximately $8\times10^{-2}$ torr at which time the oil diffusion pump was opened to the chamber and completed the transient pumpdown. For a rapid pumpdown, the transient chamber pressure decay rate between 1 atmosphere and approximately 1 torr was controlled by the control system and valves just upstream of the roughing pumps. The control valves to both roughing pumps generally became wide open at a chamber pressure of approximately 1 torr, and the chamber pumpdown rate beyond that point was dependent only on the pumping speed of the vacuum pumps and the manual operation of opening the oil diffusion pump to the chamber.

All data channels were recorded prior to and throughout the transient pumpdown of the chamber until steady-state equilibrium conditions had been reached. Data were recorded for a period of at least 30 minutes at steady-state space-hold conditions to ensure that the equilibrium condition had been achieved.

## DATA REDUCTION

The electrical output from most of the data channels could be converted directly to the parameters being measured. Appropriate correction factors were used to account for the difference between gaseous helium and nitrogen background when reading the thermocouple and ionization gages to determine chamber pressure.

The measured values of the multilayer insulation and sublayer interstitial pressure in the molecular flow and transition region were corrected for the time constant due to gaseous flow in a long tube, and for the temperature difference between the pressure transducer head and the end of the tube at which the pressure was being measured. A rough experimental evaluation of the time constant for a tubulated gage was made using a small vacuum chamber for which the transient pumpdown rate could be controlled manually and fairly closely matched to that of the Saturn V ascent pressure decay. A 2.54-meter (100-in.) long tube having a 0.95-centimeter (0.375-in.) outside diameter by 0.041-centimeter (0.016-in.) wall connected a capacitance-type pressure transducer to the vacuum chamber. The tube was flattened to a 0.64-centimeter (0.25-in.) thickness along its entire length. The experimental time constants for the tubulated capacitance gage were calculated assuming a first-order response to a step input

$$\tau = \frac{P_a - P_g}{\frac{dP_g}{dt}} \tag{1}$$

(All symbols are defined in appendix B.) The resulting time constants over a range of pressures in the transition and molecular flow regimes for both nitrogen and helium gas are noted in figures 10(a) and (b), respectively, when the tube was at either ambient temperature or liquid nitrogen temperature. The experimental values are compared with values calculated from equations presented in references 4 and 5 where the cross-sectional area of the flattened tube was equated to that of a circular tube and where the gas viscosity was assumed to be a function of both pressure and temperature as noted in references 6 and 7. The experimental data indicated somewhat longer time constants than predicted analytically, particularly at the lower pressures. The time-constant curves utilized for data reduction purposes for this investigation are noted. The experimentally determined time constants were themselves corrected analytically when applied to the data reported herein to account for variations in tube length and diameter of the actual interstitial pressure tubes (fig. 9) utilized for the transient pumpdown tests of the liquid hydrogen tank insulation.

A correction $R_p$ to the measured interstitial pressure was made due to the temperature difference between the pressure transducer head and the end of the tube at which the pressure was being measured. This correction was assumed to be a function of the temperature ratio $T_h/T_c$ and the Knudsen number Kn as noted in reference 4. The correction $R_p$ is shown in figure 11. It should be noted that in calculating the Knudsen number, the gas viscosity is assumed to be a function of temperature only and is evaluated at 1-atmosphere pressure.

The overall correction for the interstitial pressure is then

$$P_a = \left(P_g + \tau \frac{dP_g}{dt}\right) R_p \tag{2}$$

# RESULTS AND DISCUSSION

## Steady-State Data

A summary of all the test runs (in the order the data were obtained) for the three insulation systems is shown in table I. In general, tests were first conducted with each of the three insulation systems using gaseous nitrogen as the purge for the chamber and

multilayer insulation blankets and gaseous helium as the purge gas for the fiber glass sublayer. (The foam sublayer was not purged.) A rapid pumpdown of the chamber was then attempted and, in all cases, it was determined that a simulated Saturn V ascent pressure decay could not be obtained due to sublimation of frozen nitrogen somewhere on the test tank or within the vacuum chamber. Tests were then conducted utilizing gaseous helium as the purge gas in the multilayer insulation blankets as well as in the fiber glass sublayer so that rapid pumpdown tests could ultimately be achieved.

Gaseous-nitrogen-purged MLI blankets. - A comparison of the steady-state heat flux for the three insulation systems when the multilayer insulation blankets were purged with gaseous nitrogen is shown in figure 12. It was assumed, and generally validated experimentally, that during steady-state conditions, the MLI system interstitial pressure and chamber pressure were equal. At the space-hold conditions (chamber pressure $<10^{-4}$ torr), all insulation systems indicated approximately the same performance, namely, heat fluxes of 0.9 to 1.6 watts per square meter (0.3 to 0.5 Btu/(hr)(ft$^2$)). Using experimentally measured temperatures, the basic radiation component of the heat flux was calculated to be approximately 0.19 watt per square meter (0.06 Btu/(hr)(ft$^2$)), which represents only 12 to 20 percent of the total heat flux. The solid-conduction component and thermal degradation due to butt joints and nylon rod penetrations are then assumed to make up the remainder of the total heat flux.

The measured heat flux increased with an increase in chamber pressure due to the larger gaseous conduction component of heat transfer. In the transition between space-hold and ground-hold conditions, the steady-state data indicated that the measured heat flux is related to the interstitial gas pressure by an S-shaped curve, as previously noted by other investigators (e.g., ref. 8).

Under ground-hold conditions at approximately 760 torr, insulation system 1 had the highest heat flux, while insulation system 3 had the lowest. This would normally be expected since the overall thickness of system 1 was less than that of system 2, and since the foam is a more efficient ground-hold insulation (lower thermal conductivity) than the helium-purged fiber glass sublayer. The ground-hold heat flux obtained for system 2 (run 26 in table I) was 325 watts per square meter (103 Btu/(hr)(ft$^2$)); whereas the ground-hold conditions established prior to the attempted rapid pumpdown (run 27) indicated a heat flux of 200 watts per square meter (63.5 Btu/(hr)(ft$^2$)). These results emphasize the fact that repeatability is hard to achieve with these MLI systems. Based on the results obtained for systems 1 and 3, the value of 200 watts per square meter (63.5 Btu/(hr)(ft$^2$)) is a more reasonable value for ground-hold heat flux for system 2.

Gaseous-helium-purged MLI blankets. - A comparison of the steady-state heat flux for the three insulation systems when the multilayer insulation blankets were purged with gaseous helium is shown in figure 13 as a function of the chamber pressure. At the space-hold conditions (chamber pressure $<10^{-4}$ torr), all insulation systems indicated approximately the same performance, namely heat fluxes of 0.44 to 1.2 watts per

square meter (0.14 to 0.38 Btu/(hr)($ft^2$)), which was slightly better than shown previously for the nitrogen purge tests. However, the steady-state space-hold data point shown for insulation system 1 (aluminized Mylar/Dexiglas/fiber glass) was obtained immediately after a rapid pumpdown, which may have caused the insulation to "fluff" out somewhat and reduce the solid-conduction heat-transfer component.

In the transition region between space-hold and ground-hold conditions, the experimental data again indicated that the measured heat flux was related to the interstitial pressure by an S-shaped curve, as was previously noted and expected.

Under ground-hold conditions at approximately 760 torr, insulation system 1 again had the highest heat flux and system 3 the lowest; the heat flux for each insulation system was, of course, higher than for the gaseous-nitrogen-purged MLI blankets because of the higher thermal conductivity of the helium purge gas.

Ground-hold thermal performance. - The helium-purged fiber glass sublayer for insulation system 1 was intended to be of sufficient thickness (1.9 cm, or 0.75 in.) to provide a purge bag temperature of 78 K (140° R) or higher and allow the multilayer insulation blankets to be purged with gaseous nitrogen. This would then prevent freezing and/or condensation of nitrogen within the insulation system. The expected insulation system temperature profile using a hot-side boundary temperature of 247 K (445° R) from run 2 (table I) is shown in figure 14. This expected temperature profile was calculated using the average pretest-measured thickness of the sublayer and insulation blankets (table II) and the thermal conductivity of the purge gases at 1-atmosphere pressure. For these assumed conditions, the purge bag temperature should have been approximately 89 K (160° R), and the resultant heat flux should have been approximately 185 watts per square meter (58.7 Btu/(hr)($ft^2$)). However, the experimental results from run 2 (table I) indicated that the average purge bag temperature was 68 K (123° R) and that the measured heat flux was 264 watts per square meter (83.9 Btu/(hr)($ft^2$)). The most logical explanation is that the thicknesses of both the MLI blankets and sublayer decreased when liquid hydrogen was introduced into the test tank. An effective sublayer thickness of only 0.803 centimeter (0.316-in.) and an average blanket thickness of 0.330 centimeter (0.130 in.) were calculated (fig. 14) using the experimental temperature gradients. The calculated thickness of the sublayer from ground-hold test condition was slightly greater when the MLI blankets were purged with gaseous helium, as noted in table II (run 12). This may have been due, in part, to the higher temperature of the purge bag, which would have contracted somewhat less than when the MLI blankets had been purged with gaseous nitrogen.

The thermal contraction of the Aclar purge bag material has been experimentally determined to be about 1 percent when chilled from room temperature to liquid nitrogen temperature. This thermal contraction rate, when combined with the expected contraction (0.325 percent) of the copper test tank when chilled to liquid hydrogen temperature, would account for a reduction in the sublayer thickness of only about 0.28 centimeter

(0.11 in.) under ground-hold conditions. Reductions in the sublayer thickness greater than this value cannot be accounted for specifically.

Upon removal of the MLI panels for system 1 after completion of all thermal tests, the Aclar purge bag was found to be severely cracked and split over the entire surface. It is not known at what point in the thermal tests this occurred. Since there probably was a very slight positive pressure within the sublayer while it was actively purged, some helium purge gas may have leaked out into the nitrogen-purged MLI blankets and also contributed to the higher-than-expected heat flux and the lower-than-expected insulation temperatures.

Prior to the installation of the MLI blankets for system 2 on the test tank, the fiber glass sublayer had been modified as noted in figure 3 to provide (hopefully) for better control of its thickness and, hence, more predictable thermal performance. However, the control of the thickness of the helium-purged sublayer was still poor (or at least unpredictable), as indicated from runs 26 and 36 (table II). The best data for the ground-hold conditions occurred prior to the rapid pumpdown (run 27) for gaseous-nitrogen-purged MLI blankets and indicated a heat flux of 200 watts per square meter (63.5 Btu/(hr)(ft$^2$)). Even with this value and a purge bag temperature of 71 K (128$^\circ$ R), the calculated sublayer thickness was only 1.1 centimeters (0.45 in.). Upon removal of the MLI panels for insulation system 2 after all thermal tests were completed, the Mylar purge bag was found to be intact, with the exception of just one split approximately 25 centimeters (10 in.) long over the upper cold guard. The Mylar material, therefore, appears to be more suitable for the purge bag than the Aclar material.

The use of a helium-purged fiber glass mat sublayer in conjunction with nitrogen- or helium-purged multilayer insulation for ground-hold protection of liquid hydrogen tanks provided unpredictable thickness control. The result was poor thermal performance and freezing and/or condensation of nitrogen purge gas within the MLI panels. In order to reliably provide the purge bag temperature and/or heat flux required, the helium-purged fiber glass sublayer must be substantially overdesigned by increasing its nominal thickness (as also noted in ref. 1) with a resultant larger weight penalty.

The calculated thermal conductivity of the foam sublayer utilized for MLI system 3 is compared with previous data obtained for the identical foam formulation (ref. 3) in figure 15. The calculated thermal conductivity from the space-hold tests compares favorably with the previous data, while the calculated thermal conductivity from the ground-hold tests was somewhat higher. However, even though the foam sublayer ground-hold thermal performance was not as predictable as would have been desirable, the foam provided fewer problems once installed on the tank. The foam sublayer withstood all of the thermal cycles with virtually no structural damage; the one exception was one crack approximately 15 centimeters (6 in.) long found over the upper cold guard in a small area where the foam had not adhered to the tank wall. No cracks or splits were found in the vapor barrier.

Comparison of steady-state data with previous results. - The results of previous tests conducted with the aluminized Mylar/Dexiglas/fiber glass MLI system installed on a 2.10-meter (82.6-in.) diameter spherical tank (refs. 1 and 2) are summarized in table III. A comparison of these results with those obtained from this investigation (table I) again indicated that, for ground-hold conditions, the concept of a gaseous-helium-purged sublayer in conjunction with gaseous-nitrogen-purged MLI did not perform as expected. In all instances but one, the compression of the sublayer allowed a higher heat flux than expected, and the resulting purge bag temperatures were not high enough to prevent condensation or freezing of the gaseous nitrogen purge gas. The measured ground-hold heat fluxes were generally somewhat lower for the cylindrical calorimeter tests. This is most probably a result of the effort to provide an increased sublayer thickness, and the use of a cylindrical test tank on which the insulation system is more easily installed than on a spherical tank.

The measured space-hold thermal performance of this MLI system also indicated that somewhat better thermal performance was obtained on the cylindrical test tank than on the larger spherical test tank (0.95 $W/m^2$ (0.30 $Btu/(hr)(ft^2)$) compared to 1.4 and 1.2 $W/m^2$ (0.45 and 0.38 $Btu/(hr)(ft^2)$)). This is most likely due to (1) greater ease of installation, (2) less localized compression of MLI panels in the area of nylon rods and Teflon buttons, and (3) absence of thermal degradation of MLI due to penetration when this MLI system was installed on the cylindrical test tank.

## Transient Data

The original goal of this investigation was to obtain experimentally transient heat flux data for an aluminized Mylar/Dexiglas/fiber glass insulation system during a simulated Saturn V ascent pressure decay in the vacuum chamber. The insulation system, as originally conceived and tested (refs. 1 and 2), utilized a helium-purged sublayer and nitrogen-purged multilayer insulation for ground-hold conditions. However, attempts to rapidly pump the vacuum chamber down to near space-hold conditions were not successful when the chamber and multilayer insulation were purged with nitrogen. This was due to the nitrogen purge gas freezing either within the multilayer insulation system or on the test tank and/or vent lines. This problem persisted even though several attempts were made to seal the top and bottom of the test tank, as well as the vent lines, with foam. The result was that the sublimation of the frozen nitrogen would overpower the pumping system at chamber pressures less than 1 torr. Therefore, in order to obtain the desired transient data, a gaseous helium purge was utilized throughout the insulation systems (except for the foam sublayer) to achieve rapid pumpdown rates simulating the Saturn V ascent pressure decay. Experimental data from two of the

attempted pumpdowns utilizing a multilayer insulation nitrogen purge are included herein, however, for completeness.

Nitrogen-purged MLI pumpdown tests. - The aluminized Mylar/Dexiglas/fiber glass insulation system was initially subjected to a slow pumpdown to provide a transient checkout of the test facility and all control systems. The resulting pressure-against-time curves are shown in figure 16. The MLI and sublayer interstitial pressures closely matched the chamber pressure down to $10^{-1}$ torr; beyond this point, the MLI interstitial pressure and then the sublayer interstitial pressure lagged behind the chamber pressure. The lowest MLI interstitial pressure recorded was $9\times10^{-4}$ torr, which was attained 510 minutes after the initiation of the pumpdown. The resulting transient heat flux is shown in figure 17. The heat flux started at a value of 237 watts per square meter (75.3 Btu/(hr)(ft$^2$)) under ground-hold conditions, which compares to a value of 264 watts per square meter (83.9 Btu/(hr)(ft$^2$)) obtained for the previous steady-state data point (table I). The heat flux decreased as the chamber pressure decreased but never did reach the expected steady-state space-hold heat flux due to an apparent leak in the vacuum chamber and a rise in the chamber pressure beyond 534 minutes after initiation of the pumpdown. The final recorded transient heat flux prior to ending the test was 2.6 watts per square meter (0.82 Btu/(hr)(ft$^2$)), as compared to an expected space-hold heat flux of 0.949 watt per square meter (0.301 Btu/(hr)(ft$^2$)) noted in table I. During the transient pumpdown, the back-pressure control system then utilized (the first of the three systems tried) did not function correctly, and the measure-tank pressure dropped from 865.1 torr (16.73 psia) to 747.2 torr (14.45 psia) over the time period from 10 minutes to 95 minutes after the start of the pumpdown. No corrections were made to the instantaneous values of the measured boiloff during this time period, however, since the pressure drop occurred over such a long period of time and since the increased boiloff due to the decreasing tank pressure was small ($<$10 percent) when compared to that due to the heat flux through the insulation. The transient heat flux is plotted as a function of the multilayer interstitial pressure and compared to the steady-state heat flux data in figure 18. The transient data are plotted as a function of the multilayer interstitial pressure rather than the chamber pressure since this is more representative of the actual pressure within the insulation which is controlling the gaseous conduction component of heat transfer. The comparison of transient and steady-state data required the assumption that, during the transient pumpdown, the insulation is at a quasi-steady-state condition at each instant in time. The transient and steady-state data generally agree quite well down to at least $10^{-2}$ torr.

A rapid pumpdown test was attempted for each of the three insulation systems with the multilayer insulation panels purged with gaseous nitrogen. None of the tests, however, were successful in achieving a satisfactory chamber pressure decay rate. The resulting pressure decay rate within the chamber, MLI, and sublayer for the aluminized Mylar/silk net/fiber glass insulation system (typical for all systems tested) is shown in

figure 19. The chamber pressure decay provided a good simulation of a Saturn V ascent pressure decay only for the first $1\frac{1}{2}$ minutes of the pumpdown. Between $1\frac{1}{2}$ and 3 minutes, some difficulty was experienced with the chamber pressure controller which momentarily slowed the chamber pumpdown rate. Beyond 3 minutes after the initiation of the pumpdown, the chamber pressure decay rate was slowed up by the sublimation of frozen nitrogen, and a vacuum level of $1\times10^{-4}$ torr was not achieved in the chamber until approximately 200 minutes after the pumpdown had been initiated. The MLI interstitial pressure again tended to follow the chamber pressure curve throughout most of the pumpdown. The indication that the sublayer interstitial pressure decayed even faster than the chamber pressure may be a consequence of the sublayer vent lines being connected just upstream of the roughing pumps rather than directly into the chamber. The transient heat flux (noted in fig. 20) started at a ground-hold heat flux of 200 watts per square meter (63.5 Btu/(hr)($ft^2$)). The transient heat flux curve again showed the tendency to follow the MLI interstitial and chamber pressure decay curves. The last recorded space-hold heat flux was 2.5 watts per square meter (0.78 Btu/(hr)($ft^2$)), which was higher than the value of 1.6 watts per square meter (0.50 Btu/(hr)($ft^2$)) obtained during steady-state testing (table I, run 18). This was probably caused by a higher MLI interstitial pressure at the end of the transient test. During the transient pumpdown, the measure-tank back-pressure controller functioned properly and maintained the measure-tank pressure at 901.3±1.6 torr (17.42±0.03 psia). Therefore, no correction to the boiloff due to changes in measure-tank pressure need be considered. The transient heat flux as a function of the MLI interstitial pressure is compared to the steady-state data for this insulation system in figure 21. In this case, the transient data agreed very well with the steady-state data.

The average MLI temperature profiles within MLI systems 1 and 2 as recorded during the chamber pumpdown tests discussed previously are noted in table IV. Both the specific and average temperatures at some locations within the MLI tend to fluctuate with time and chamber pressure. The reason for this is not apparent. It may be due, in part, to sublimation of frozen nitrogen influencing the gaseous conduction and, therefore, the MLI temperature profiles, at varying times during the pumpdown. Or, it may be due to small pressure gradients, which were created by uneven venting of the interstitial purge gas, expanding or compressing the MLI panels in localized areas.

The data from these transient pumpdown tests of gaseous-nitrogen-purged MLI systems indicated that, for at least the vacuum chamber pumpdown rates achieved, there was close agreement between the transient and steady-state heat flux when plotted as a function of MLI interstitial pressure. Therefore, it may be said that, over all, a quasi-steady-state heat-transfer condition existed at each point in time during the transient pumpdown. In addition, the data indicated that the expected space-hold heat flux (as determined from steady-state tests) could not be achieved within a relatively

short period of time after the vacuum chamber had been pumped down to a pressure of $10^{-4}$ torr or less.

Helium-purged MLI pumpdown tests. - A good simulation of the Saturn V ascent pressure decay down to a chamber pressure of $10^{-1}$ torr (fig. 22) was achieved with the aluminized Mylar/Dexiglas/fiber glass MLI systems when a gaseous helium purge was utilized in the MLI as well as in the sublayer. The chamber reached a vacuum level of $1\times10^{-4}$ torr at 6.2 minutes after the pumpdown was initiated. The MLI interstitial pressure followed the chamber pressure curve down to $3\times10^{-2}$ torr and then lagged behind, as shown in the figure. The lowest MLI interstitial pressure recorded was $6.5\times10^{-4}$ torr at 102 minutes after initiation of the rapid pumpdown. The helium-purged sublayer appeared to pump down very rapidly. The indication that the sublayer pumped down faster than the chamber during the latter stages of the pumpdown was again most likely a result of connecting the sublayer vent line directly upstream of the roughing pumps.

The measured transient heat flux recorded during the rapid pumpdown is shown in figure 23. The initial ground-hold heat flux was 536 watts per square meter (170 Btu/(hr)(ft$^2$)) at the start of the test. The measured heat flux decayed rapidly during the pumpdown and attained a steady-state space-hold value of 0.44 watt per square meter (0.14 Btu/(hr)(ft$^2$)) at 110 minutes after initiation of the pumpdown. The space-hold heat flux was lower than that obtained during the steady-state tests conducted initially after purging the MLI with nitrogen (table I, run 9). This may be due to the very rapid venting of the sublayer plus the delayed venting of the MLI interstitial purge gas, which could have fluffed out the MLI somewhat (both radially inward as well as outward) and reduced the solid-conduction component of heat transfer. During the transient pumpdown (1 to 14 min), the back-pressure controller again did not function properly and the measure-tank pressure dropped from 1201 torr (23.23 psia) to 741.0 torr (14.33 psia). This time, a correction to the measured boiloff was required because of the relatively large pressure drop involved and the relatively short period of time in which the pressure drop occurred. The corrected heat flux is also shown in figure 23; the procedure used in making the correction is discussed in the following paragraph.

The measured transient heat flux as a function of the MLI interstitial pressure is compared with the steady-state data in figure 24. The measured transient heat flux was considerably higher than the steady-state heat flux over the pressure range from about 350 torr to $10^{-2}$ torr. This range represents the data obtained during the time interval of 1 to 14 minutes after the initiation of the pumpdown. This is the time interval during which the measure-tank pressure drop was noted. Normally, in order to make a correction for the measure-tank pressure drop, the amount of saturated liquid hydrogen in the measure tank at the start of the pumpdown would have to be accurately known. For these tests, however, suitable instrumentation within the measure tank had not been provided, and the amount of saturated liquid hydrogen in the measure tank was not accurately known because of the fill procedure and the amount of tank pressure rise

encountered while setting up the initial ground-hold conditions. However, the previous data had indicated that the curve of transient heat flux against MLI interstitial pressure should coincide with the steady-state data (figs. 18 and 21). Therefore, the measured liquid hydrogen boiloff was corrected by means of the following procedure.

The total boiloff gas flow rate, and hence the measured heat flux, included some quantity of boiloff gas resulting from the heat lost (reduction in saturation temperature) by the bulk of the liquid hydrogen contained within the measure tank. The actual heat transferred through the MLI system can be expressed as

$$Q_a = Q_m - m_{LH,\,s} C_s \frac{\Delta T_s}{\Delta t} \tag{3}$$

where the saturation temperature of the bulk of liquid hydrogen experienced a decrease of $\Delta T_s$ corresponding to the decrease in measure-tank pressure over a small time interval $\Delta t$. The mass of saturated liquid hydrogen within the measure tank at a particular point in time was initially determined by assuming that $Q_m$ was equal to a value $Q_{ss}$ determined from a previous steady-state test so that

$$m_{LH,\,s} = \left( \frac{Q_m - Q_{ss}}{C_s \, \Delta T_s} \right) \Delta t \tag{4}$$

For this case, $Q_{ss}$ was arbitrarily determined from run 16, where the chamber pressure was $9.0 \times 10^{-2}$ torr; and $Q_m$ was determined from the transient data at a point in time where the MLI interstitial pressure was approximately $8.7 \times 10^{-2}$ torr. The calculated mass of saturated liquid hydrogen (11.58 kg, or 25.52 lb) at that point in time was approximately 26 percent less than the total mass (saturated and subcooled) of liquid hydrogen (16.39 kg, or 36.13 lb) calculated to be in the measure tank by integrating the measured boiloff gas flow rate from the time at which the filling procedure had been completed. A new curve of saturated liquid hydrogen mass $m_{LH,\,s}$ was generated by integrating the measured boiloff gas flow rate both forward and backward in time from the point at which the MLI interstitial pressure was recorded. Other values of transient measured heat flux recorded while the measure tank pressure dropped were then corrected as follows:

$$\left( \frac{Q}{A} \right)_a = \frac{Q_m - m_{LH,\,s} C_s \dfrac{\Delta T_s}{\Delta t}}{A} \tag{5}$$

where $C_s$ and $\Delta T_s$ were determined by the curve of measure-tank pressure decay against time that had been recorded during the transient test. The three major assumptions for the procedure just described are as follows:

(1) A quasi-steady-state heat-transfer condition for the MLI system existed at each point in time during the transient test.

(2) The initial value of $Q_{ss}$ used is a true value.

(3) The mass of liquid hydrogen in the measure tank assumed to be subcooled (not at saturated conditions) remained constant with time.

The corrected heat flux data are also shown in figures 23 and 24. The corrected transient heat flux now agrees closely with the steady-state data over the entire pressure range for which the MLI pressure was recorded.

The aluminized Mylar/silk net/fiber glass insulation was subjected to the rapid pumpdown indicated by the chamber pressure curve in figure 25. The pumpdown curve provided a fairly good simulation of the Saturn V ascent pressure decay down to $3\times10^{-3}$ torr. However, the chamber did not achieve a pressure of $1\times10^{-4}$ torr until 48 minutes after the initiation of the pumpdown; this was most probably caused by a small leak in the chamber. The MLI interstitial pressure again followed the chamber pressure curve down to almost $10^{-2}$ torr and then lagged behind. The lowest recorded MLI interstitial pressure was $7.4\times10^{-3}$ torr at 17 minutes after the pumpdown had been initiated. From the data obtained, the MLI system utilizing the silk net spacer appears to vent slightly faster (more rapid pressure decay rate) than the system utilizing the Dexiglas spacers (for comparison see figs. 22 and 25). The measured transient heat flux is shown in figure 26. The initial ground-hold heat flux at the start of the test was 416 watts per square meter (132 Btu/(hr)($ft^2$)). The measured transient heat flux again decayed rapidly and attained a steady-state space-hold value of 0.44 watt per square meter (0.14 Btu/(hr)($ft^2$)) at 240 minutes after the initiation of the pumpdown. This is the same space-hold heat flux as obtained for insulation system 1 after the rapid pumpdown test. However, the space-hold heat flux was obtained much later, after the initiation of the pumpdown; this delay may be due, at least in part, to the slower chamber pumpdown rate at reduced pressures noted in this test. The back-pressure controller again did not function properly during the transient pumpdown (0 to 18 min) and the measure-tank pressure dropped from 1084.9 torr (20.98 psia) to 745.1 torr (14.41 psia). Therefore, the measured boiloff and heat flux were corrected in a manner similar to that described previously for MLI system 1. The measured transient heat flux is plotted as a function of the MLI pressure and compared with steady-state data in figure 27. Again the measured transient heat flux for MLI interstitial pressures above $10^{-2}$ torr was considerably higher than the steady-state data. Once corrected, however, the transient data showed good agreement with the steady-state data throughout the entire range of pressures for which transient data were obtained.

The aluminized Mylar/Dexiglas/foam insulation was subjected to a rapid chamber pressure decay, as shown in figure 28. The chamber pressure decay was a good simulation of the Saturn V ascent pressure decay to pressures less than $10^{-4}$ torr. Only a limited amount of data for the MLI interstitial pressure decay was obtained due to difficulty with the data recording system. However, the data indicate that the MLI interstitial pressure followed the chamber pressure decay curve closely into the $10^{-2}$-torr pressure range. The MLI vented slightly faster than the previous two insulation systems because of the higher MLI and purge gas temperatures occurring during the initial ground-hold condition. Calibration tests had also shown that rapid pumpdowns conducted with ambient-temperature gaseous helium or gaseous nitrogen (no liquid hydrogen in the test tank) in MLI systems 1 and 2 produced very rapid venting of the interstitial purge gases. MLI interstitial pressures in the low $10^{-4}$-torr region were achieved within 10 minutes after the initiation of the pumpdown. The gaseous helium also tended to provide a slightly faster venting rate than gaseous nitrogen.

The transient heat flux for MLI system 3 is shown in figure 29. The initial ground-hold heat flux was 237 watts per square meter (75.4 Btu/(hr)($ft^2$)) compared to 228 watts per square meter (72.3 Btu/(hr)($ft^2$)) obtained for the steady-state tests. MLI system 3 attained space-hold heat flux of 1.2 watts per square meter (0.37 Btu/(hr)($ft^2$)) 99 minutes after the initiation of the pumpdown, which compares to a steady-state space-hold heat flux of 1.2 watts per square meter (0.38 Btu/(hr)($ft^2$)). Apparently, the rapid chamber pressure decay did not fluff out the MLI panels because of the relatively firm foam sublayer, which prevented the radially inward movement of the MLI which the fiber glass sublayer could have allowed. For this test, the back-pressure controller functioned properly and maintained the measure-tank pressure at 900.3 ±5.2 torr (17.41±0.10 psia). Therefore, no correction to the measured boiloff and heat flux due to a variation in the measure-tank pressure was required. The transient heat flux, however, decayed more slowly (particularly during the early part of the pumpdown) than that noted for the first two MLI systems tested. In all probability, the energy given up by the foam sublayer and the inner layers of MLI as that portion of the insulation system chills down from its ground-hold temperature profile accounts for, at least, a considerable part of the measured transient heat input. An estimate of the heat lost by the foam was made by, first of all, calculating the temperature profiles through the foam sublayer corresponding to the ground hold (surface temperature, 240 K (432° R)) and to the space hold (surface temperature, 36 K (65° R)) using the faired thermal conductivity curve in figure 15. The only value for specific heat C of low-density foam insulation that could be located in the literature available was $1.2\times10^{-3}$ joule per kilogram per K (0.29 Btu/(lb)(°R)) at a temperature of 296 K (532° R) (ref. 9). Therefore, a linear specific-heat function $C = 4.05\times10^{-6}$ T (in K) ($C = 5.45\times10^{-4}$ T (in °R)), along with a density of 34.3 kilograms per cubic meter (2.14 lb/$ft^3$) (ref. 9), was assumed. Using the equation expressing the heat lost from the foam as $mC\,\Delta T$, the estimated value of heat

lost by the foam sublayer during the transient pumpdown was $4.18 \times 10^4$ joules per square meter (3.68 Btu/ft$^2$).

MLI system temperature profiles. - The temperature profiles recorded within all three insulation systems during the helium-purge rapid pumpdown tests are noted in table V. The temperatures at a given location tended to fluctuate much less with time than those noted for the tests where the MLI was purged with nitrogen.

Integrated heat flux. - The curves of corrected transient heat flux against time (figs. 23, 26, and 29) for the helium-purged MLI panels were integrated time-wise to determine the total heat input through the insulation system after any specified time until steady-state space-hold conditions were reached. The results are shown in figure 30. The aluminized Mylar/Dexiglas/fiber glass insulation system showed the highest integrated heat input during the early part of the pumpdown due to the high ground-hold heat flux. The aluminized Mylar/silk net/fiber glass showed a slightly slower increase in the initial heat input, but about the same total heat input at 150 minutes after initiation. This may be at least partially attributed to a somewhat slower chamber pressure decay rate at reduced pressures for the rapid pumpdown test for insulation system 2. The aluminized Mylar/Dexiglas/foam insulation system, although it had the lowest total heat input initially due to the low ground-hold heat flux, ended up with highest total heat input for any time greater than $6\frac{1}{2}$ minutes after the initiation of the pumpdown. However, at least $4.18 \times 10^4$ joules per square meter (3.68 Btu/ft$^2$) of the total heat input can be attributed to heat given up by the foam sublayer during the transient period. The heat given up by the foam sublayer could be significantly reduced by optimizing the foam sublayer thickness at the sacrifice of a slightly higher ground-hold heat flux.

A comparison of the actual (corrected) and ideal integrated heat input for the three insulation systems (MLI helium purged for ground-hold) is shown in table VI. The ideal integrated heat input assumes that the MLI interstitial pressure was at all times equal to the chamber pressure during the transient pumpdown. The curves of steady-state heat flux against chamber pressure were then utilized for time-wise integration of the heat flux. The comparison indicates that not too much is to be gained by attempting to improve the venting rates of MLI systems 1 and 2. The large difference between the actual and ideal heat inputs for MLI system 3 can be partially resolved by optimizing the foam sublayer thickness. Improvements in the total heat input might be achieved for all three MLI systems by utilizing a nitrogen purge within the MLI panels during the initial ground-hold conditions. However, an experimental demonstration requires a well-designed insulation and a test tank that can be adequately sealed to ensure that no freezing of the nitrogen purge gas will occur and that a rapid pumpdown can be achieved.

# CONCLUDING REMARKS

Both steady-state and transient heat flux data were obtained to determine the extent to which the total integrated heat input through three 30-layer multilayer insulation systems determined under simulated ascent pressure decay conditions differed from that predicted by using equivalent steady-state conditions. The multilayer insulation systems utilized (1) glass-fiber paper (Dexiglas) or silk netting as the spacer between the double-aluminized Mylar radiation shields, and (2) helium-purged fiber glass or sealed foam sublayers to reduce the ground-hold heat flux. Experimental data were obtained for each insulation system with the multilayer insulation panels purged with both gaseous nitrogen or gaseous helium. However, a simulated transient ascent pressure decay representative of a Saturn V launch could be achieved only when the MLI panels had been purged with gaseous helium.

The initial steady-state data indicated that the space-hold thermal performance of the three multilayer insulation systems was approximately the same (0.9 to 1.6 $W/m^2$, or 0.3 to 0.5 Btu/(hr)($ft^2$)). The transition between space-hold and ground-hold conditions was characterized by an S-shaped curve of heat flux as a function of interstitial pressure. The ground-hold data indicated that the MLI system utilizing a sublayer of polyurethane foam had a lower and more predictable ground-hold heat leak than those utilizing a gaseous-helium-purged fiber glass sublayer. Each MLI system showed an increase in the ground-hold heat flux when the MLI blankets were purged with gaseous helium rather than with gaseous nitrogen, as expected.

The values of thermal conductivity of the foam sublayer calculated from steady-state data were close to values observed from other tests conducted at the Lewis Research Center. The foam sublayer remained structurally intact throughout the test program. However, it was concluded that for MLI systems utilizing the gaseous-helium-purged fiber glass sublayer, the thickness of the sublayer could neither be maintained nor controlled to the desired value. This resulted in condensation and/or freezing of the gaseous nitrogen purge within the multilayer insulation, which is undesirable if the MLI blankets must vent rapidly to a low interstitial pressure. A more reliable concept could utilize either an optimized foam sublayer with either gaseous-nitrogen- or helium-purged multilayer insulation, or just a gaseous-helium-purged multilayer insulation without a sublayer.

The rapid pumpdown tests simulating the Saturn V ascent pressure decay (conducted with the multilayer insulation purged with gaseous helium) indicated that the interstitial pressure within the insulation blankets decayed rapidly down to less than the $10^{-2}$-torr pressure level. However, a considerably longer period of time (approx. 2 hr) was required for the interstitial pressure to drop to less than $10^{-3}$ torr. The interstitial pressure decay rate appeared to be a function of the purge gas temperature. Rapid pumpdown tests conducted with all components at ambient temperature (no liquid hydrogen in

the test tank) indicated that the interstitial pressure decayed into the low $10^{-4}$-torr region within less than 10 minutes after the pumpdown was initiated. Also the pressure decayed somewhat more rapidly when the multilayer insulation was purged with gaseous helium as compared to gaseous nitrogen.

The transient heat flux, starting from the initial ground-hold condition, decayed in a manner very similar to the interstitial pressure decay during the rapid pumpdown tests. The measured heat flux generally reached the steady-state space-hold values approximately 2 hours after the rapid pumpdown had been initiated. The steady-state space-hold heat leak measured after a rapid pumpdown for the two multilayer insulation systems utilizing a fiber glass sublayer was 0.44 watt per square meter (0.14 Btu/(hr)($ft^2$)), which apparently resulted from some fluffing out of the MLI caused by rapid venting of the interstitial purge gas. The total integrated heat flux for the first 150 minutes was also the same ($9.4\times10^4$ J/$m^2$, or 8.3 Btu/$ft^2$) for the two multilayer insulation systems utilizing the fiber glass sublayer. The idealized heat input (calculated from steady-state data and assuming the interstitial pressure decayed at the same rate as the Saturn V ascent pressure) was $7.4\times10^4$ and $7.7\times10^4$ joules per square meter (6.5 and 6.8 Btu/$ft^2$) for the aluminized Mylar/Dexiglas and aluminized Mylar/silk net MLI systems, respectively. The integrated measured heat flux for the MLI system utilizing the foam sublayer was $16.8\times10^4$ joules per square meter (14.8 Btu/$ft^2$), while the idealized value was calculated to be only $4.7\times10^4$ joules per square meter (4.1 Btu/$ft^2$). However, the foam sublayer was actually thicker than would have been required for an optimized insulation system, and the heat storage capacity of the foam under ground-hold conditions provided a sizable portion (rough calculation indicated at least $4.2\times10^4$ joules per square meter (3.7 Btu/$ft^2$)) of the total integreated measured heat flux.

Lewis Research Center,
National Aeronautics and Space Administration,
Cleveland, Ohio, April 1, 1971,
180-31.

# APPENDIX A

# ANALYTICAL PREDICTION OF INTERSTITIAL PRESSURE DECAY

As indicated in the main body of the report, the multilayer insulation panels were sized such that the point where maximum interstitial pressure occurs (center of panel) experiences nearly identical pressure decay rates as the corresponding point in a panel of the 2.10-meter (82.6-in.) diameter tank insulation system. For completeness, a description of the analytical program used for predicting pressure decay rates is included.

## Analytical Model

The analytical model utilized to predict the interstitial pressure decay within multilayer insulation has been discussed previously in references 1 and 10. The model assumes that the interstitial purge gas within the multilayer insulation during groundhold conditions is vented edgewise from each insulation panel during the ascent pressure decay. Interstitial gas flow in both the continuum, or viscous gas flow, regime and the free molecular regime is considered.

The continuum, or viscous gas flow, regime can be described by Darcy's classical relation for porous, one-dimensional flow (see fig. 31):

$$G_v = - \frac{k}{\mu} \frac{dP}{dx} \tag{A1}$$

If it is assumed that the gas flowing through the porous media is subject to the perfect-gas law, performing a mass balance on a differential control volume of length dx results in the following nonlinear differential equation:

$$P \frac{\partial^2 P}{\partial x^2} + \left(\frac{\partial P}{\partial x}\right)^2 = \frac{\mu}{k}\left(\frac{\partial P}{\partial t}\right) \tag{A2}$$

which is subject to the following boundary conditions:

$$P(L, t) = P_b(t)$$

$$P(x, 0) = P_i$$

$$\left(\frac{\partial P}{\partial x}\right)_{x=0} = 0$$

Transforming equation (A2) into a cylindrical coordinate system for two-dimensional flow within a multilayer insulation panel results in the following equation for describing the interstitial pressure decay:

$$\frac{\partial P}{\partial t} = \frac{Pk}{\mu}\left(\frac{1}{r^2}\frac{\partial^2 P}{\partial \theta^2} + \frac{\partial^2 P}{\partial z^2}\right) + \frac{k}{\mu}\left[\frac{1}{r^2}\left(\frac{\partial P}{\partial \theta}\right)^2 + \left(\frac{\partial P}{\partial z}\right)^2\right] + \frac{2Pkg}{\mu RT}\frac{\partial P}{\partial z} \tag{A3}$$

The two-dimensional flow equation for an oblate spheroidal coordinate system (used for both spherical and oblate spheroidal tank configurations) is

$$\frac{\partial P}{\partial t} = \frac{Pk}{\mu}\left\{\left(\frac{\cos^2\varphi}{a^2} + \frac{\sin^2\varphi}{b^2}\right)\frac{\partial^2 P}{\partial \varphi^2} + \frac{1}{a^2 \sin^2\varphi}\frac{\partial^2 P}{\partial \theta^2} + \left[\frac{1}{a^2}\cot\varphi + \left(\frac{1}{b^2} - \frac{1}{a^2}\right)\sin 2\varphi\right]\frac{\partial P}{\partial \varphi}\right\}$$

$$+ \frac{k}{\mu}\left[\left(\frac{\cos^2\varphi}{a^2} + \frac{\sin^2\varphi}{b^2}\right)\left(\frac{\partial P}{\partial \varphi}\right)^2 + \frac{1}{a^2 \sin^2\varphi}\left(\frac{\partial P}{\partial \theta}\right)^2\right] + \frac{2Pkg}{\mu RT}\left(-\frac{\sin\varphi}{b}\frac{\partial P}{\partial \varphi}\right) \tag{A4}$$

Gas flow in the free molecular regime is assumed to be a mass diffusion process which can be described by Fick's law as follows (one-dimensional flow):

$$G = -D\frac{d\rho}{dx} \tag{A5}$$

The transient equation is then obtained (using the perfect-gas law $\rho = P/RT$) in a manner similar to that for the viscous flow equation:

$$D\frac{\partial^2 P}{\partial x^2} + \eta RT = \frac{\partial P}{\partial t} \tag{A6}$$

The mass generation term $\eta RT$ (included in eq. (A6) to account for outgassing of the multilayer insulation materials at reduced pressures) can be written as

$$\eta RT = 9.835\times10^{-2}\,\frac{(1 - 2N)g}{X} \tag{A7}$$

for this program. The boundary conditions for equation (A6) are the same as those for equation (A2). Transforming equation (A6) into a cylindrical coordinate system for two-dimensional flow within a multilayer insulation panel results in the following equation for describing the interstitial pressure decay:

$$\frac{\partial P}{\partial t} = D\left(\frac{1}{r^2}\frac{\partial^2 P}{\partial \theta^2} + \frac{\partial^2 P}{\partial z^2}\right) + \eta RT \tag{A8}$$

The two-dimensional flow equation for an oblate spheroidal coordinate system is

$$\frac{\partial P}{\partial t} = D\left\{\left(\frac{\cos^2\varphi}{a^2} + \frac{\sin^2\varphi}{b^2}\right)\frac{\partial^2 P}{\partial \varphi^2} + \frac{1}{a^2\sin^2\varphi}\frac{\partial^2 P}{\partial \theta^2} + \left[\frac{1}{a^2}\cot\varphi + \left(\frac{1}{b^2} - \frac{1}{a^2}\right)\sin 2\varphi\right]\frac{\partial P}{\partial \varphi}\right\} + \eta RT \tag{A9}$$

The transition from continuum, or viscous, flow to free molecular flow within a multilayer insulation panel was assumed to occur between 10 torr and 0.1 torr (as indicated by ref. 11 for an aluminized Mylar/Dexiglas insulation system) in a smooth fashion as obtained from the following equation:

$$\%\ WC = 100 - \%\ WM = 100\left[1 - (2.25\,J - 1.5\,J^2 + 0.25\,J^3)\right] \tag{A10}$$

where $J = \log(100\,P)$. The transition region for the helium-purged sublayer was arbitrarily assumed to occur between 1000 torr and 10 torr; therefore, for equation (A10), $J = \log P$.

The experimental values of the permeability constant determined as a result of the investigation reported in reference 1 were utilized. A permeability constant of $8.4\times10^{-10}$ square meter ($9\times10^{-9}$ ft$^2$) was used for the fiber-glass sublayer and a permeability constant of $5.9\times10^{-9}$ square meter ($6.4\times10^{-8}$ ft$^2$) was used for the aluminized Mylar/Dexiglas multilayer insulation panels at a layer density of 28 layers per centimeter (70 layers/in.). The value of the permeability constant is dependent only on the porosity of the materials assumed and is independent of the interstitial purge gas and temperature.

The diffusion constant, which is dependent on the interstitial purge gas and temperature, was determined from experimental data presented in reference 1 and the following equation:

$$D = D_H\left(\frac{T}{T_H}\frac{M_H}{M}\right)^{1/2} = 0.00269\left(\frac{T}{M}\right)^{1/2} \qquad \text{(A11)}$$

Values for the diffusion constant determined in reference 1 were for an aluminized Mylar/Dexiglas multilayer insulation panel. Since no experimental data were available for the fiber glass sublayer, diffusion constants predicted by equation (A11) were utilized.

The computer program was written to calculate the pressure profile across a multilayer insulation panel or fiber glass sublayer at (1) a specified number of points between the no-flow boundary and the edge of the panel, and (2) a specified time increment throughout the assumed ascent-pressure-decay-against-time profile. The multilayer insulation panel configurations utilized in this program for both the cylindrical and spherical tank configurations are shown in figure 32. The analytical model actually considered only a quarter segment of the cylindrical panel and/or one-half of the spherical panel because of the symmetry of the flow pattern.

The analytical model assumes that the values of the permeability and diffusion constants used for the interstitial purge gas also applied to the gas generated within the multilayer insulation due to outgassing. This is an arbitrary assumption which may or may not be strictly valid.

## Analytical Results

A comparison of the interstitial pressure decay for the aluminized Mylar/Dexiglas multilayer insulation panels considered for both the 0.76-meter (2.50-ft) diameter cylindrical calorimeter and the 2.10-meter (6.88-ft) diameter spherical tank is shown in figure 33. The interstitial pressures shown are for the point at or near the center of each panel where the maximum interstitial pressure at any point in time was predicted to occur. The interstitial purge gas was assumed to be gaseous nitrogen at a temperature of 79.5 K (143$^{\circ}$ R), which represented an average temperature under ground-hold conditions at a point within the multilayer insulation panel where the experimental interstitial pressure measurements were made. The results indicated that, for the panel sizes considered, the interstitial pressure decay rate of the cylindrical tank MLI panel was very close to that of the MLI panel for the spherical tank. The MLI panels theoretically vent very rapidly during the ascent pressure decay for a zero outgassing rate. However, the interstitial pressures can remain high enough ($>10^{-4}$ torr) to affect the space-hold heat flux if the outgassing rate of the insulation material remains higher than $1.08\times10^{-6}$ torr-liter per square meter per second ($10^{-7}$ torr-liter/(ft$^2$)(sec)). The maximum pressure differential between the center and the edge of the MLI panel

analytically predicted was 0.28 torr for the spherical tank and 0.26 torr for the cylindrical tank; both occurred at 140 seconds into the ascent pressure decay.

The interstitial pressure profile across the width of the MLI panels in the plane of the maximum interstitial pressure (along the no-flow boundary) is shown in figure 34. The ambient or boundary pressure was $1.82\times10^{-6}$ torr, corresponding to 300 seconds of the assumed ascent pressure decay. The results indicate that the interstitial pressure was relatively constant across most of the width of the panel. This indicates that, for practical purposes in correlating experimentally measured heat flux with interstitial pressure, the interstitial pressure measured at the center of a cylindrical panel can be considered as the average panel pressure without creating unduly large errors. It should also be noted that the pressure profiles are nearly identical for the cylindrical and spherical MLI panels.

The interstitial pressure profile along the length of the MLI panels in the plane of the maximum interstitial pressure (along the no-flow boundary) is shown in figure 35. The ambient or boundary pressure is again $1.82\times10^{-6}$ torr. The interstitial pressure is lower near the top of the spherical MLI panel than near the bottom because of the shorter distance from the no-flow boundary to the edge of the panel. The pressure profile is still very similar to that predicted for the cylindrical MLI panel, which exhibited a relatively flat pressure profile except close to the edge of the panel.

As noted in the discussion of figure 33, multilayer insulation outgassing rates higher than $1.08\times10^{-6}$ torr-liter per square meter per second ($10^{-7}$ torr-liter/(ft$^2$)(sec)) would have been sufficient to maintain the interstitial pressure above $10^{-4}$ torr. This would adversely affect the space-hold thermal performance of the multilayer insulation by increasing the gaseous conduction component of the total heat transferred. Experimentally determined outgassing rates for three multilayer insulation materials (refs. 11 to 13) are noted in figure 36. These values were determined from transient, controlled pumpdown tests in small vacuum tanks. The ranges of absolute values of the outgassing rates are indicative of what can be expected. Since the outgassing rate would be expected to be a function of the ambient or vacuum tank pressure decay, however, the curves of outgassing rate as a function of time are questionable because the vacuum tank pumpdown may vary from one test to another and, also, is considerably different from the expected launch vehicle ascent pressure decay curve. The data presented indicate that for the multilayer insulation panels considered in this investigation, the outgassing rate should decay to $1.08\times10^{-6}$ torr-liter per square meter per second ($10^{-7}$ torr-liter/(ft$^2$)(sec)) within 15 hours after the launch (a conservative estimate).

The interstitial pressure decay for helium-purged multilayer insulation is compared with that for nitrogen-purged insulation for the cylindrical tank in figure 37. The helium gas temperature was assumed to be 147 K (265$^\circ$ R), which was the expected temperature of the insulation at the point where the interstitial pressure was experimentally measured. The analytical results indicate that the helium-purged MLI panels should vent

slightly more rapidly and achieve slightly lower pressures within a panel than nitrogen-purged MLI for the same outgassing rates. The maximum differential pressure across the helium-purged MLI panel was 0.44 torr and occurred at 130 seconds into the ascent pressure decay.

A comparison of the theoretical interstitial pressure decay within the helium-purged sublayer for the cylindrical and spherical tank configurations is shown in figure 38. The analytical model was altered to consider only one-dimensional flow for this case because, for each tank configuration, the purge gas was allowed to vent only from the top and bottom of the sublayer and not from the vertical edges. The gas temperature was assumed to be 49 K ($88^{\circ}$ R) and the outgassing rate was assumed to be zero. Even though the values of the diffusion constant and transition region were arbitrarily chosen, the analytical results indicate that the interstitial pressure decay for the sublayer on the cylindrical tank should be very close to that expected for the spherical tank.

# APPENDIX B

## SYMBOLS

| | |
|---|---|
| A | area of measure tank surface, $m^2$; $ft^2$ |
| a | major semi-axis of oblate spheroidal coordinate system, m; ft |
| b | minor semi-axis of oblate spheroidal coordinate system, m; ft |
| C | specific heat, J/(kg)(K); Btu/(lbm)($^oR$) |
| D | diffusion coefficient, $m^2$/sec; $ft^2$/sec |
| G | mass flow rate per unit cross-sectional area, kg/(sec)($m^2$); lbm/(sec)($ft^2$) |
| $G_v$ | volumetric flow rate per unit cross-sectional area, m/sec; ft/sec |
| g | gravitational constant, 9.8066 m/$sec^2$; 32.174 ft/$sec^2$ |
| J | log P or log(100 P) |
| Kn | Knudsen number, ratio of mean free path of gas to tube radius |
| k | permeability constant, $m^2$; $ft^2$ |
| L | total length of flowpath from no-flow boundary to edge of panel, m; ft |
| M | molecular weight, kg/mole; lbm/mole |
| m | mass, kg; lbm |
| N | number of radiation shields |
| P | pressure, torr or $N/m^2$; lbf/$ft^2$ or psia |
| Q | heat rate, W; Btu/hr |
| q | outgassing rate, torr-liter/($m^2$)(sec); torr-liter/($ft^2$)(sec) |
| R | gas constant, J/(K)(mole); ft-lbf/(lbm)($^oR$) |
| $R_p$ | pressure ratio, $P_c/P_h$ |
| r | radius of cylindrical MLI panel, m; ft |
| $r_o$ | radius of upper edge of MLI panel for oblate spheroidal coordinate system, m; ft |
| T | temperature, K; $^oR$ |
| t | time |
| WC | percent continuum flow |
| WM | percent molecular flow |
| X | thickness of MLI blanket, m; ft |

| | |
|---|---|
| x | distance from no-flow boundary, m; ft |
| z | height of cylindrical MLI panel from no-flow boundary, m; ft |
| $\eta$ | mass generation due to outgassing, $kg/(m^3)(sec)$; $lbm/(ft^3)(sec)$ |
| $\theta$ | angle in horizontal plane, rad; deg |
| $\mu$ | absolute viscosity, $N\text{-}sec/m^2$; $lbf\text{-}sec/ft^2$ |
| $\rho$ | density, $kg/m^3$; $lbm/ft^3$ |
| $\tau$ | time constant, sec |
| $\varphi$ | angle from vertical centerline of tank, rad; deg |

Subscripts:

| | |
|---|---|
| a | actual or corrected value |
| b | boundary condition at edge of panel |
| c | cold |
| g | tubulated gage |
| H | helium |
| h | hot |
| i | initial conditions |
| LH | liquid hydrogen |
| m | measured during transient conditions |
| s | saturated liquid conditions |
| ss | steady-state conditions |

# REFERENCES


1. Sterbentz, W. H.; and Baxter, J. W.: Thermal Protection System for a Cryogenic Spacecraft Propulsion Module. Rep. LMSC-A794993, Lockheed Missiles and Space Co. (NASA CR-54879), Nov. 15, 1966.

2. Dewitt, Richard L.; and Mellner, Max B.: Experimental Evaluation of a Purged Substrate Multilayer Insulation System for Liquid Hydrogen Tankage. NASA TN D-6331, 1971.

3. Sumner, Irving E.: Low-Density Foam for Insulating Liquid-Hydrogen Tanks. NASA TN D-5114, 1969.

4. Youngblood, W. W.; and Usher, L. H.: Feasibility Study of Vacuum Pressure Measurement Beneath and Within Battens of High Performance Insulation. Rep. HTL-TR-37, Heat Technology Lab., Inc. (NASA CR-82938), Jan. 18, 1967.

5. Hord, Jesse: Response of Pneumatic Pressure-Measurement Systems to a Step Input in the Free Molecule, Transition, and Continuum Flow Regimes. ISA Trans., vol. 6, no. 3, July 1967, pp. 252-260.

6. Johnson, Victor J., ed.: A Compendium of the Properties of Materials at Low Temperatures (Phase I). Part 1. Properties of Fluids. National Bureau of Standards (WADD TR 60-56, pt. 1), Oct. 1960.

7. Keesom, Willem H.: Helium. Elsevier Publ. Co., reprinted, 1959.

8. Glaser, Peter E.; Black, Igor A.; Lindstrom, Richard S.; Ruccia, Frank E.; and Wechsler, Alfred E.: Thermal Insulation Systems. NASA SP-5027, 1967.

9. Baer, Eric, ed.: Engineering Design for Plastics. Reinhold Publ. Corp., 1964.

10. Nast, T. C.; and Coston, R. M.: Investigation of the Gas Flow Within Multilayer Insulations and its Effect on Cryogenic Space Vehicle Design. Chem. Eng. Prog. Symp. Ser., vol. 62, no. 61, 1966, pp. 184-192.

11. Anon.: Investigation Regarding Development of a High-Performance Insulation System. Final Rep., Lockheed Missiles and Space Co., July 25, 1968. (Work done under Contract NAS 8-20758.)

12. Niendorf, L. R.; and Nies, G. E.: Investigation of a Lightweight Self-Evacuating Prefabricated Multi-Layer Insulation System for Cryogenic Space Propulsion Stages. Union Carbide Corp. (NASA CR-72017), July 15, 1966.

13. Coston, R. M.: A Study on High-Performance Insulation Thermal Design Criteria. Vol. 1. Rep. LMSC-A847882, vol. 1, Lockheed Missiles and Space Co. (NASA CR-87021), June 25, 1967.

TABLE I. - SUMMARY OF MULTILAYER INSULATION SYSTEM TESTS

| Run | MLI system | Sublayer gaseous helium purge rate | | MLI purge gas | Test conditions | Chamber pressure, torr | Measured heat flux | | Insulation temperature | | | | | | | | | |
|---|---|---|---|---|---|---|---|---|---|---|---|---|---|---|---|---|---|---|
| | | | | | | | | | Purge bag | | Inside inner blanket | | Outside inner blanket | | Outside intermediate blanket | | Outside outer blanket | |
| | | scmh | scfh | | | | $W/m^2$ | $Btu/(hr)(ft^2)$ | K | $^oR$ | K | $^oR$ | K | $^oR$ | K | $^oR$ | K | $^oR$ |
| 1 | 1 | 0.107 | 3.79 | $N_2$ | Steady state | 738 | 260 | 82.5 | --- | --- | --- | --- | --- | --- | --- | --- | --- | --- |
| 2 | | .111 | 3.92 | | | 744 | 264 | 83.9 | 68 | 123 | 77 | 139 | 156 | 280 | 214 | 386 | 247 | 445 |
| 3 | | .022 | .79 | | | 96.4 | 195 | 61.8 | 80 | 144 | 96 | 173 | 148 | 267 | 189 | 341 | 232 | 418 |
| 4 | | .0054 | .19 | | | 1.83 | 140 | 44.5 | 69 | 124 | 83 | 150 | 142 | 255 | 186 | 335 | 232 | 417 |
| 5 | | .0057 | .20 | | | 1.00 | 128 | 40.5 | 60 | 108 | 73 | 132 | 137 | 246 | 191 | 343 | 246 | 443 |
| 6 | | 0 | 0 | | | $2.1\times10^{-1}$ | 64.3 | 20.4 | 46 | 82 | 52 | 93 | 120 | 216 | 196 | 352 | 275 | 495 |
| 7 | | 0 | 0 | | | $4.0\times10^{-2}$ | 11.5 | 3.65 | 163 | 293 | 167 | 300 | 219 | 395 | 262 | 471 | 295 | 531 |
| 8 | | 0 | 0 | | | $2.6\times10^{-4}$ | 1.02 | .322 | 91 | 163 | 109 | 196 | 194 | 350 | 261 | 470 | 296 | 533 |
| 9 | | 0 | 0 | | | $6.2\times10^{-6}$ | .95 | .301 | 83 | 150 | 108 | 194 | 201 | 362 | 261 | 469 | 296 | 532 |
| 10 | | .113 | 4.0 | | Transient | -------- | ------ | ------ | --- | --- | --- | --- | --- | --- | --- | --- | --- | --- |
| 11 | | .113 | 4.0 | | Transient | -------- | ------ | ------ | --- | --- | --- | --- | --- | --- | --- | --- | --- | --- |
| 12 | | .113 | 4.0 | He | Steady state | 747 | 539 | 170 | 121 | 218 | 129 | 233 | 164 | 296 | 191 | 343 | 216 | 389 |
| 13 | | .113 | 4.0 | | Transient | -------- | ------ | ------- | --- | --- | --- | --- | --- | --- | --- | --- | --- | --- |
| 14 | | ----- | --- | | Steady state | $4.3\times10^{-6}$ | .44 | .14 | 37 | 67 | 51 | 91 | 113 | 203 | 238 | 429 | 293 | 528 |
| 15 | | ----- | --- | | | $7.1\times10^{-2}$ | 38.8 | 12.3 | 29 | 52 | 32 | 58 | 99 | 178 | 204 | 368 | 283 | 510 |
| 16 | | ----- | --- | | | $9.0\times10^{-2}$ | 47.6 | 15.1 | --- | --- | --- | --- | --- | --- | --- | --- | --- | --- |
| 17 | | ----- | --- | | | $2.2\times10^{-1}$ | 79.1 | 25.1 | 43 | 78 | 47 | 84 | 108 | 194 | 198 | 356 | 273 | 491 |
| 18 | 2 | 0 | 0 | $N_2$ | Steady state | $3.6\times10^{-5}$ | 1.57 | 0.499 | 56 | 100 | 78 | 140 | 203 | 365 | 268 | 483 | 297 | 535 |
| 19 | | 0 | 0 | | | $3.0\times10^{-4}$ | 2.45 | .777 | 90 | 162 | 104 | 187 | 203 | 365 | 255 | 459 | 296 | 533 |
| 20 | | .0008 | .03 | | | $1.8\times10^{-3}$ | 9.27 | 2.94 | 183 | 330 | 185 | 333 | 212 | 382 | 253 | 456 | 290 | 522 |
| 21 | | .0014 | .05 | | | $1.3\times10^{-2}$ | 12.5 | 3.96 | 203 | 366 | 206 | 370 | 234 | 421 | 263 | 473 | 292 | 526 |
| 22 | | .0028 | .10 | | | $9.4\times10^{-2}$ | 38.8 | 12.3 | 184 | 332 | 188 | 339 | 219 | 394 | 254 | 457 | 286 | 515 |
| 23 | | .0057 | .20 | | | $9.2\times10^{-1}$ | 187 | 59.3 | 96 | 172 | 103 | 186 | 143 | 258 | 190 | 342 | 233 | 420 |
| 24 | | .0156 | .55 | | | 9.93 | 157 | 49.9 | 82 | 147 | 94 | 169 | 144 | 259 | 197 | 354 | 241 | 433 |
| 25 | | .042 | 1.50 | | | 99.6 | 158 | 50.0 | 58 | 104 | 65 | 117 | 128 | 231 | 192 | 346 | 249 | 449 |
| 26 | | .149 | 5.25 | | | 738 | 325 | 103 | 59 | 107 | 64 | 115 | 110 | 198 | 193 | 348 | 255 | 459 |
| 27 | | .297 | 10.5 | | Transient | -------- | ------- | ------- | --- | --- | --- | --- | --- | --- | --- | --- | --- | --- |
| 28 | | ------ | ----- | He | Steady state | $2.9\times10^{-6}$ | 0.835 | 0.265 | 63 | 114 | 77 | 138 | 155 | 279 | 217 | 390 | 293 | 527 |
| 29 | | ------ | ----- | | | $4.0\times10^{-4}$ | 1.90 | .604 | 76 | 136 | 86 | 155 | 157 | 283 | 211 | 380 | 296 | 532 |
| 30 | | ------ | ----- | | | $2.3\times10^{-3}$ | 3.85 | 1.22 | 64 | 116 | 71 | 128 | 157 | 282 | 231 | 415 | 296 | 533 |
| 31 | | ------ | ----- | | | $1.1\times10^{-2}$ | 31.1 | 9.85 | 51 | 92 | 57 | 103 | 121 | 217 | 200 | 360 | 285 | 513 |
| 32 | | ------ | ----- | | | $1.1\times10^{-1}$ | 94.3 | 29.9 | 72 | 129 | 79 | 143 | 131 | 236 | 198 | 356 | 269 | 485 |
| 33 | | ------ | ----- | | | 1.02 | 243 | 77.2 | 113 | 204 | 120 | 216 | 152 | 274 | 189 | 340 | 226 | 407 |
| 34 | | ------ | ----- | | | 9.98 | 297 | 94.2 | 126 | 226 | 130 | 234 | 151 | 272 | 177 | 319 | 198 | 356 |
| 35 | | ------ | ----- | | | 99.5 | 350 | 111 | 139 | 251 | 144 | 259 | 166 | 298 | 191 | 343 | 214 | 385 |
| 36 | | ------ | ----- | | | 751 | 363 | 115 | 149 | 268 | 156 | 281 | 181 | 325 | 210 | 378 | 236 | 424 |
| 37 | | .297 | 10.5 | | Transient | -------- | ------- | ------- | --- | --- | --- | --- | --- | --- | --- | --- | --- | --- |
| 38 | 3 | ------ | ----- | $N_2$ | Steady state | 752 | 173 | 55.0 | 177 | 319 | 186 | 334 | 211 | 380 | 248 | 447 | 264 | 475 |
| 39 | | ------ | ----- | $N_2$ | Transient | -------- | ------- | ------- | --- | --- | --- | --- | --- | --- | --- | --- | --- | --- |
| 40 | | ------ | ----- | $N_2$ | Steady state | $1.2\times10^{-3}$ | 1.36 | .432 | 38 | 68 | 72 | 130 | 176 | 317 | 259 | 467 | 299 | 538 |
| 41 | | ------ | ----- | He | Steady state | $3.7\times10^{-5}$ | 1.19 | 0.378 | 63 | 113 | 77 | 138 | 188 | 338 | 259 | 467 | 301 | 541 |
| 42 | | ------ | ----- | | | $1.1\times10^{-3}$ | 2.33 | .740 | 49 | 88 | 82 | 147 | 127 | 228 | 218 | 392 | 297 | 534 |
| 43 | | ------ | ----- | | | $1.3\times10^{-2}$ | 10.9 | 3.47 | --- | --- | --- | --- | 107 | 192 | 203 | 365 | 290 | 522 |
| 44 | | ------ | ----- | | | 1.03 | 126 | 40.1 | 148 | 267 | 148 | 266 | 182 | 328 | 238 | 429 | 265 | 477 |
| 45 | | ------ | ----- | | | 103 | 214 | 68.0 | 216 | 389 | 217 | 391 | 224 | 404 | 241 | 433 | 248 | 447 |
| 46 | | ------ | ----- | | | 746 | 228 | 72.3 | 236 | 425 | 240 | 432 | 246 | 442 | 259 | 466 | 266 | 479 |
| 47 | | ------ | ----- | | Transient | -------- | ------- | ------- | --- | --- | --- | --- | --- | --- | --- | --- | --- | --- |

TABLE II. - SUMMARY OF MULTILAYER INSULATION SYSTEM THICKNESS

| MLI system | Ground-hold test | Average measured MLI blanket thickness | | Thickness based on ground-hold tests | | | | | | | | | |
|---|---|---|---|---|---|---|---|---|---|---|---|---|---|
| | | | | Sublayer | | Inner blanket | | Intermediate blanket | | Outer blanket | | Average blanket | |
| | | cm | in. | cm | in. | cm | in. | cm | in. | cm | in. | cm | in. |
| 1 | 2 | 0.462 | 0.182 | 0.803 | 0.316 | 0.339 | 0.133 | 0.391 | 0.154 | 0.259 | 0.102 | 0.330 | 0.130 |
| | 12 | .462 | .182 | 1.080 | .425 | .620 | .244 | .523 | .206 | .572 | .225 | .574 | .226 |
| 2 | 26 | 0.635 | 0.250 | 0.493 | 0.194 | 0.177 | 0.046 | 0.381 | 0.150 | 0.335 | 0.132 | 0.279 | 0.110 |
| | 36 | .635 | .250 | 2.330 | .917 | .701 | .276 | .945 | .372 | .874 | .344 | .838 | .330 |
| 3 | 38 | 0.462 | 0.182 | ----- | ----- | 0.274 | 0.108 | 0.445 | 0.179 | 0.206 | 0.081 | 0.312 | 0.123 |
| | 46 | .462 | .182 | ----- | ----- | .218 | .086 | .805 | .317 | .376 | .148 | .467 | .184 |

TABLE III. - SUMMARY OF PREVIOUS TEST DATA OBTAINED WITH ALUMINIZED MYLAR/DEXIGLAS/FIBER GLASS MLI SYSTEM

[Tank diameter, 2.10 m (82.6 in.).]

| Test type | Reference | Chamber wall temperature | | MLI purge gas | Heat flux | | Temperature profile location on tank | MLI temperature profile | | | | | | | |
|---|---|---|---|---|---|---|---|---|---|---|---|---|---|---|---|
| | | | | | | | | Purge bag | | Outside inner blanket | | Outside intermediate blanket | | Outside outer blanket | |
| | | K | $^{o}R$ | | $W/m^2$ | $Btu/(hr)(ft^2)$ | | K | $^{o}R$ | K | $^{o}R$ | K | $^{o}R$ | K | $^{o}R$ |
| Ground hold | 1 | Ambient | | $N_2$ | 410 | 130 | Top | 79 | 142 | 133 | 240 | 179 | 323 | 233 | 419 |
| | | | | | | | Bottom | 59 | 106 | 118 | 213 | 170 | 306 | 215 | 387 |
| | 2 | 265 | 477 | $N_2$ | 372 | 118 | Top | 75 | 135 | 113 | 203 | 151 | 271 | 197 | 355 |
| | | | | | | | Bottom | 51 | 91 | 111 | 200 | 186 | 335 | 233 | 419 |
| | | 271 | 487 | $N_2$ | 504 | 160 | Top | 71 | 128 | 111 | 200 | 159 | 286 | 212 | 382 |
| | | | | | | | Bottom | 50 | 90 | 88 | 158 | 193 | 347 | 240 | 432 |
| | | 285 | 513 | He | 630 | 200 | ------ | --- | --- | --- | --- | --- | --- | --- | --- |
| Space hold | 1 | 222 | 400 | -- | 1.4 | 0.45 | Top | 72 | 130 | 137 | 246 | 164 | 296 | 209 | 376 |
| | | | | | | | Bottom | 47 | 85 | 110 | 198 | 167 | 300 | 218 | 392 |
| | 2 | 283 | 509 | -- | 1.2 | 0.38 | Top | 66 | 119 | 181 | 325 | 244 | 439 | 281 | 505 |
| | | | | | | | Bottom | 57 | 102 | 184 | 331 | 238 | 429 | 281 | 505 |

TABLE IV. - GASEOUS-NITROGEN-PURGED MLI SYSTEM AVERAGE TEMPERATURE PROFILES

DURING PUMPDOWN TESTS

| MLI system | Purge gas (sublayer / MLI) | Time, min | Chamber pressure, torr | MLI temperature profile | | | | | | | | | |
|---|---|---|---|---|---|---|---|---|---|---|---|---|---|
| | | | | Purge bag | | Inside inner blanket | | Outside inner blanket | | Outside intermediate blanket | | Outside outer blanket | |
| | | | | K | °R | K | °R | K | °R | K | °R | K | °R |
| 1 (run 10) | $He/N_2$ | 0 | 745 | 68 | 122 | 80 | 144 | 152 | 273 | 214 | 386 | 251 | 451 |
| | | 30 | 199 | 81 | 145 | 89 | 161 | 154 | 277 | 208 | 374 | 241 | 434 |
| | | 60 | 4.50 | 67 | 120 | 84 | 152 | 160 | 288 | 214 | 385 | 251 | 452 |
| | | 90 | $7.0\times10^{-2}$ | 39 | 71 | 51 | 91 | 126 | 227 | 195 | 351 | 266 | 478 |
| | | 115 | $4.0\times10^{-3}$ | 89 | 161 | 94 | 170 | 134 | 242 | 185 | 333 | 281 | 505 |
| | | 150 | $1.4\times10^{-4}$ | 118 | 212 | 120 | 216 | 149 | 268 | 198 | 356 | 283 | 509 |
| | | 180 | $1.8\times10^{-5}$ | 122 | 219 | 124 | 223 | 146 | 262 | 191 | 343 | 283 | 510 |
| | | 210 | ↓ | 118 | 212 | 119 | 215 | 143 | 258 | 184 | 331 | 286 | 514 |
| | | 270 | ↓ | 114 | 206 | ↓ | 214 | 137 | 247 | 191 | 344 | 286 | 515 |
| | | 330 | ↓ | 119 | 214 | ↓ | 215 | 144 | 259 | 197 | 355 | 287 | 517 |
| | | 390 | ↓ | 117 | 210 | ↓ | 214 | 152 | 274 | 207 | 372 | 286 | 515 |
| | | 450 | ↓ | 114 | 205 | 116 | 208 | 152 | 273 | 221 | 398 | 281 | 506 |
| | | 510 | ↓ | 114 | 206 | 118 | 213 | 183 | 330 | 234 | 421 | 284 | 512 |
| 2 (run 27) | $He/N_2$ | 0 | 725 | 71 | 128 | 82 | 147 | 141 | 254 | 211 | 379 | 256 | 461 |
| | | 3 | 13.2 | 92 | 166 | 100 | 180 | 138 | 248 | 187 | 336 | 222 | 399 |
| | | 10 | 1.10 | 76 | 137 | 79 | 142 | 134 | 242 | 212 | 382 | 237 | 427 |
| | | 64 | $1.3\times10^{-1}$ | 85 | 153 | 98 | 176 | 133 | 240 | 204 | 368 | 266 | 478 |
| | | 244 | $<10^{4}$ | 124 | 224 | 130 | 234 | 181 | 325 | 241 | 433 | 290 | 522 |

TABLE V. - GASEOUS-HELIUM-PURGED MLI SYSTEM AVERAGE TEMPERATURE

PROFILES DURING PUMPDOWN TESTS

| MLI system | Purge gas (sublayer / MLI) | Time, min | Chamber pressure, torr | MLI temperature profile | | | | | | | | | |
|---|---|---|---|---|---|---|---|---|---|---|---|---|---|
| | | | | Purge bag | | Inside inner blanket | | Outside inner blanket | | Outside intermediate blanket | | Outside outer blanket | |
| | | | | K | °R | K | °R | K | °R | K | °R | K | °R |
| 1 (run 13) | He He | 0 | 748 | 121 | 218 | 129 | 233 | 164 | 296 | 191 | 343 | 217 | 390 |
| | | 1.3 | 33.1 | 112 | 202 | 118 | 213 | 142 | 255 | 171 | 307 | 199 | 359 |
| | | 2.8 | $3.7\times10^{-1}$ | 91 | 163 | 94 | 169 | 138 | 248 | 177 | 318 | 208 | 375 |
| | | 5 | $3.6\times10^{-2}$ | 44 | 79 | 47 | 85 | 124 | 224 | 183 | 329 | 231 | 416 |
| | | 9 | $2.1\times10^{-5}$ | 22 | 40 | 25 | 45 | 118 | 212 | 186 | 334 | 233 | 419 |
| | | 28 | $9.3\times10^{-6}$ | 23 | 41 | 32 | 57 | 108 | 194 | 189 | 341 | 263 | 474 |
| | | 162 | 4.3 | 37 | 67 | 51 | 91 | 113 | 203 | 238 | 429 | 293 | 528 |
| 2 (run 37) | He He | 0 | 728 | 147 | 265 | 150 | 270 | 167 | 301 | 205 | 369 | 223 | 401 |
| | | 3 | $2.5\times10^{-1}$ | 79 | 142 | 92 | 165 | 149 | 269 | 196 | 353 | 244 | 440 |
| | | 6 | $1.2\times10^{-3}$ | 46 | 83 | 54 | 98 | 137 | 247 | 194 | 349 | 246 | 443 |
| | | 13 | $3.6\times10^{-4}$ | 31 | 56 | 49 | 88 | 135 | 243 | 197 | 355 | 256 | 460 |
| | | 20 | 2.2 | 33 | 60 | 42 | 75 | 132 | 237 | 199 | 359 | 263 | 474 |
| | | 31 | 1.8 | 20 | 36 | 29 | 53 | 121 | 217 | 184 | 331 | 271 | 487 |
| | | 40.5 | 1.2 | 25 | 45 | 34 | 61 | 120 | 216 | 202 | 363 | 279 | 502 |
| | | 51 | $9.5\times10^{-5}$ | 38 | 68 | 45 | 81 | 123 | 221 | 207 | 372 | 287 | 516 |
| 3 (run 47) | --- He | 0 | 794 | 240 | 432 | 245 | 441 | 246 | 443 | 262 | 471 | 267 | 481 |
| | | 5.5 | $6\times10^{-5}$ | 208 | 375 | 219 | 395 | 236 | 424 | 254 | 458 | 275 | 495 |
| | | 9.5 | ↓ | 156 | 280 | 185 | 333 | 238 | 429 | 258 | 464 | 282 | 507 |
| | | 16 | | 91 | 163 | 141 | 253 | 237 | 426 | 258 | 465 | 287 | 516 |
| | | 23 | | 53 | 96 | 113 | 204 | 234 | 421 | 257 | 463 | 288 | 519 |
| | | 42 | | 59 | 107 | 93 | 167 | 233 | 420 | 263 | 473 | 298 | 537 |
| | | 272 | | 36 | 65 | 82 | 148 | 201 | 362 | 263 | 473 | 301 | 541 |

TABLE VI. - COMPARISON OF ACTUAL AND IDEALIZED INTEGRATED HEAT FLUX FOR HELIUM-PURGED MLI

[Time, 0 to 150 min.]

| MLI system | Total heat input | | | |
|---|---|---|---|---|
| | Actual (corrected) | | Ideal | |
| | $J/m^2$ | $Btu/ft^2$ | $J/m^2$ | $Btu/ft^2$ |
| 1 | $9.4\times10^4$ | 8.3 | $7.4\times10^4$ | 6.5 |
| 2 | 9.4 | 8.3 | 7.7 | 6.8 |
| 3 | 16.8 | 14.8 | 4.7 | 4.1 |

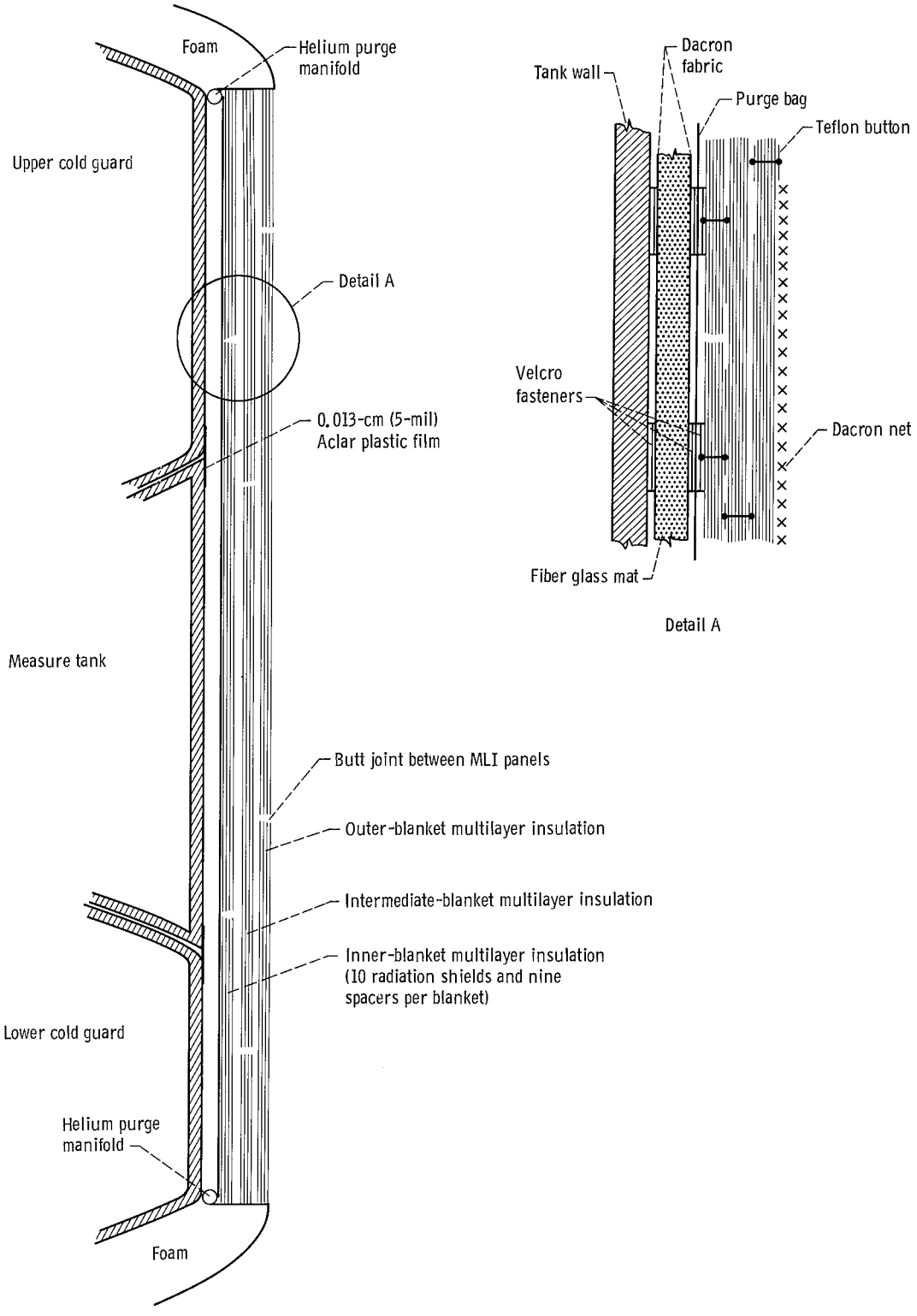


Figure 1. - Installation of multilayer insulation (MLI) system on cylindrical calorimeter.

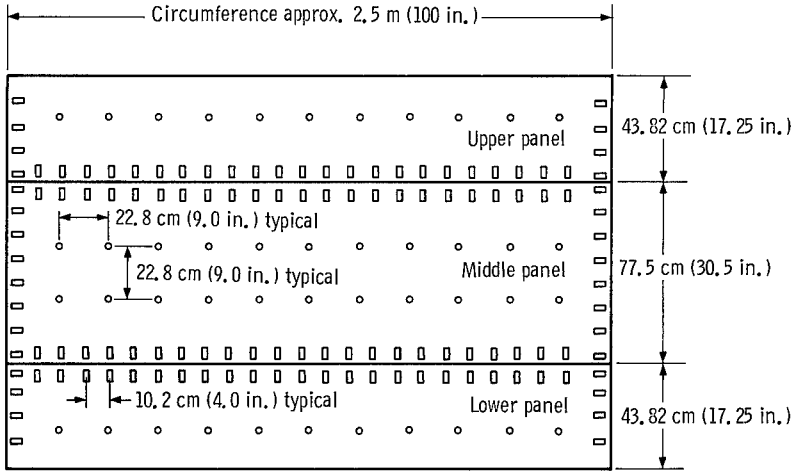


(a) Inner blanket.

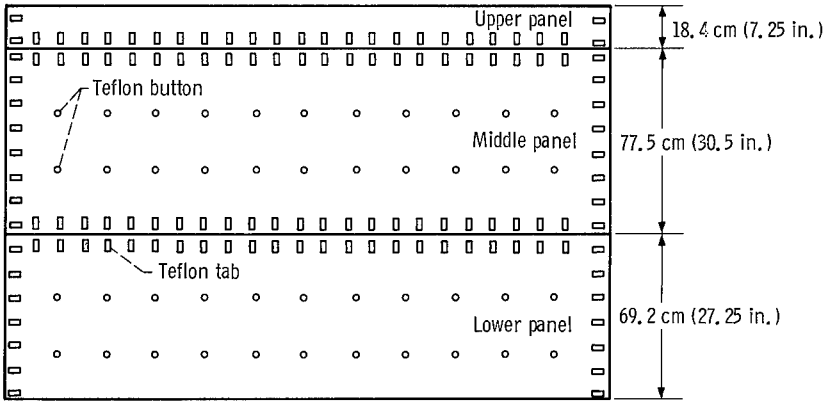


(b) Intermediate blanket.

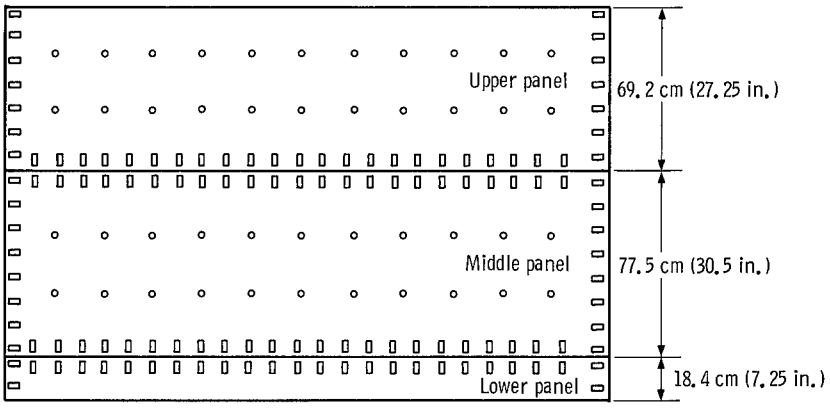


(c) Outer blanket.

Figure 2. - Multilayer insulation blanket configuration.

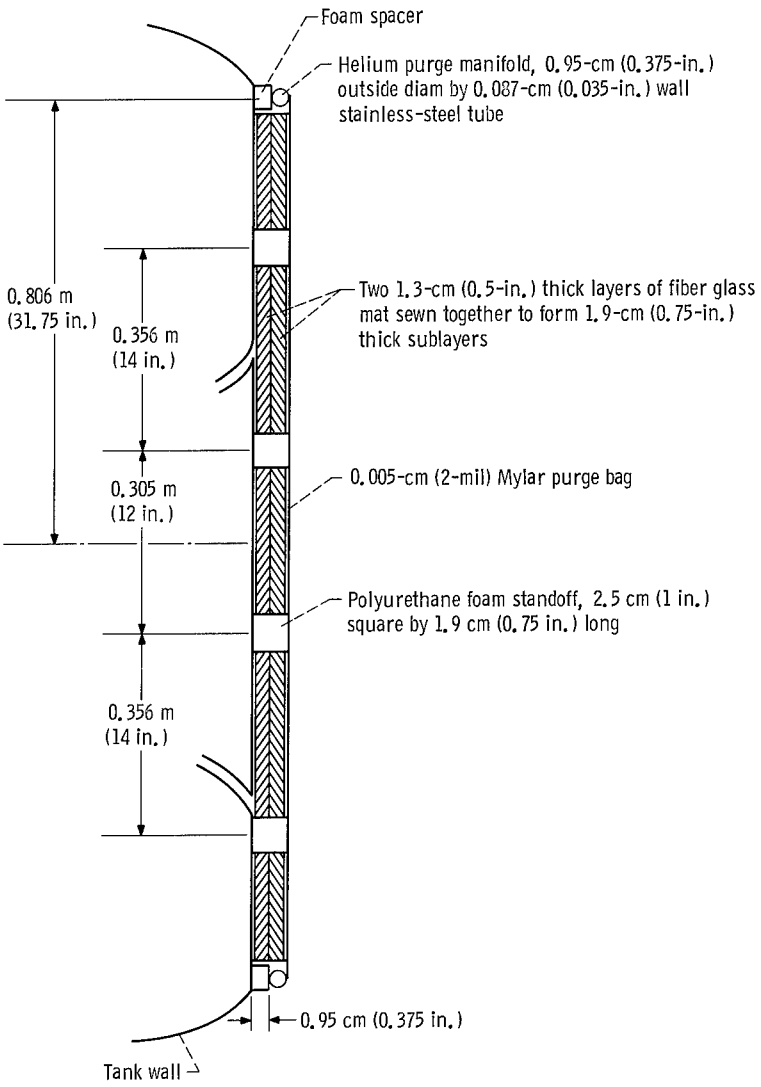


Figure 3. - Modifications to fiber glass sublayer for multilayer insulation system 2.

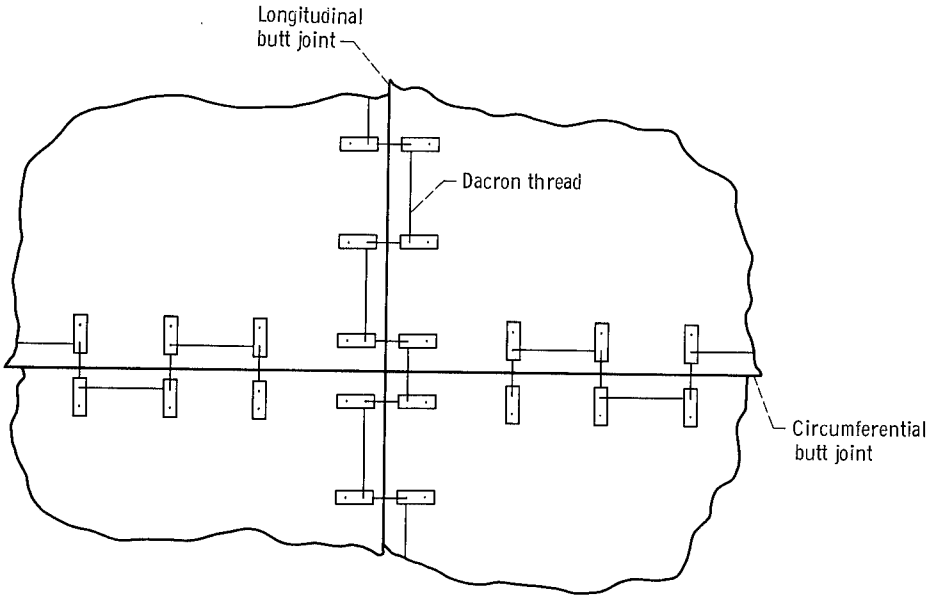


(a) Typical of lacing panels into blanket assembly.

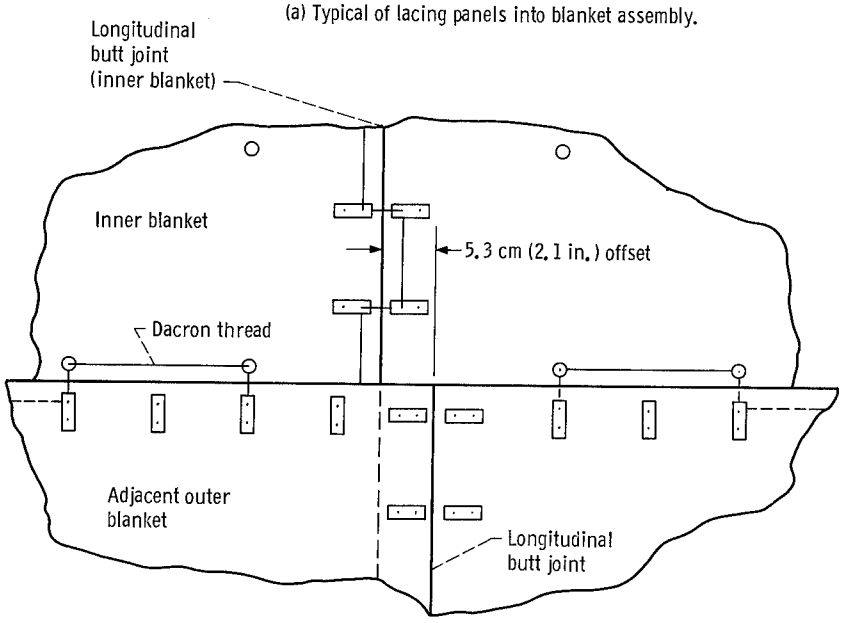


(b) Typical of lacing of one panel on adjacent inner blanket.

Figure 4. - Typical lacing for blanket assembly and installation.

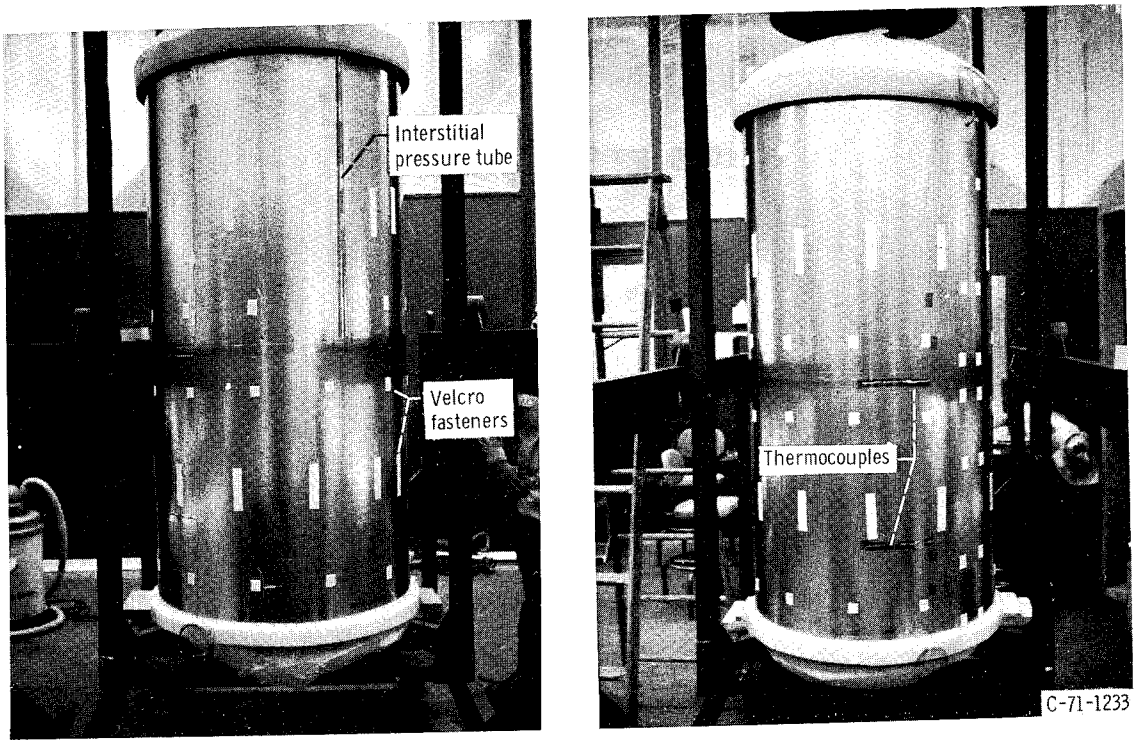


(a) Front view.

(b) Back view.

Figure 5. - Completed foam sublayer installed on cylindrical calorimeter.

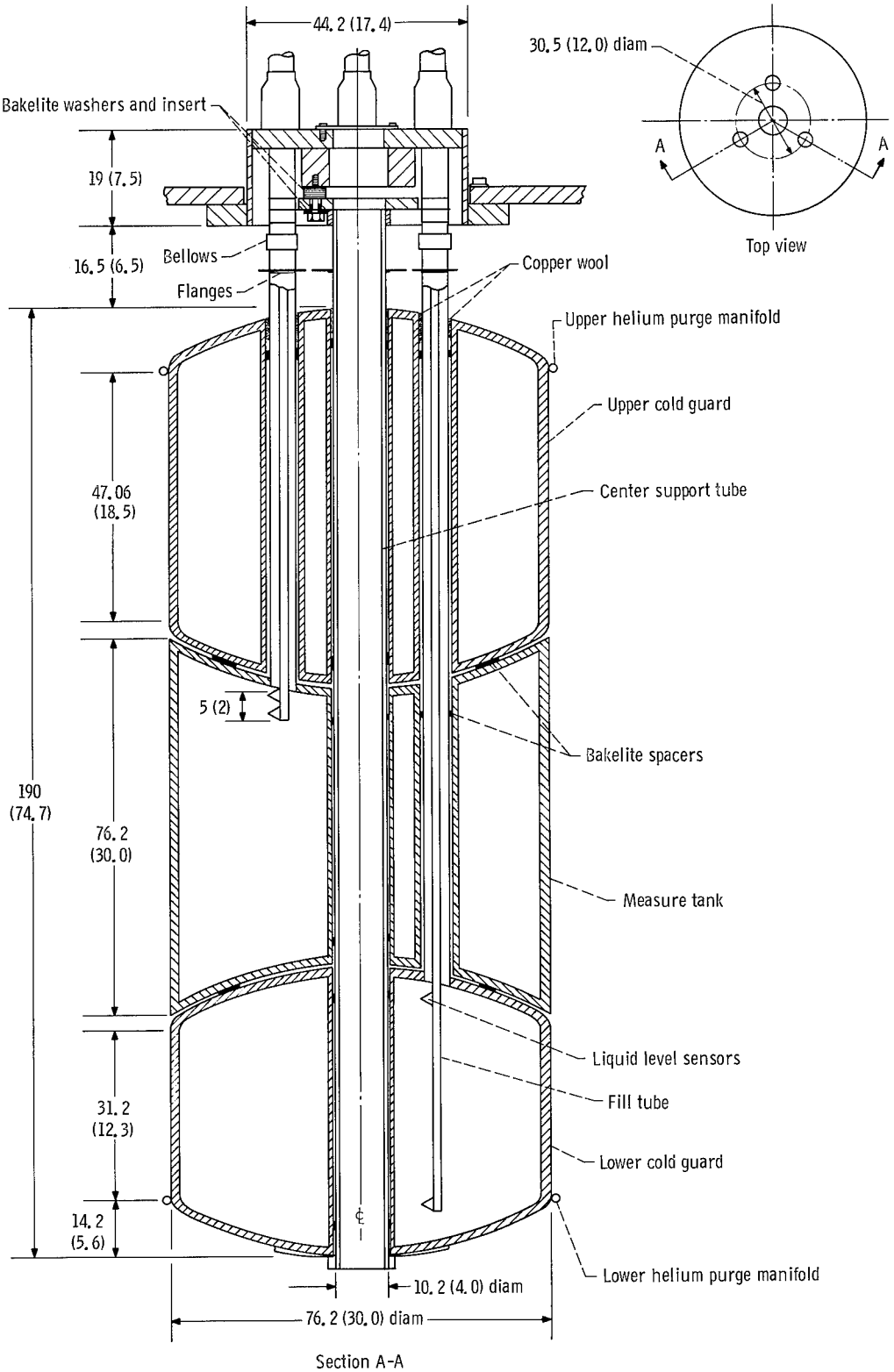


Figure 6. - Double-guarded cylindrical calorimeter. Dimensions are in centimeters (in.).

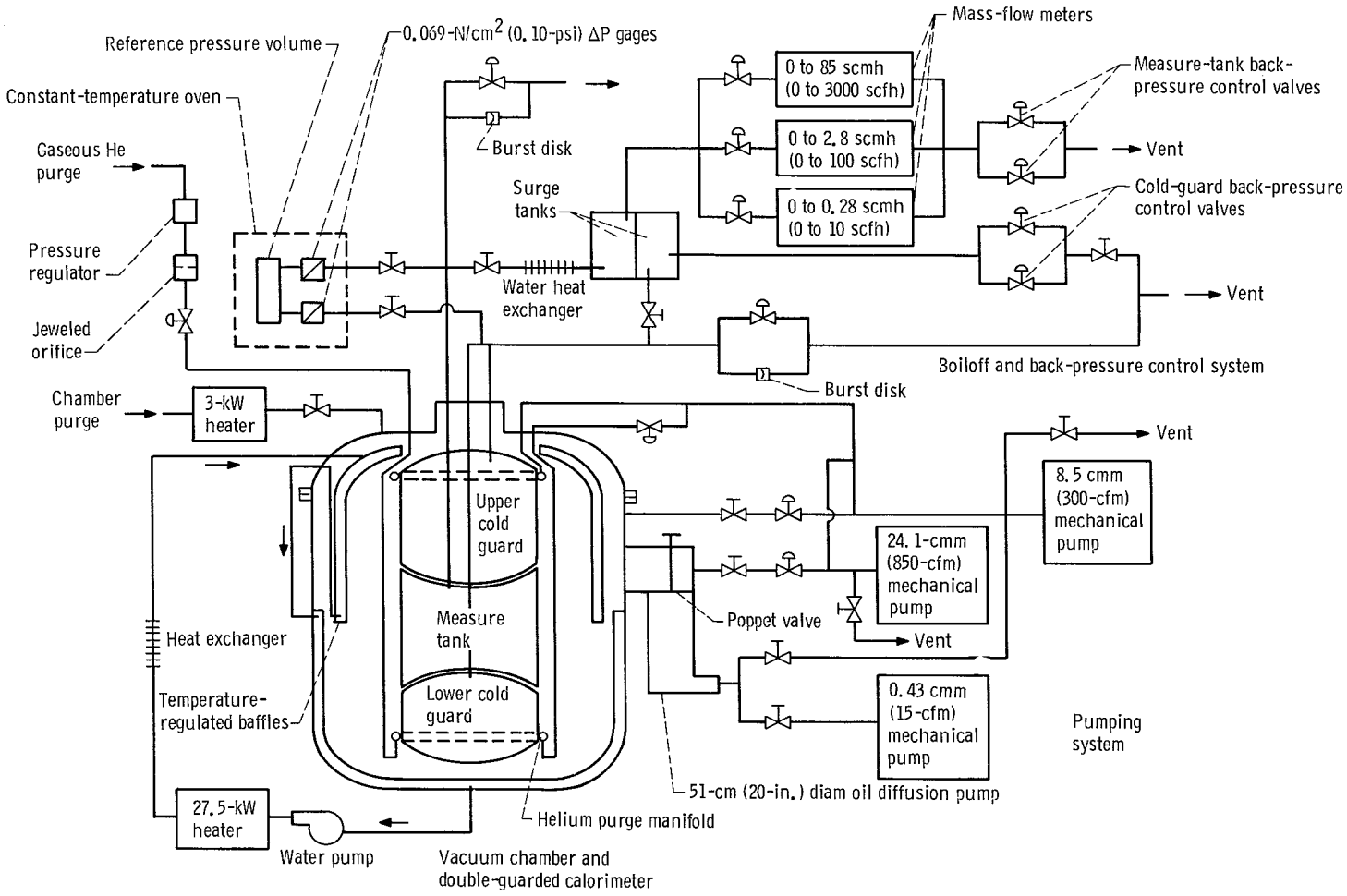


Figure 7. - Final schematic of test facility and major control systems.

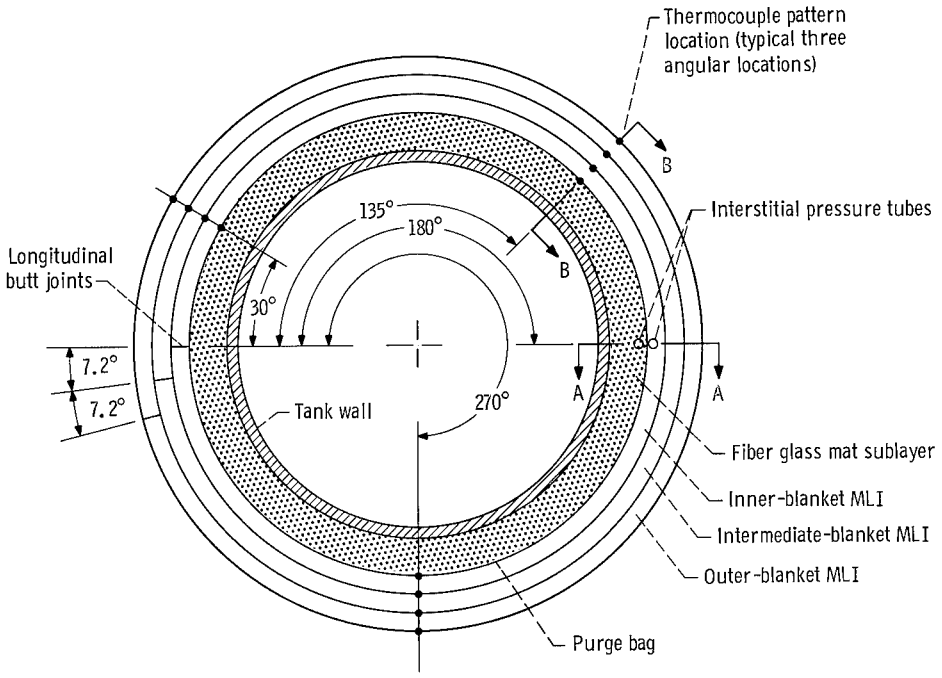


(a) Top view of insulation assembly.

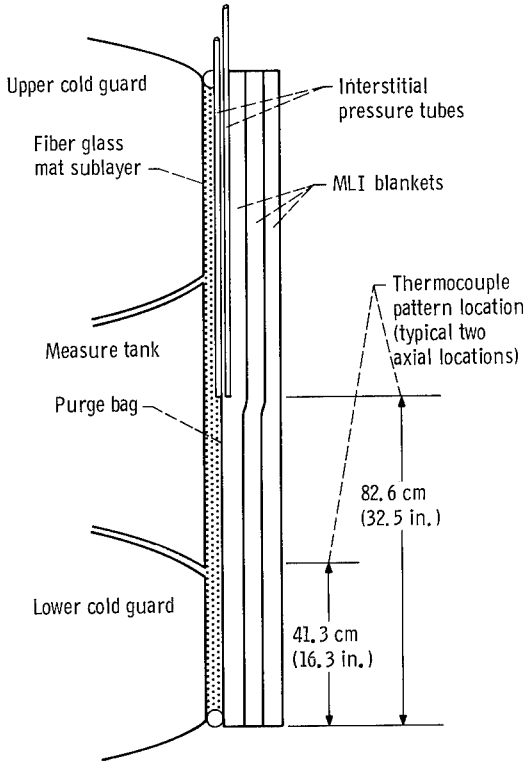


(b) Section A-A: interstitial pressure and longitudinal thermocouple pattern location.

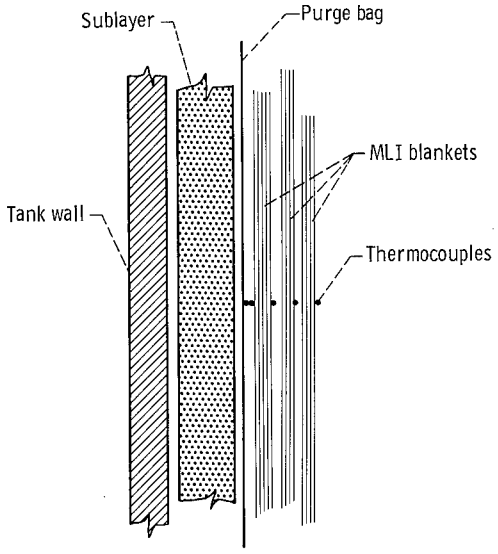


(c) Section B-B: location of thermocouples within individual pattern.

Figure 8. - Instrumentation location.

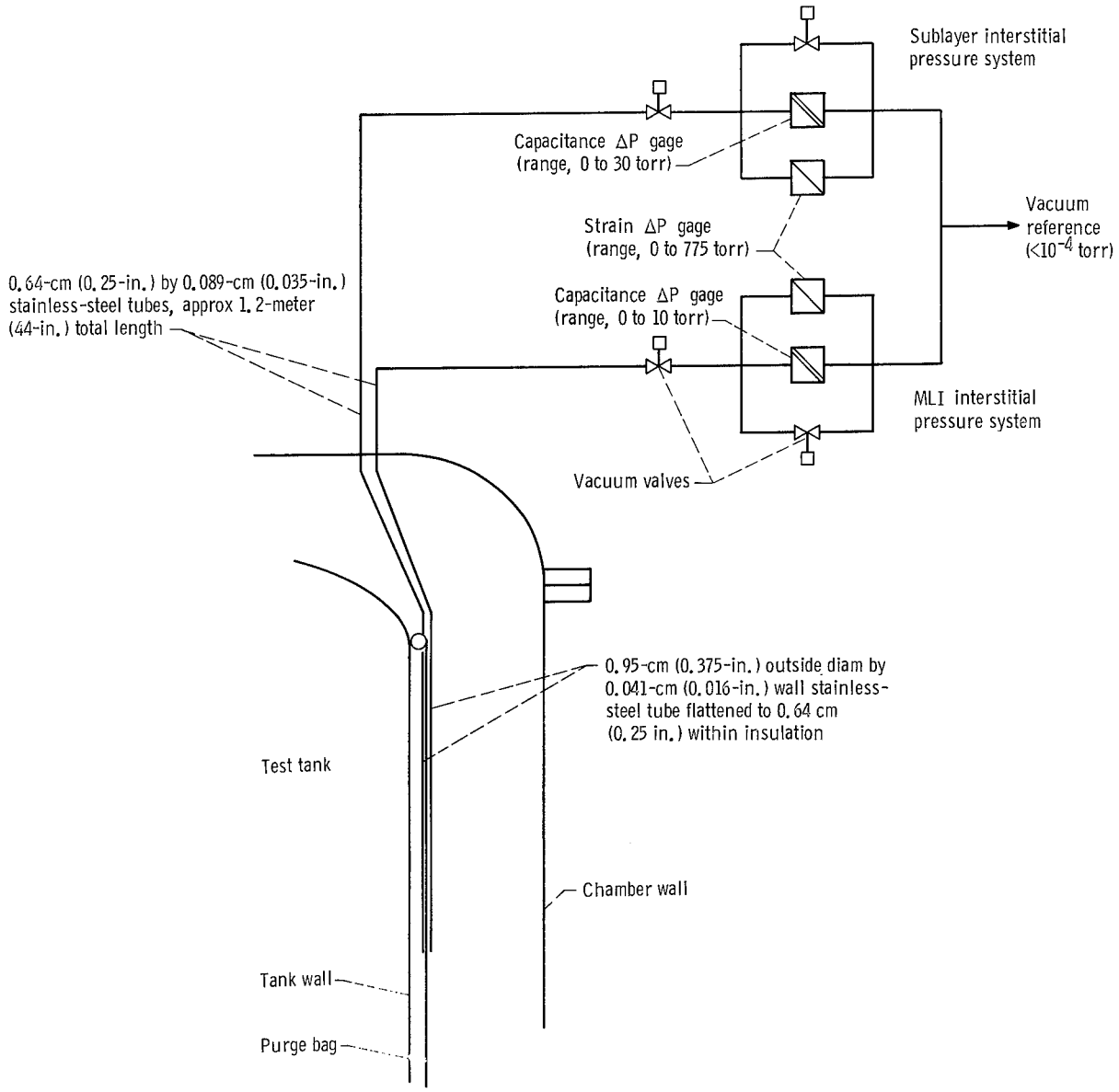


Figure 9. - Schematic of tubulated interstitial pressure transducers.

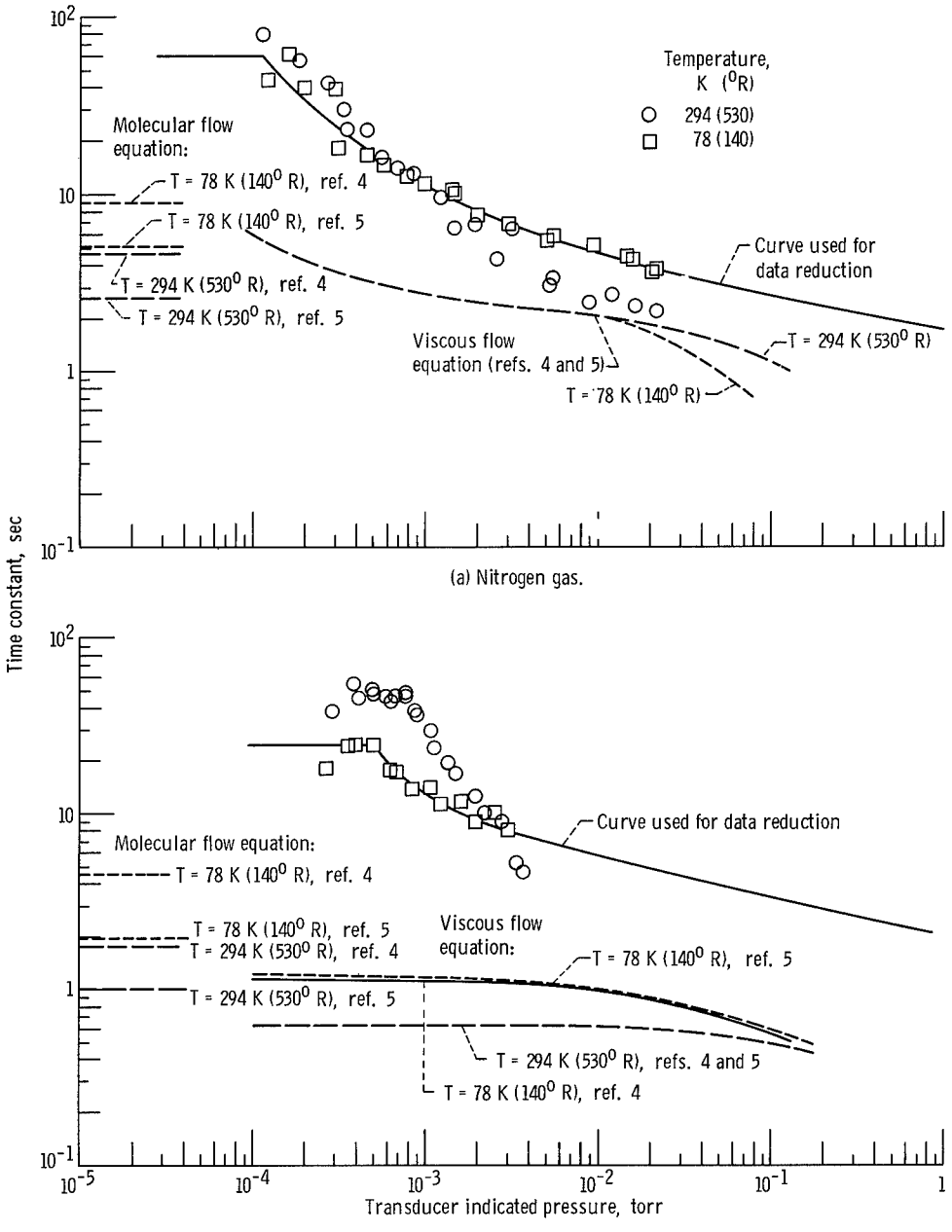


Figure 10. - Time constant for tubulated gage. Tube length, 2.54 meters (10 ft); 0.871-centimeter (0.343-in.) inside diameter tube flattened to 0.55 centimeter (0.22 in.).

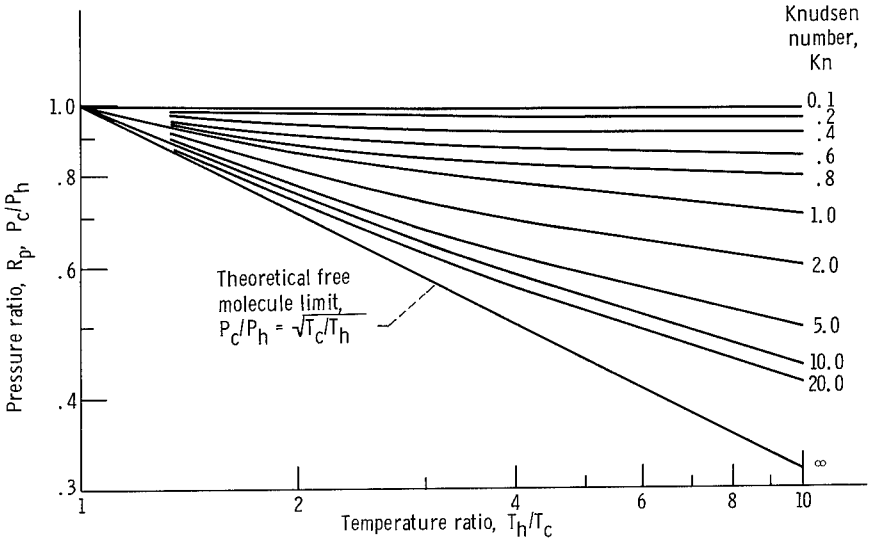


Figure 11. - Correction for thermolecular pressure effects in tubes.

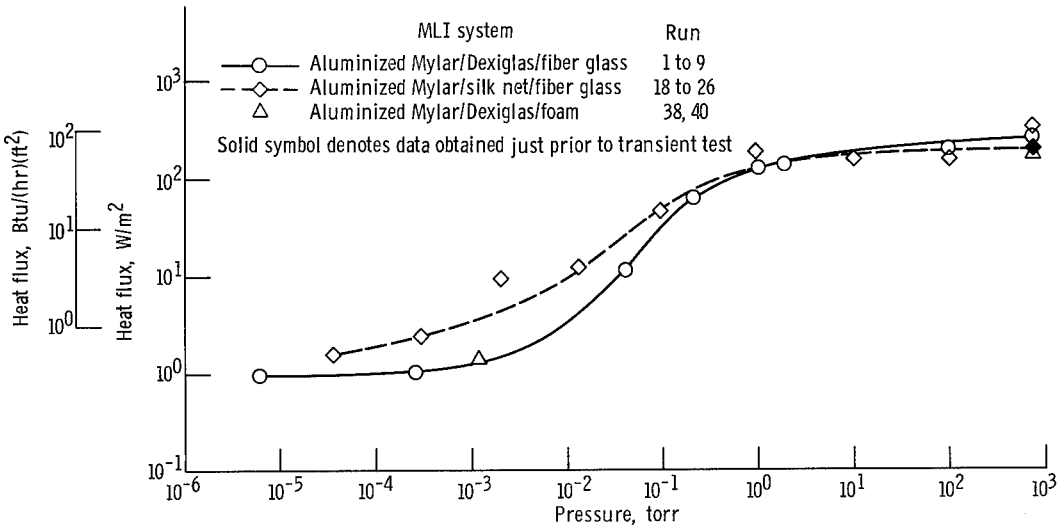


Figure 12. - Steady-state heat flux as function of chamber pressure for gaseous nitrogen multilayer insulation purge.

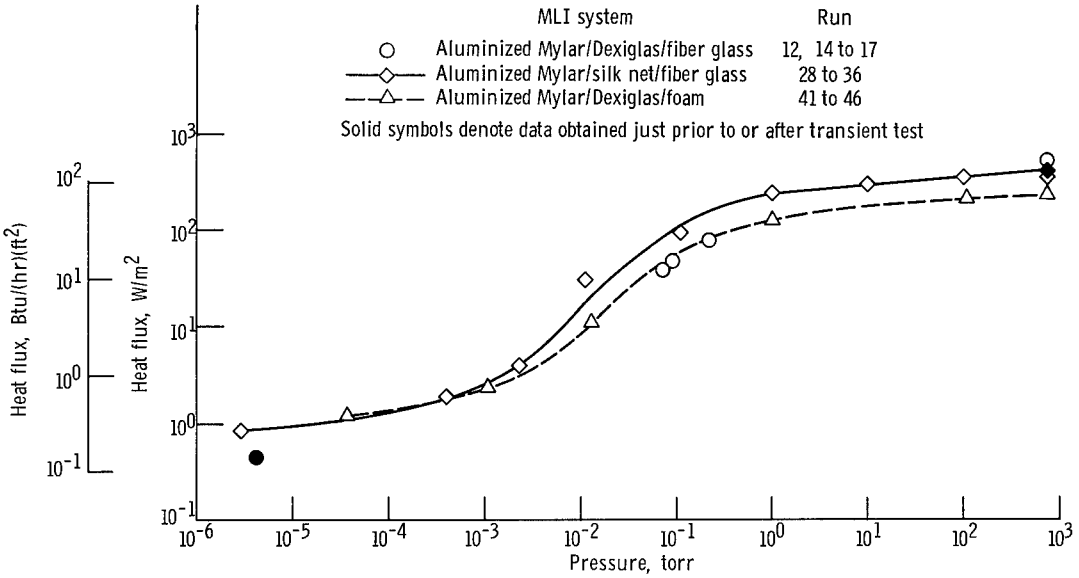


Figure 13. - Steady-state heat flux as function of chamber pressure for gaseous helium multilayer insulation purge.

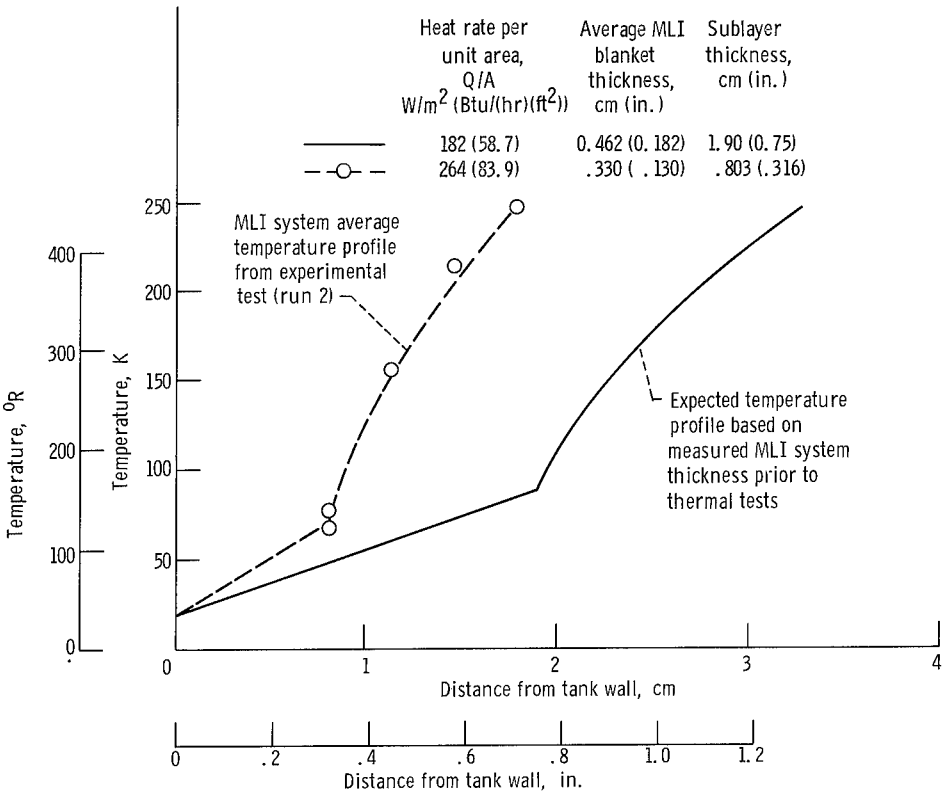


Figure 14. - Comparison of calculated and experimentally determined temperature profiles and ground-hold conditions for multilayer insulation (MLI) system 1.

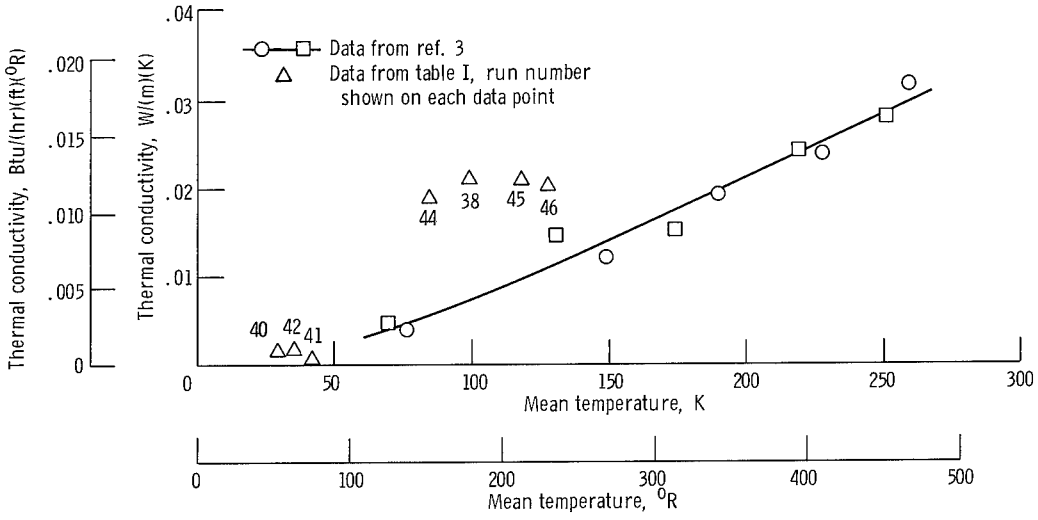


Figure 15. - Thermal conductivity of polyurethane foam sublayer.

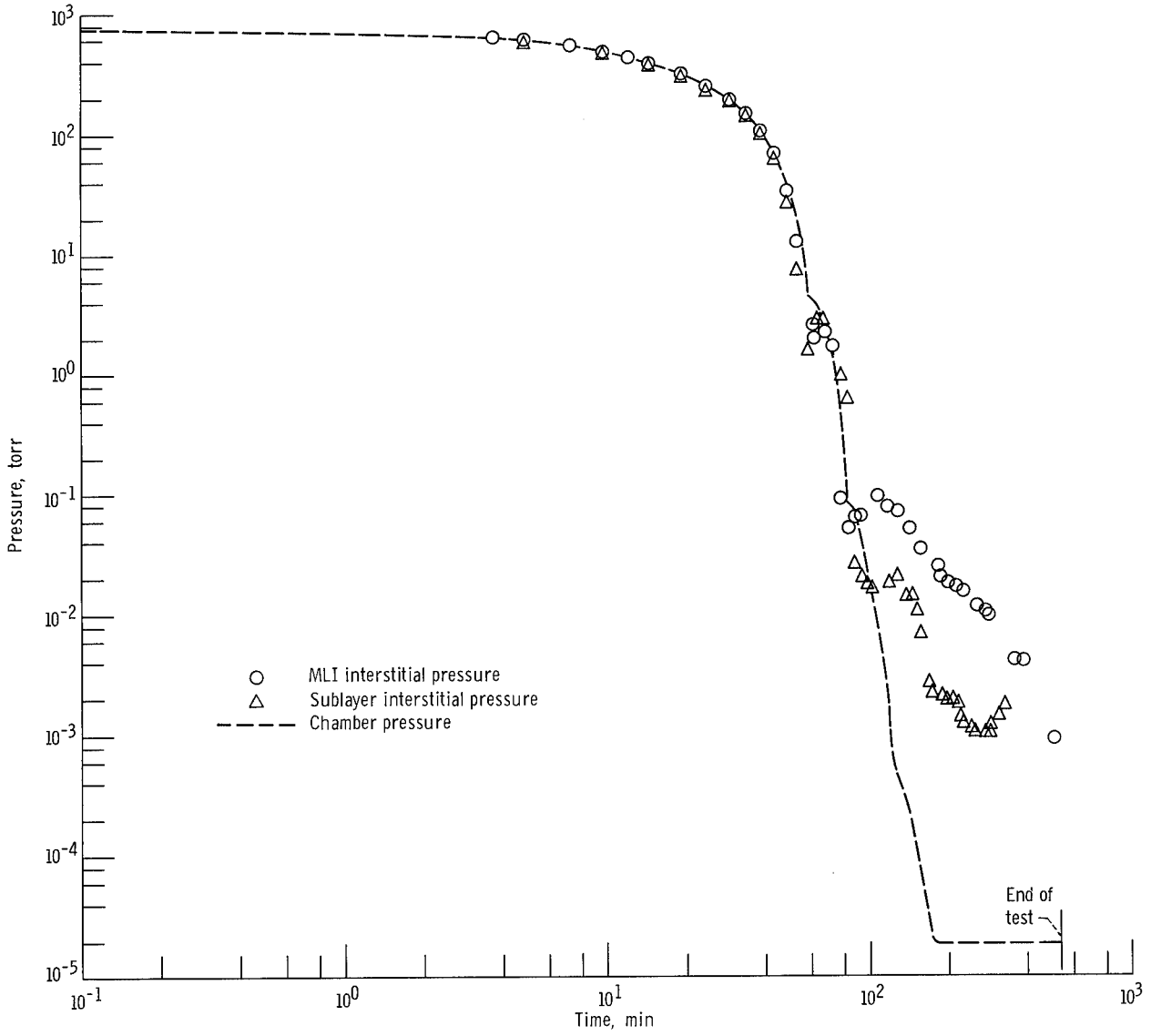


Figure 16. - Pressure as function of time for aluminized Mylar/Dexiglass/fiber glass sublayer insulation system. MLI nitrogen-purged, sublayer helium-purged for ground hold; run 10.

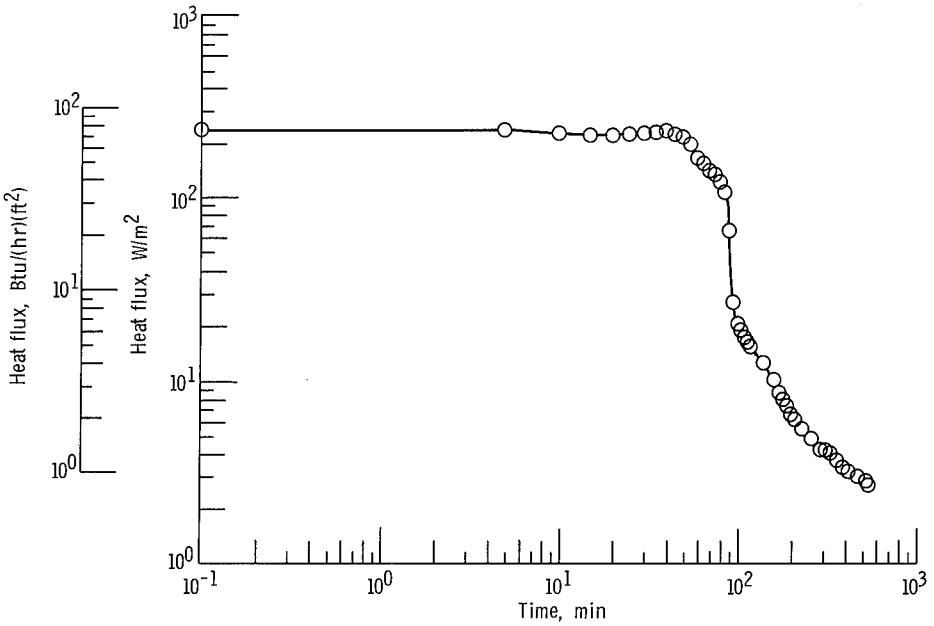


Figure 17. - Transient heat flux for aluminized Mylar/Dexiglas/fiber glass sublayer insulation system. MLI nitrogen-purged, sublayer helium-purged for ground hold; run 10.

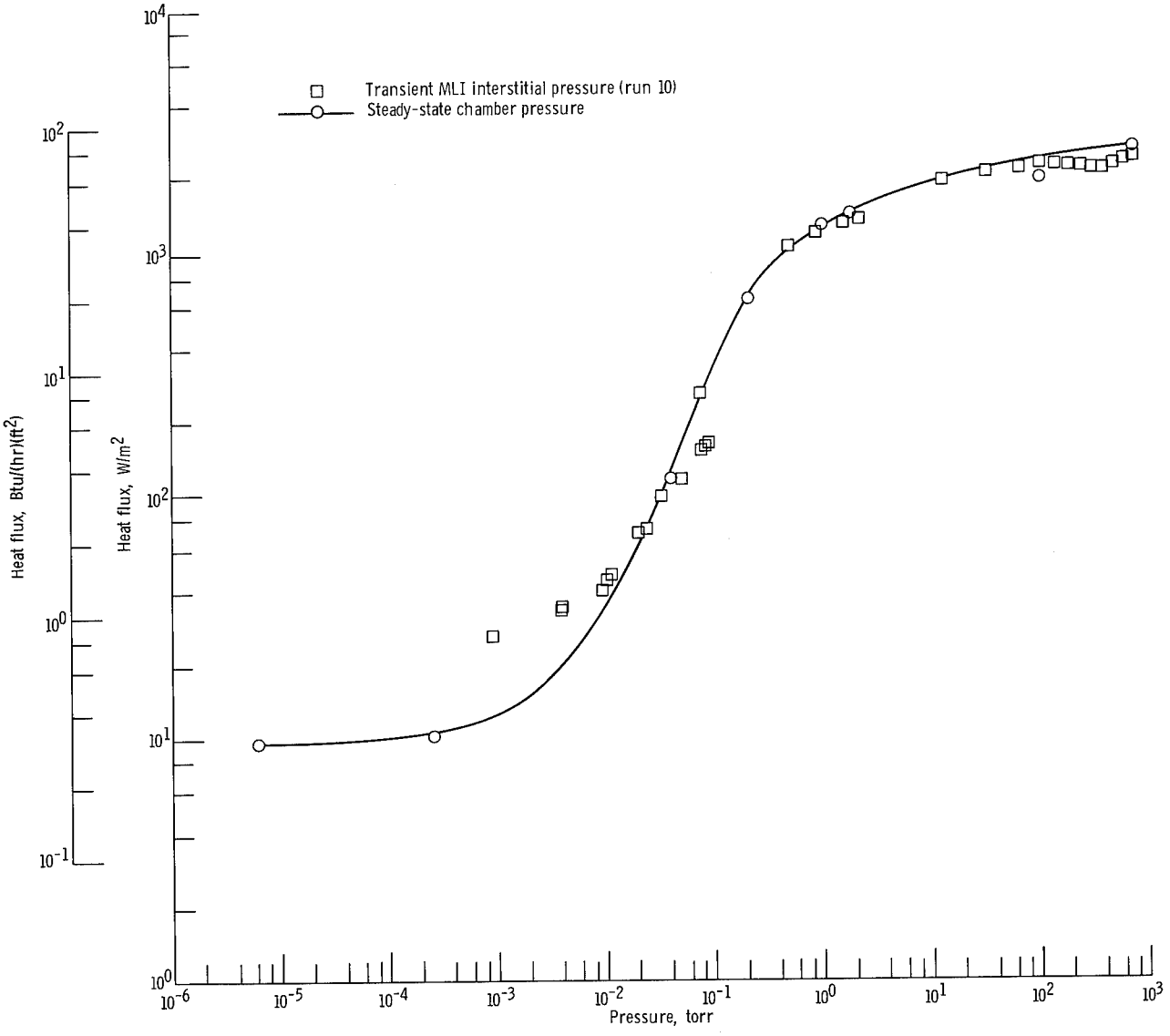


Figure 18. - Heat flux as function of pressure for aluminized Mylar/Dexiglas/fiber glass sublayer insulation system. MLI nitrogen-purged, sublayer helium-purged for ground hold.

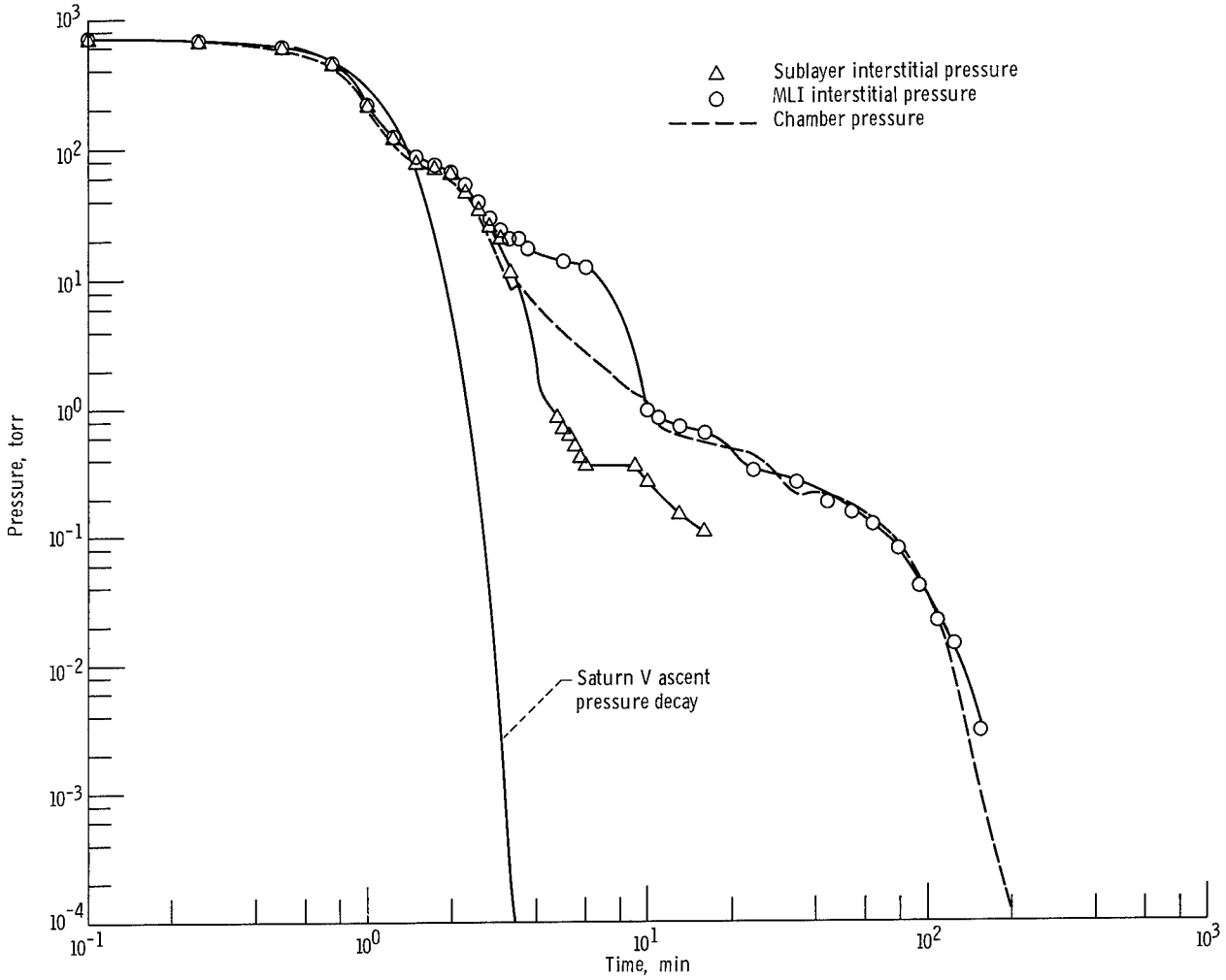


Figure 19. - Pressure as function of time for aluminized Mylar/silk netting/fiber glass sublayer insulation system. MLI nitrogen-purged, sublayer helium-purged for ground hold; run 27.

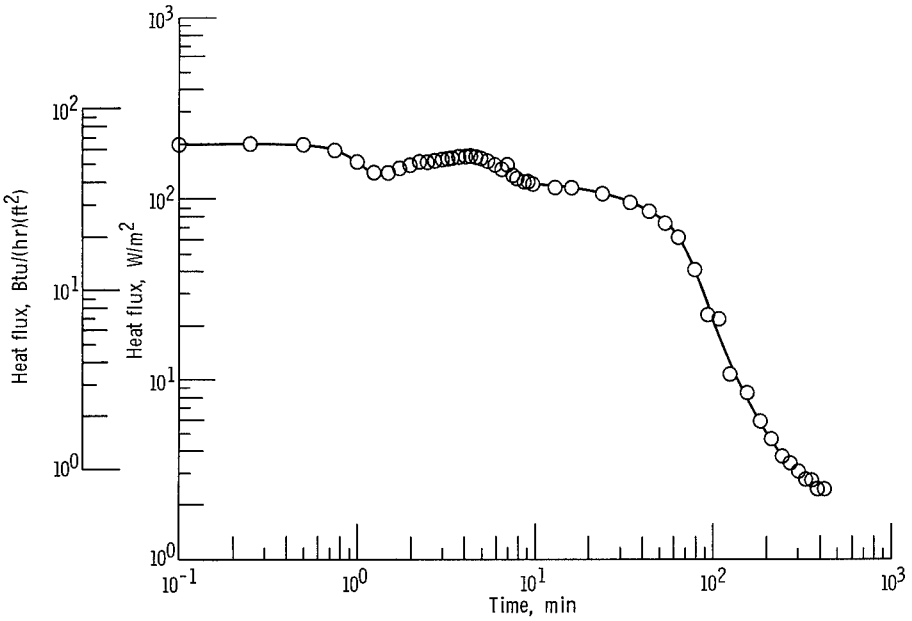


Figure 20. - Transient heat flux for aluminum Mylar/silk netting/fiber glass sublayer insulation system. MLI nitrogen-purged, sublayer helium-purged for ground hold; run 27.

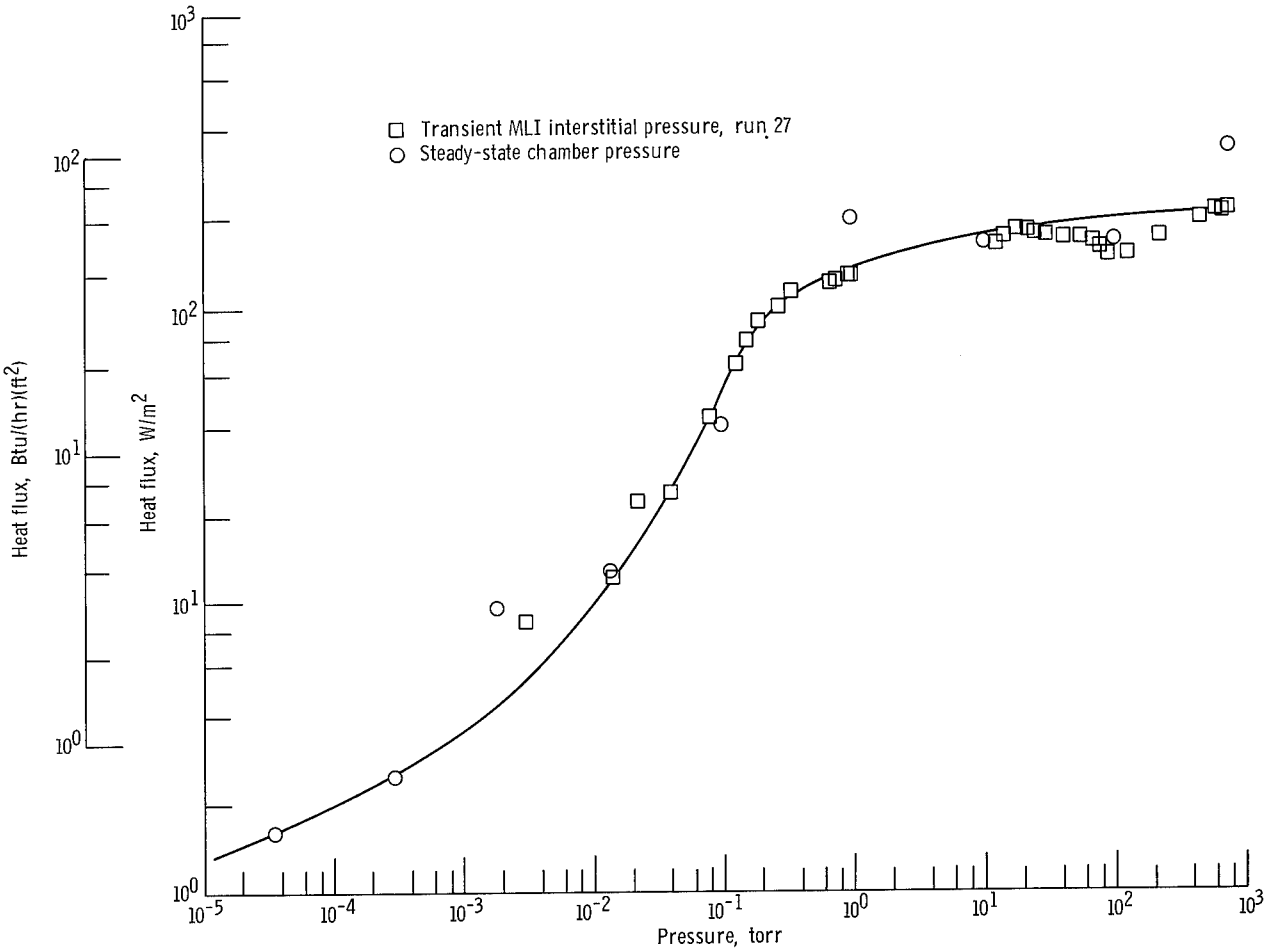


Figure 21. - Heat flux as function of pressure for aluminized Mylar/silk netting/fiber glass sublayer insulation system. MLI nitrogen-purged, sublayer helium-purged for ground hold.

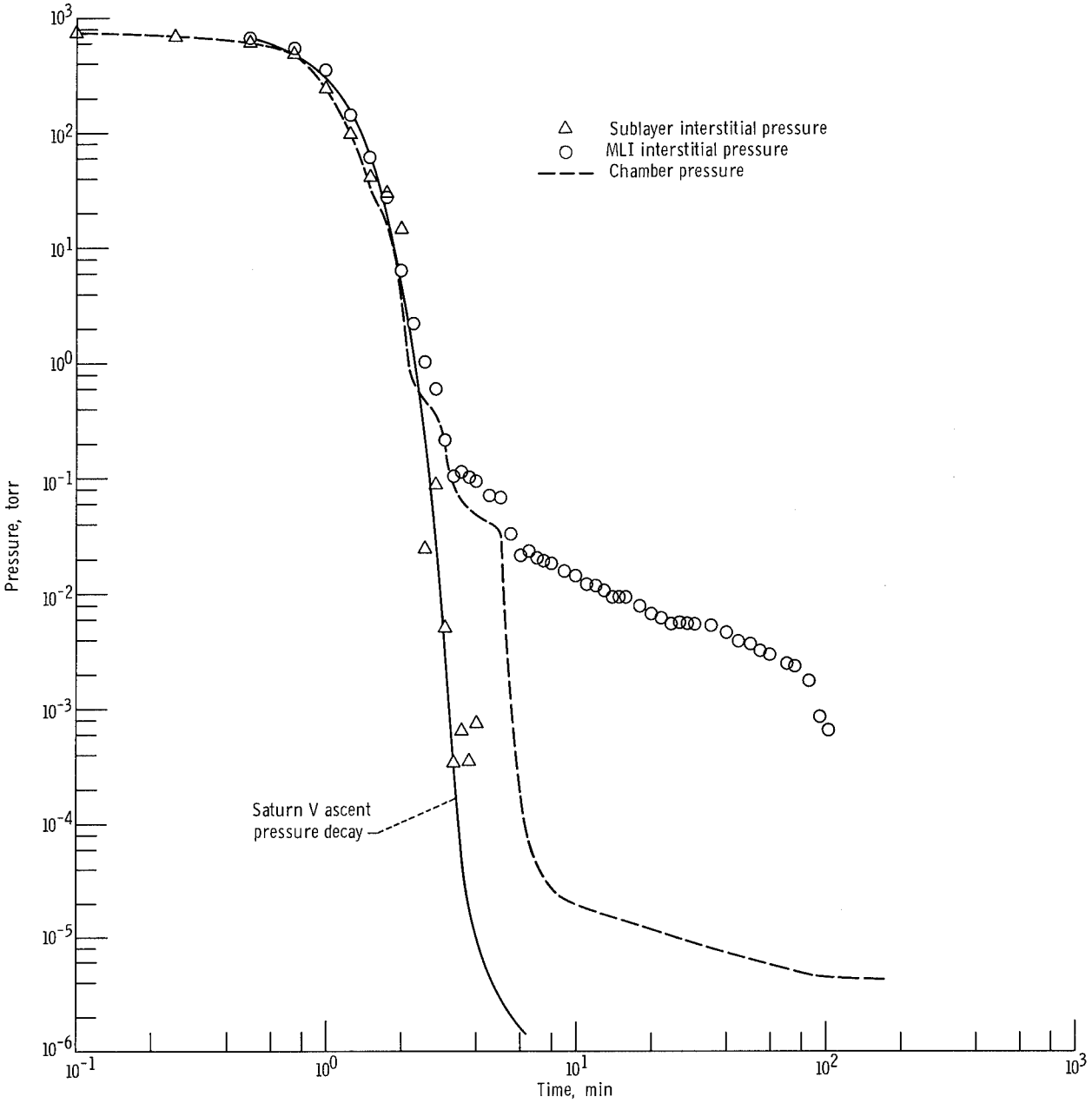


Figure 22. - Pressure as function of time for aluminized Mylar/Dexiglas/fiber glass sublayer insulation system. Helium-purged for ground hold; run 13.

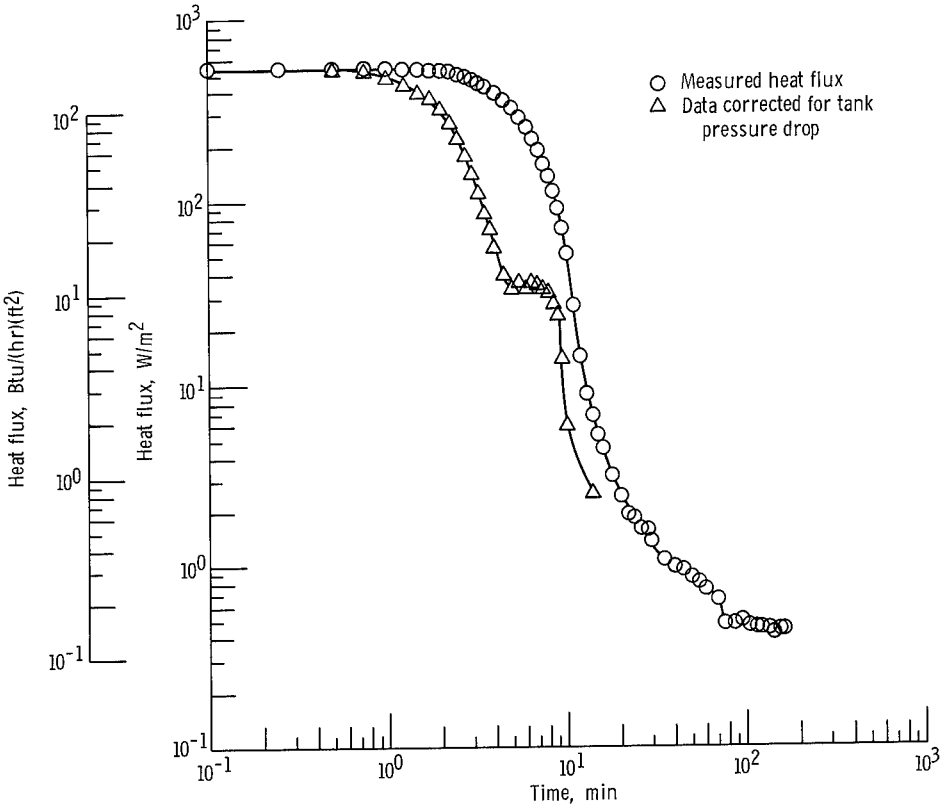


Figure 23. - Transient heat flux for aluminized Mylar/Dexiglas/fiber glass sublayer insulation system. Helium-purged for ground hold; run 13.

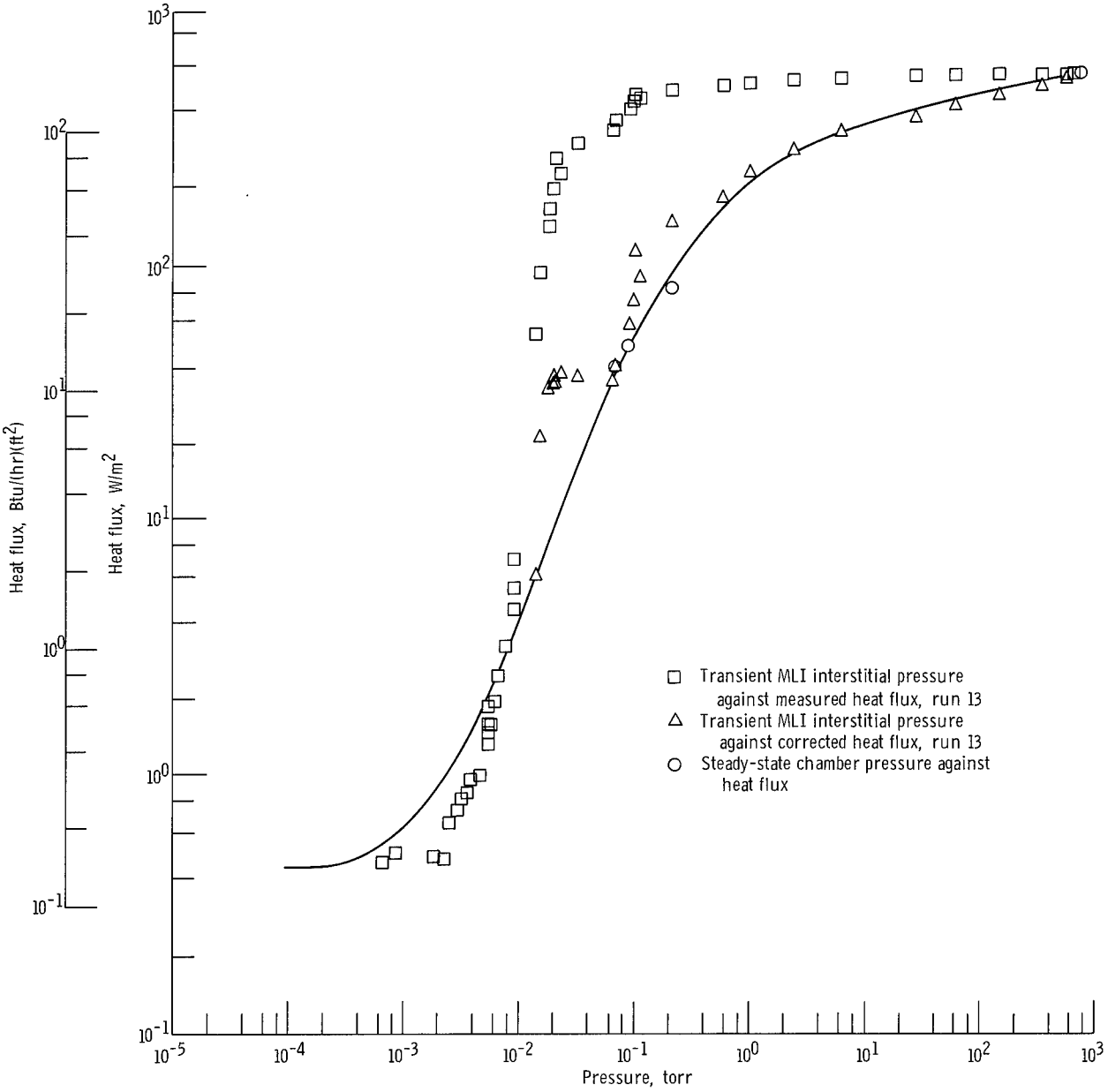


Figure 24. - Heat flux as function of pressure for aluminized Mylar/Dexiglas/fiber glass sublayer. Helium-purged for ground hold.

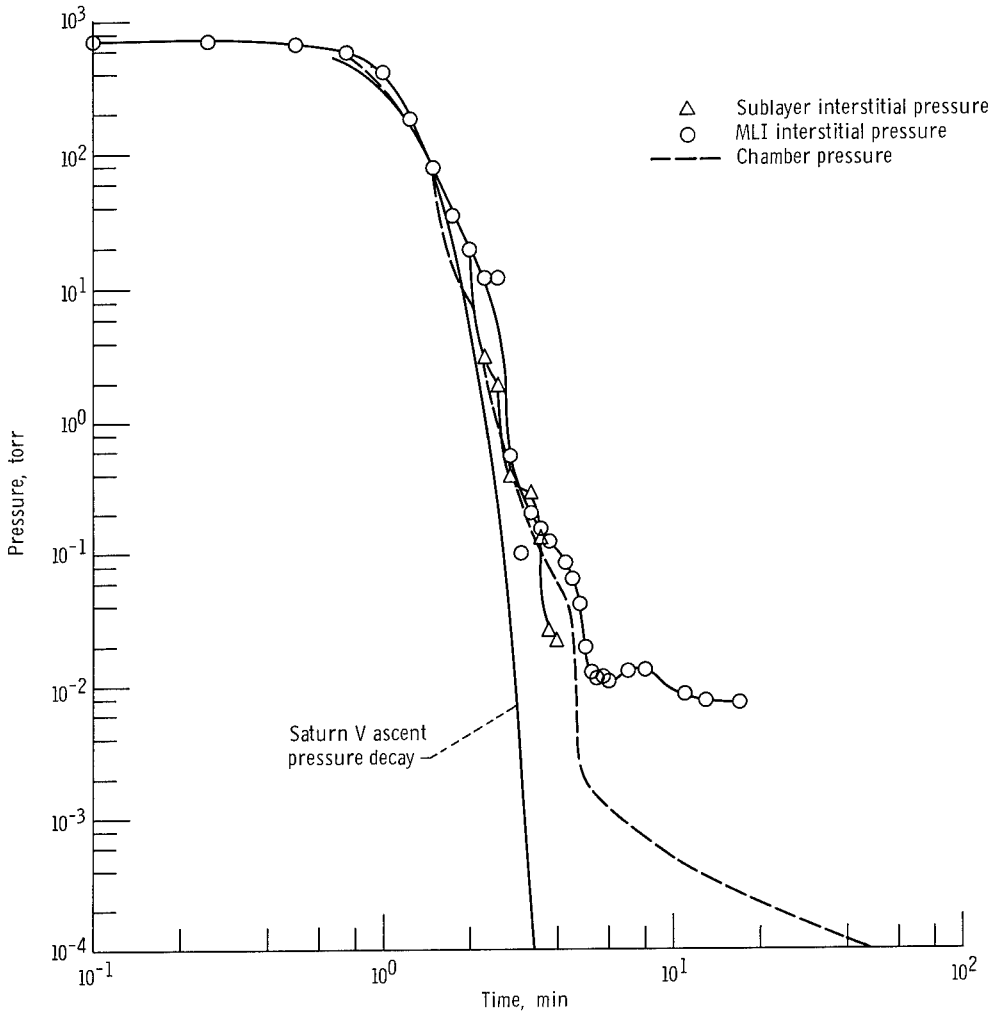


Figure 25. - Pressure as function of time for aluminized Mylar/silk netting/fiber glass sublayer insulation system. Helium-purged for ground hold; run 37.

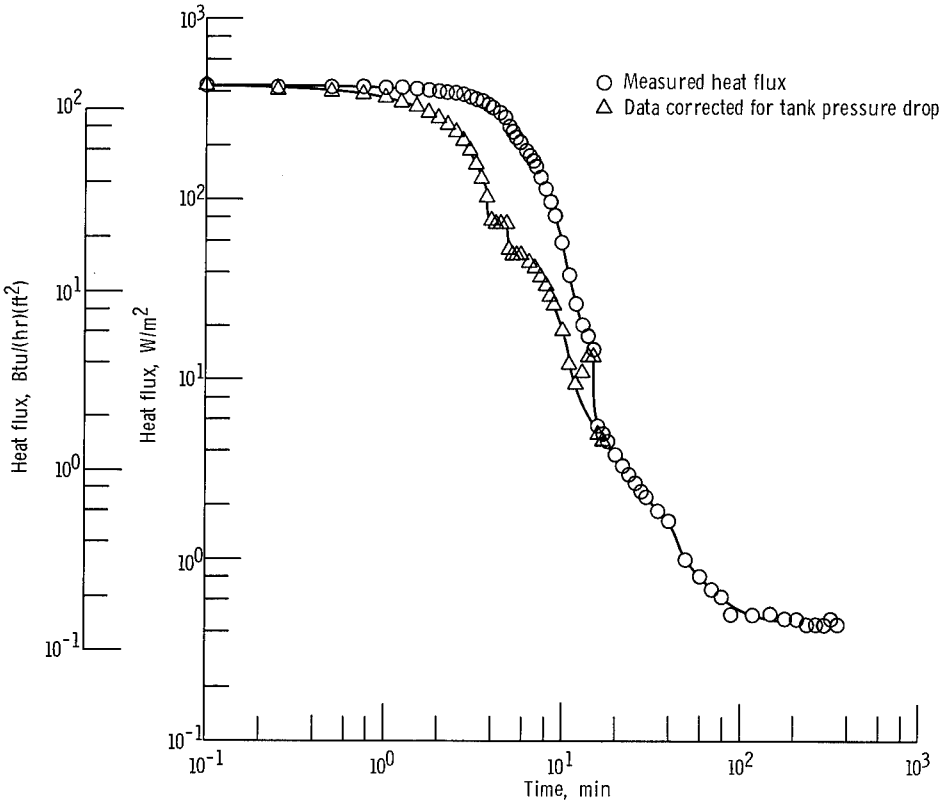


Figure 26. - Transient heat flux for aluminized Mylar/silk netting/fiber glass sublayer insulation system. Helium-purged for ground hold; run 37.

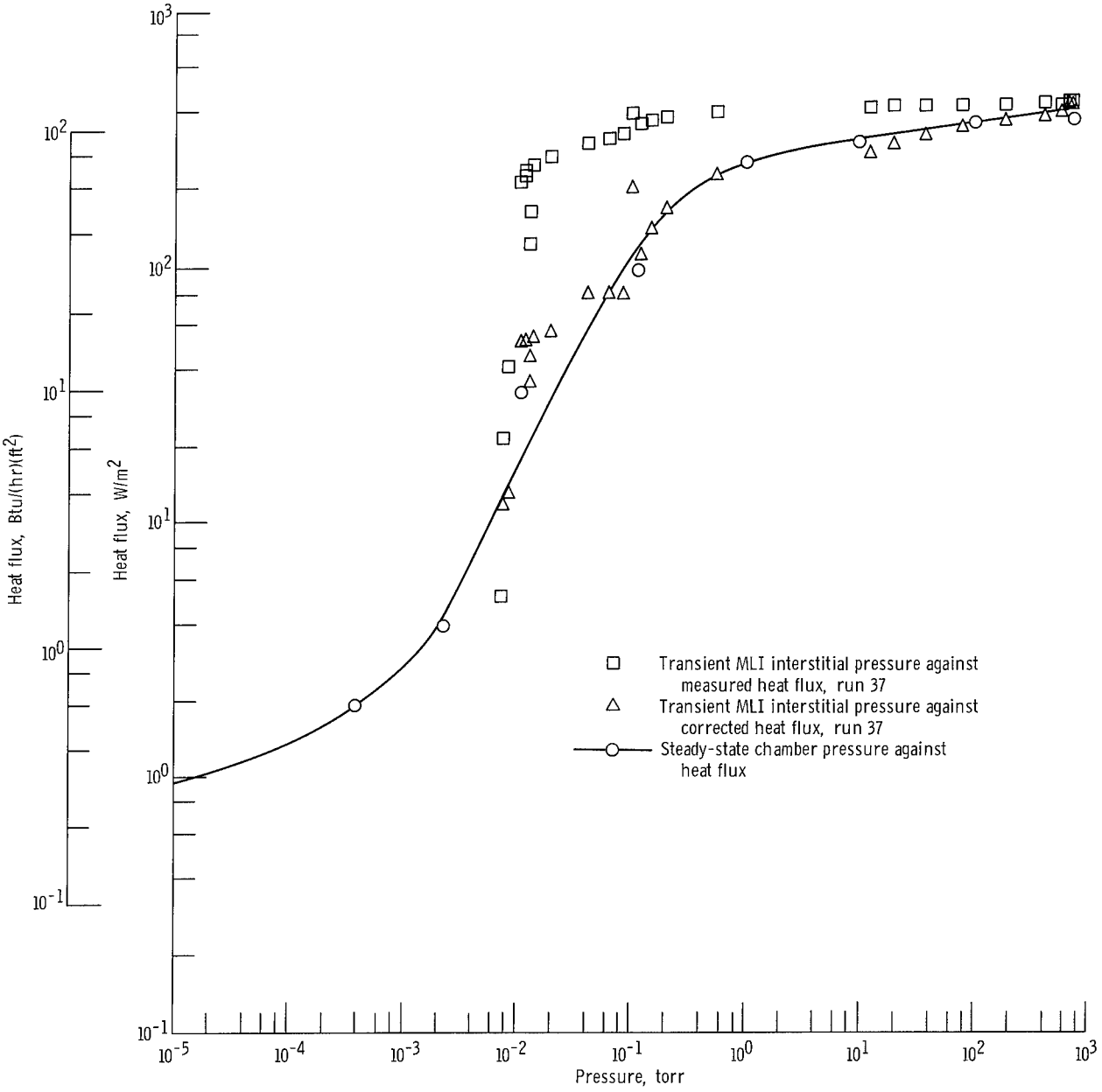


Figure 27. - Heat flux as function of pressure for aluminized Mylar/silk netting/fiber glass sublayer insulation system. Helium-purged for ground hold.

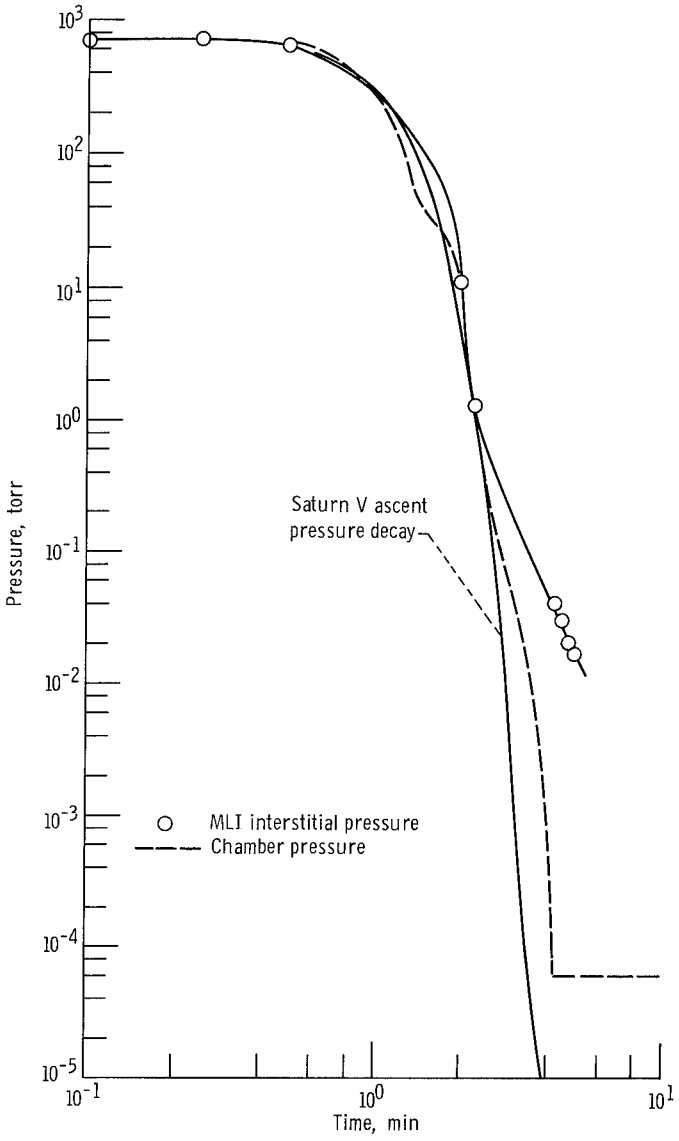


Figure 28. - Pressure as function of time for aluminized Mylar/ Dexiglas/foam sublayer insulation system. MLI helium-purged for ground hold; run 47.

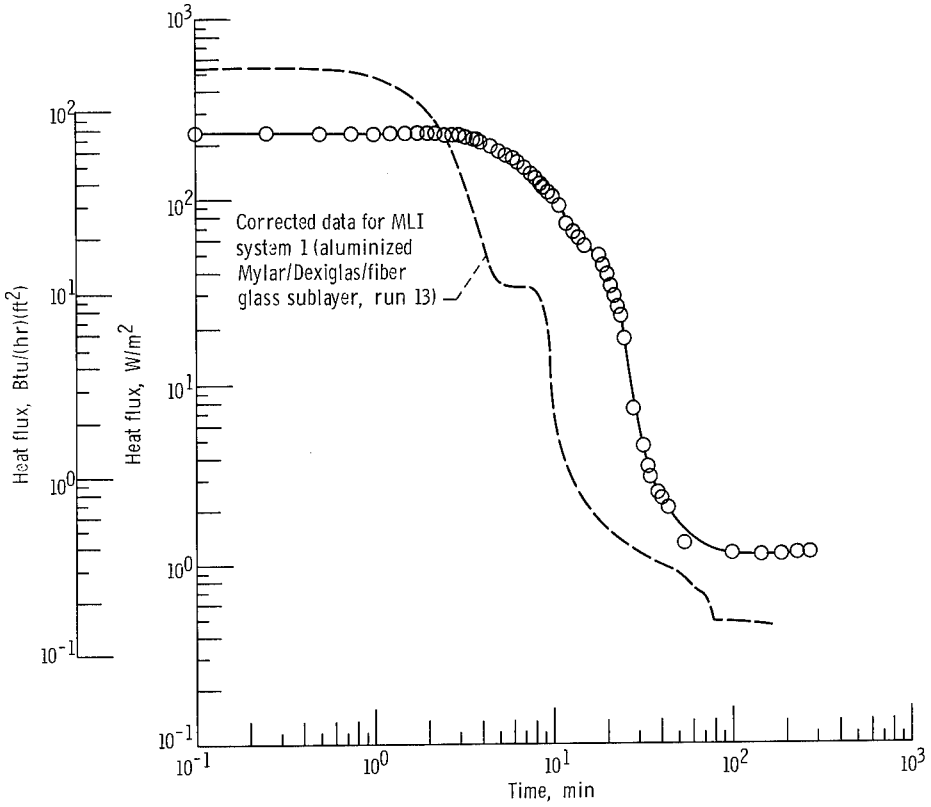


Figure 29. - Transient heat flux for aluminized Mylar/Dexiglas/foam sublayer insulation system. MLI helium-purged for ground hold; run 47.

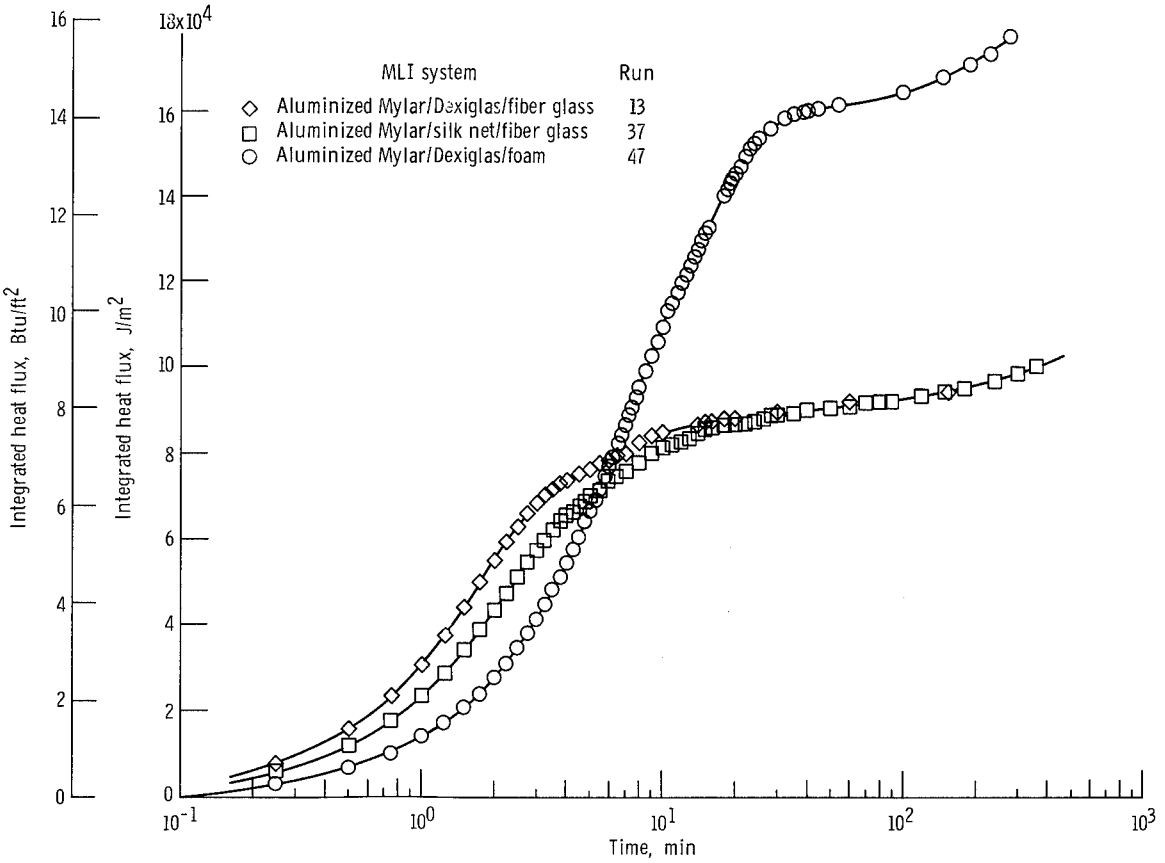


Figure 30. - Integrated heat flux as function of time for helium-purged multilayer insulation systems.

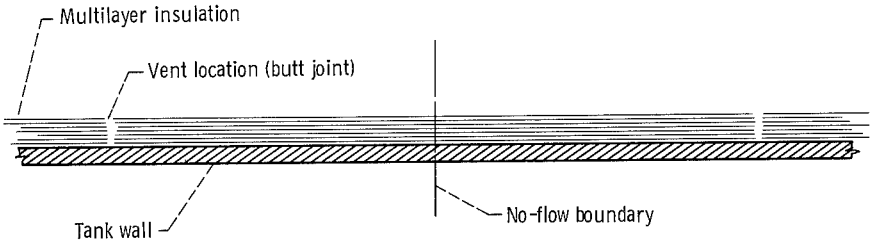


(a) Multilayer insulation system.

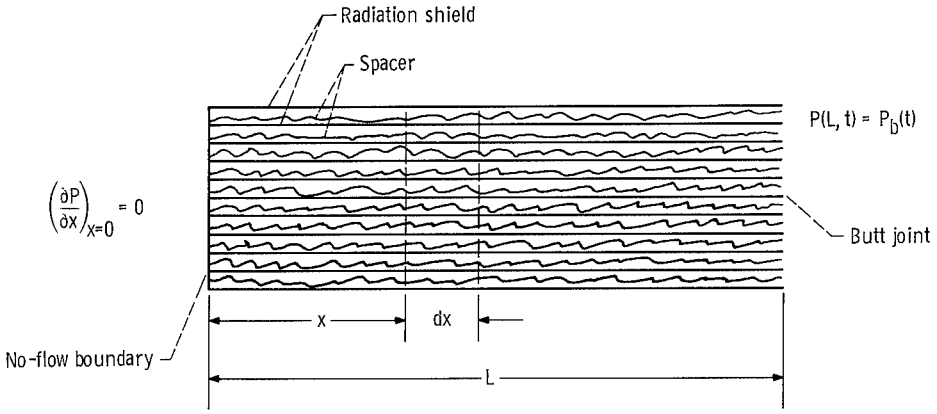


(b) Analytical gas flow model.

Figure 31. - Analytical model for edgewise evacuation of multilayer insulation.

| Dimensions for quarter panel considered | | | | | |
|---|---|---|---|---|---|
| r | | z | | θ | |
| m | ft | m | ft | rad | deg |
| 0.4014 | 1.3470 | 0.3874 | 1.271 | 3.14 | 180 |

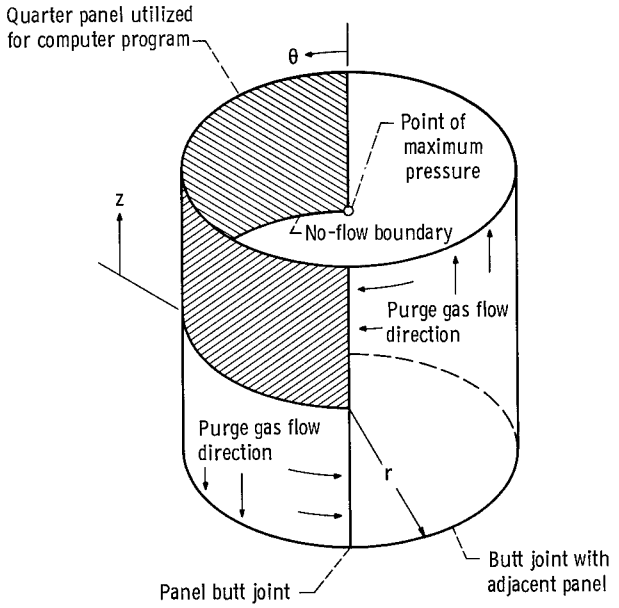


(a) Cylindrical multilayer insulation panel.

| Dimensions for half panel considered | | | | | | | |
|---|---|---|---|---|---|---|---|
| a | | b | | $r_o$ | | θ | |
| m | ft | m | ft | m | ft | rad | deg |
| 1.062 | 3.4833 | 1.062 | 3.4833 | 0.1334 | 0.4375 | 0.52 | 30 |

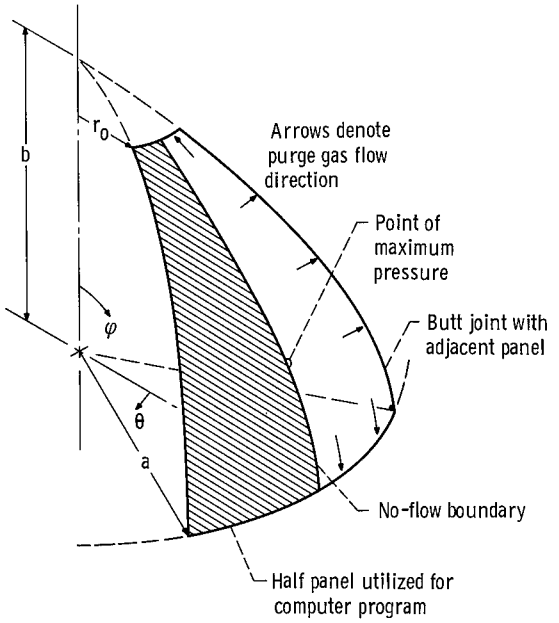


(b) Spherical multilayer insulation panel.

Figure 32. - Multilayer insulation panel configurations utilized for venting analysis.

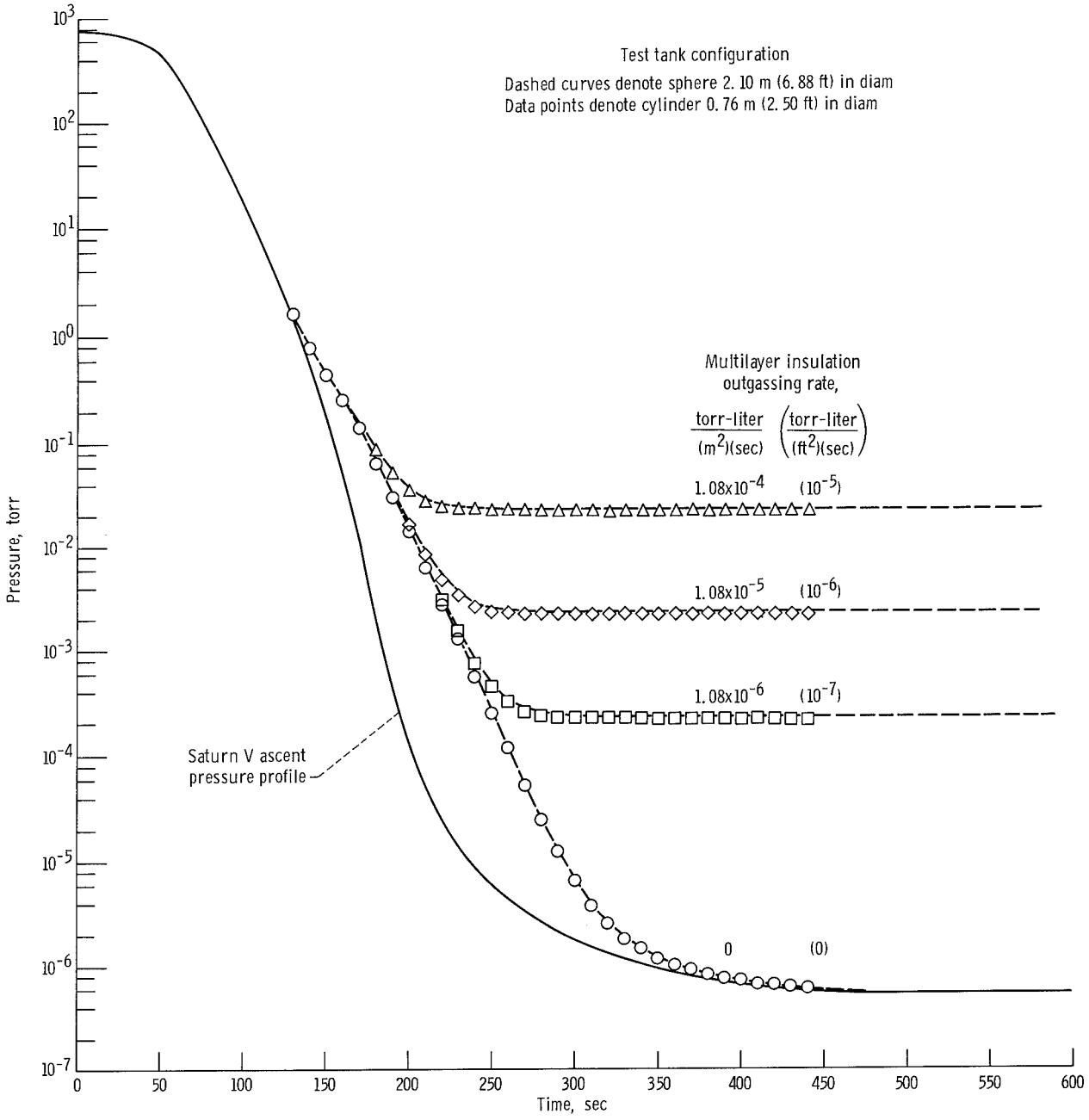


Figure 33. - Interstitial pressure decay for various outgassing rates within gaseous-nitrogen-purged multilayer insulation. Purge gas temperature, 79.5 K (143° R).

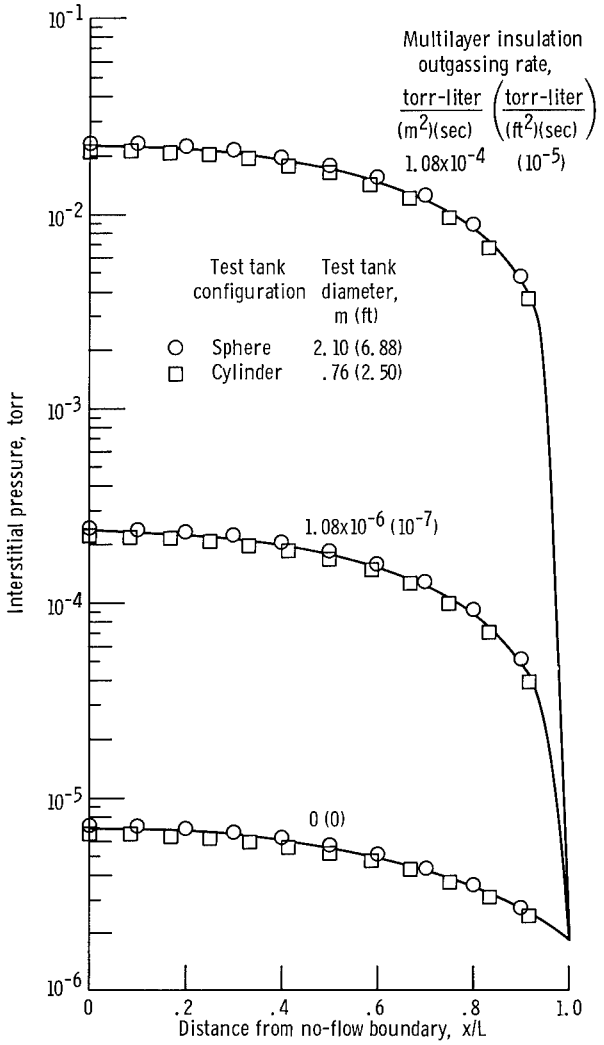


Figure 34. - Interstitial pressure profile across width of multilayer insulation panel in plane of maximum interstitial pressure. Ambient pressure ($1.82 \times 10^{-6}$ torr) corresponding to 300 seconds of Saturn V ascent pressure decay; gaseous nitrogen purge at 79.5 K ($143^{0}$ R).

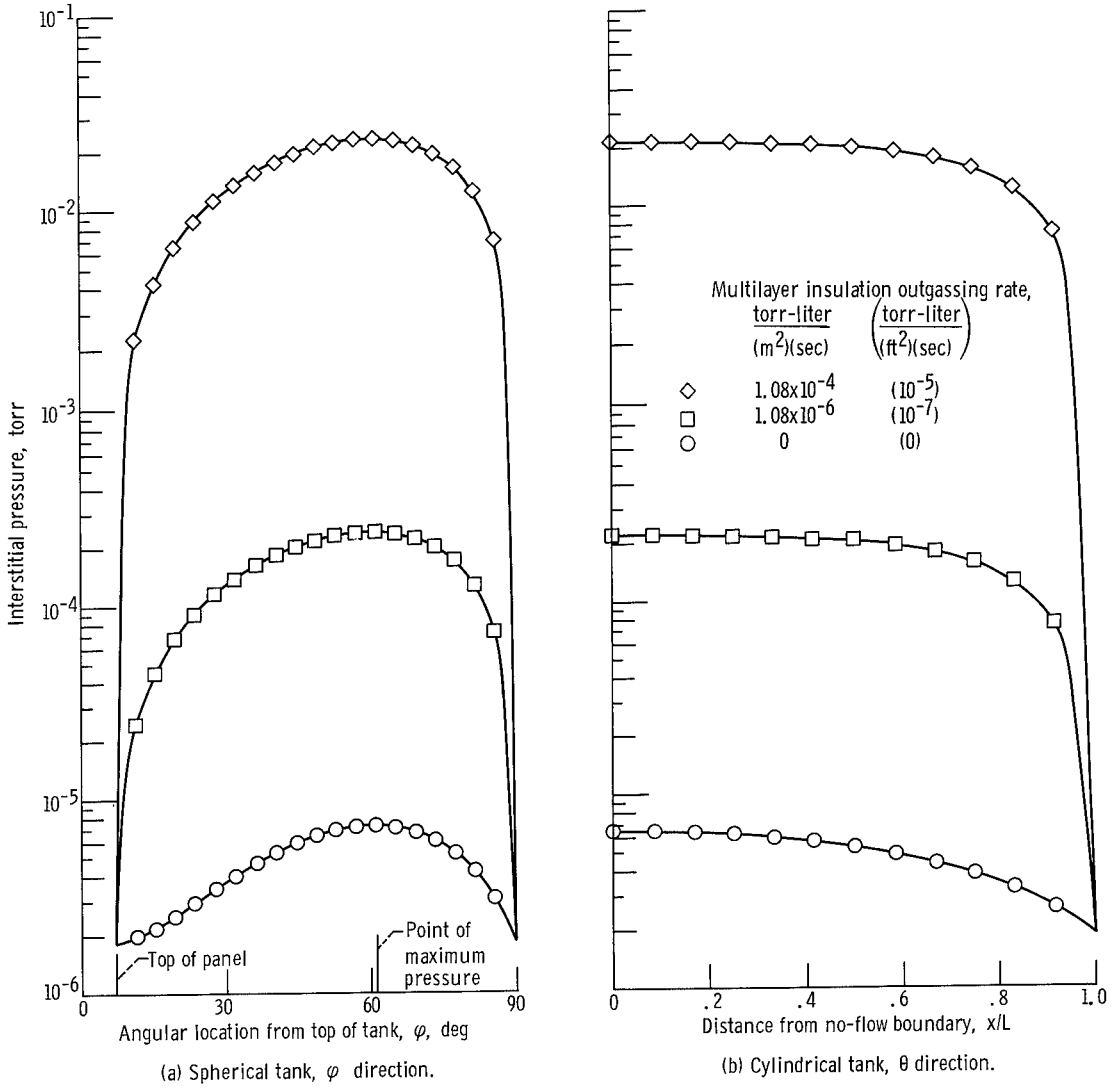


Figure 35. - Interstitial pressure profile along length of multilayer insulation panel in plane of maximum interstitial pressure. Ambient pressure ($1.82 \times 10^{-6}$ torr) corresponding to 300 seconds of Saturn V ascent pressure decay; gas-nitrogen purge at 79.5 K ($143^{0}$ R).

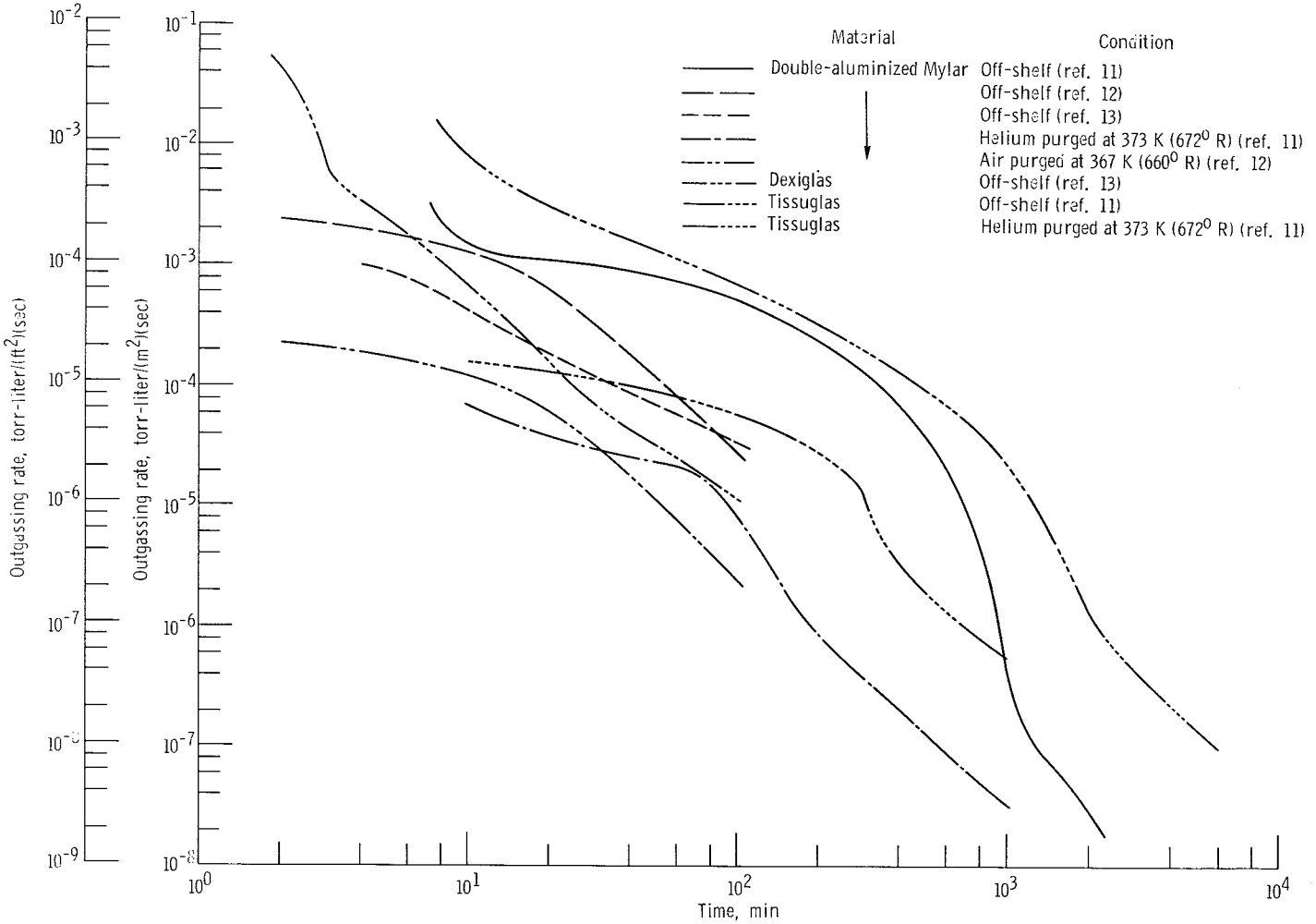


Figure 36. - Outgassing rate for several multilayer insulation materials.

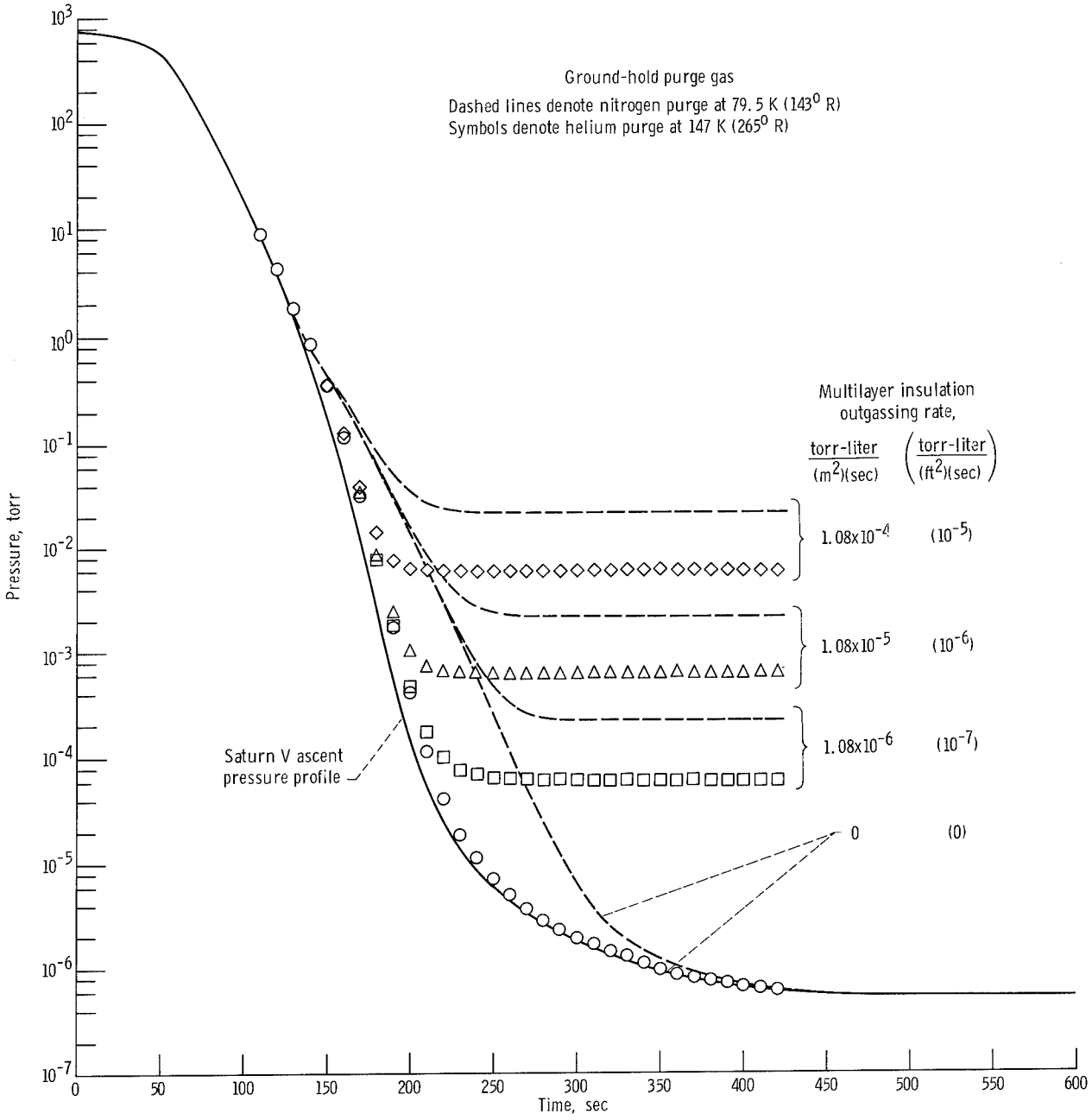


Figure 37. - Comparison of interstitial pressure decay for gaseous-nitrogen- and helium-purged multilayer insulation panels for cylindrical tank.

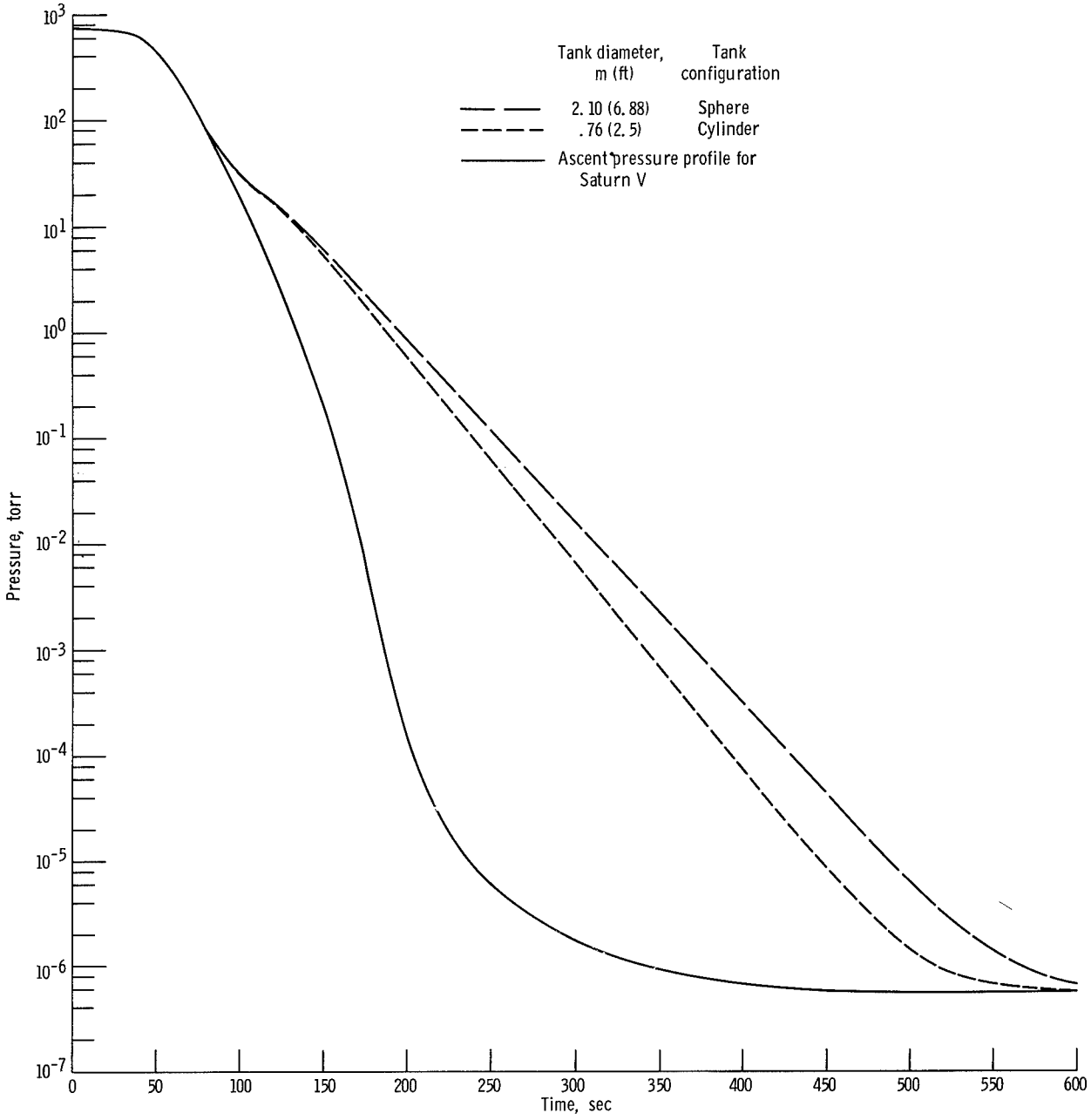


Figure 38. - Interstitial pressure decay within helium-purged fiber glass sublayer. Outgassing rate, 0; purge gas temperature, 49 K ($88^{0}$ R).